

**TRIBLOCK COPOLYMER MICELLE AS A MODEL FOR
DRUG DELIVERY SYSTEM: MOLECULAR MODELING
AND EXPERIMENTAL STUDY**

Mantana Chansuna



**A Thesis Submitted in Partial Fulfillment of the Requirements for the
Degree of Doctor of Philosophy in Chemistry
Suranaree University of Technology
Academic Year 2012**

การจำลองเชิงโมเลกุลและการทดลองบล็อกโพลีเมอร์ไมเซลล์
เพื่อเป็นต้นแบบในระบบนำส่งยา



วิทยานิพนธ์นี้เป็นส่วนหนึ่งของการศึกษาตามหลักสูตรปริญญาวิทยาศาสตรดุษฎีบัณฑิต
สาขาวิชาเคมี
มหาวิทยาลัยเทคโนโลยีสุรนารี
ปีการศึกษา 2555

**TRIBLOCK COPOLYMER MICELLE AS A MODEL FOR DRUG
DELIVERLY SYSTEM: MOLECULAR MODELING AND
EXPERIMENTAL STUDY**

Suranaree University of Technology has approved this thesis submitted in partial fulfillment of the requirements for the Degree of Doctor of Philosophy.

Thesis Examining Committee

(Assoc. Prof. Dr. Jatuporn Wittayakun)

Chairperson

(Asst. Prof. Dr. Visit Vao-soongnern)

Member (Thesis Advisor)

(Assoc. Prof. Dr. Vinich Promarak)

Member

(Asst. Prof. Dr. Siriporn Jungsuttiwong)

Member

(Dr. Nuttaporn Pimpha)

Member

(Prof. Dr. Sukit Limpijumnong)

Vice Rector for Academic Affairs

(Assoc. Prof. Dr. Prapun Manyum)

Dean of Institute of Science

มณฑนา จันสุนา : การจำลองเชิงโมเลกุลและการทดลองไทรบล็อกโคพอลิเมอร์ไมเซลล์
เพื่อเป็นต้นแบบในระบบนำส่งยา (TRIBLOCK COPOLYMER MICELLE AS A MODEL
FOR DRUG DELIVERY SYSTEM : MOLECULAR MODELING AND
EXPERIMENTAL STUDY) อาจารย์ที่ปรึกษา : ผู้ช่วยศาสตราจารย์ ดร.วิศิษฐ์ แวสูงเนิน,
180 หน้า.

พอลิแลคไทด์-พอลิเอธิลีนไกลคอล-พอลิแลคไทด์ไทรบล็อกโคพอลิเมอร์ไมเซลล์ได้รับความสนใจในด้านการนำส่งยาเนื่องจากมีสมบัติที่พิเศษ โดยการพิจารณาสมบัติที่เกี่ยวข้องกับไทรบล็อกโคพอลิเมอร์ไมเซลล์ทั้งหมดช่วยให้เข้าใจรายละเอียดของไทรบล็อกโคพอลิเมอร์ไมเซลล์นี้ต่อการนำไปประยุกต์ใช้งาน พอลิเมอร์แบบแปรงจาก PEO ซึ่งใช้เป็นต้นแบบของส่วนโคโรนาของไมเซลล์ถูกนำมาศึกษาโดยใช้แบบจำลองมอนติคาร์โลบนผลึก ในการจำลองแบบหยาบจะเทียบสายโซ่ PEO เป็นบีดแต่ละบีดแทนการเชื่อมต่อกันของหน่วยเอธิลีน (CH_2CH_2) และ CH_2O แรงกระทำระยะใกล้คำนวณโดยใช้ rotational isomeric state model (RIS) และแรงกระทำระยะไกลใช้การคำนวณโดยใช้ฟังก์ชันศักย์ของ Lennard-Jones (LJ) จากนั้นศึกษาผลของความหนาแน่นการยึดจับ (grafting density) ค่าการกระจายตัวแบบผสม (polydispersity) รวมถึงสมบัติของตัวทำละลายต่อสมบัติเชิงโครงสร้างของพอลิเมอร์แบบแปรง ผลการศึกษาที่ได้พบว่าทั้งความหนาแน่นการยึดจับและค่าการกระจายตัวแบบผสม เป็นปัจจัยหลักที่ส่งผลต่อสมบัติของพอลิเมอร์ และพอลิเมอร์แบบแปรงจะถูกอัดมากขึ้นเมื่ออยู่ในตัวทำละลายที่ไม่ดี (poor solvent) ซึ่งเห็นได้จากโปรไฟล์ความหนาแน่นและการกระจายตัวของบีดบนสายโซ่พอลิเมอร์ จากนั้นนำแบบจำลองมอนติคาร์โลนี้ไปใช้จำลองการรวมกลุ่มเชิงโครงสร้างของอนุภาคนาโนของ PEO (ซึ่งในงานวิจัยนี้ใช้เป็นต้นแบบสำหรับส่วนแกนกลางของไมเซลล์) ที่อยู่ภายใต้สภาวะตัวทำละลายที่แตกต่างกัน พบว่าอนุภาคนาโนสามารถจัดเรียงตัวได้หนาแน่นขึ้นและเปลี่ยนรูปร่างจนเกือบเป็นรูปทรงรีเมื่ออยู่ในตัวทำละลายแบบไม่ดี สมบัติของตัวทำละลายไม่มีผลต่อการกระจายตัวของบีดตรงกลางแต่มีผลอย่างมากต่อการกระจายตัวของบีดตรงปลาย และการจัดเรียงพันธะของสายโซ่ภายในอนุภาคนาโนเป็นแบบสุ่ม นอกจากนี้ได้ใช้การจำลองมิโซคายน์ ศึกษาผลของอัตราส่วน A/B ความเข้มข้นของพอลิเมอร์และการเติมส่วนประกอบที่สามต่อการเปลี่ยนแปลงรูปร่างของไทรบล็อกโคพอลิเมอร์แบบ ABA เมื่อ A แทนหน่วยเอธิลีนออกไซด์ในขณะที่ B แทนหน่วยโพรพิลีนออกไซด์ ผลที่ได้พบว่าคุณค่าความเข้มข้นเริ่มต้นของการเกิดไมเซลล์ (cmc) และอัตราการเกิดไมเซลล์เพิ่มขึ้นเมื่อเพิ่มอัตราส่วน A/B การเติมโมเลกุลยาและการเปลี่ยนแปลงสมบัติความไม่ชอบน้ำของส่วนที่ไม่ชอบน้ำในโครงสร้างของบล็อกโคพอลิเมอร์ส่งผลต่อการเปลี่ยนแปลงรูปร่างของไมเซลล์ทรงกลม นอกจากนี้

ในงานวิจัยได้ใช้การจำลองเชิง โมเลกุลเพื่อออกแบบพอลิแลคไทด์-พอลิเอธิลีนไกลคอล-พอลิแลคไทด์ไตรบล็อกโคพอลิเมอร์ที่มีการเปลี่ยนแปลงอัตราส่วน LA/EG ก่อนจะทำการสังเคราะห์จริง โดยใช้เทคนิคมีโซคายนัน และ DPD ศึกษาพฤติกรรมเฟส ค่า cmc และอัตราการเกิดไมเซลล์ จากนั้นได้ทำการสังเคราะห์พอลิแลคไทด์-พอลิเอธิลีนไกลคอล-พอลิแลคไทด์ไตรบล็อกโคพอลิเมอร์และศึกษาการเกิด ไมเซลล์ จากผลการทดลองที่ได้พบว่าสอดคล้องกับการจำลอง โมเลกุลคือ ที่ค่าอัตราส่วน LA/EG ที่เหมาะสมเท่านั้นที่สามารถเตรียมให้เกิดไมเซลล์ทรงกลมได้ และบล็อกโคพอลิเมอร์ที่มีอัตราส่วน LA/EG ที่สูงกว่าจะสามารถห่อหุ้ม โมเลกุลยาได้มากกว่า



สาขาวิชาเคมี

ปีการศึกษา 2555

ลายมือชื่อนักศึกษา _____

ลายมือชื่ออาจารย์ที่ปรึกษา _____

ลายมือชื่ออาจารย์ที่ปรึกษาร่วม _____

MANTANA CHANSUNA : TRIBLOCK COPOLYMER MICELLE AS A
MODEL FOR DRUG DELIVERY SYSTEM: MOLECULAR MODELING
AND EXPERIMENTAL STUDY. THESIS ADVISOR : ASST. PROF.
VISIT VAO-SOONGNERN, Ph.D. 180 PP.

TRIBLOCK COPOLYMER/MICELLE/MESOSCALE/MONTE
CARLO/POLYMER BRUSH/ NANOPARTICLE

The $PLA_x-PEG_y-PLA_x$ triblock copolymer micelle has gained attention in the field of drug delivery due to its excellent properties. To get the sufficient details of this triblock copolymer micelle all effective properties were considered. The PEO brush, model for corona part of micelle, was studied by a novel Monte Carlo (MC) of coarse-grained model on high coordination lattice. A PEO chain was mapped to a coarse-grained model which each bead represents series of linked vector connecting the CH_2CH_2 and CH_2O unit. The short and long-range interactions were based on the rotational isomeric state (RIS) and the Lennard-Jones (LJ) potential energy, respectively. The effects of grafting density, polydispersity and solvent quality on structure properties of polymer brushes were investigated. The results suggested that both polydispersity and grafting density were the major effects on the brush properties. The brush under poorer solvent was more compressed as clearly seen by brush density profile and bead distribution of grafted chains. Moreover, this MC method was also employed to simulate the structure aggregation of PEO nanoparticle as a model for the micelle core, under varying implicit solvent quality. The nanoparticle was denser packed themselves, increasing its density at the bulk region

and transforming to a nearly ellipsoid shape when the solvent quality was poorer. The distribution of middle beads was no significant effected by solvent quality, while the end beads distribution were strongly dependent. Bond orientations of chain in the nanoparticle were relatively random. Then, the aggregation behavior of triblock copolymer solution was simulated for molecular design. The ABA triblock copolymer (A = EO, B = PO) was investigated by MesoDyn. The effect of A/B block ratio, concentration and adding the third component on the morphology change were investigated. The results showed that the critical micelle concentration (cmc) and micelle formation rate were increased with increasing A/B block ratio. Introducing of hydrophobic drug and changing the strength of hydrophobicity part of the block copolymer were resulted in changing the shape of spherical micelle. Besides, PLA_x-PEG_y-PLA_x triblock copolymer micelle with varying LA/EG block ratio was simulated for molecular design before real synthesis. MesoDyn and DPD were used to gain more understanding about the phase aggregation, cmc and micelle formation rate. After that, the PLA_x-PEG_y-PLA_x triblock copolymers were experimentally prepared and characterized. The results were in a good agreement with simulation results that only the appropriated LA/EG block ratio could induce the formation of a spherical micelle. The block copolymer with higher LA/EG ratio could encapsulate more drug.

School of Chemistry

Academic Year 2012

Student's Signature_____

Advisor's Signature_____

Co-advisor's Signature_____

ACKNOWLEDGEMENTS

I would like to express my gratitude to all those who encouraged me and made it possible for me to complete this thesis.

I am thank to my thesis advisor, Asst. Prof. Dr. Visit Vao-soongnern, for his valuable advices, comments for my thesis and for kindness. I am also very thankful for thesis examining committee members for their efforts throughout the entire process. These include Assoc. Prof. Dr. Jatuporn Wittayakun, Assoc. Prof. Dr. Vinich Promarak, Asst. Prof. Dr. Siriporn Jungsuttiwong and Dr. Nuttaporn Pimpha. I thank all professors at School of Chemistry, Suranaree University of Technology (SUT) for their kind attitude and providing me valuable knowledge. The gratitude is for all lecturers at Department of Chemistry, Maharakham University (MSU) who gave me valuable advices and knowledge during my study for a bachelor's degree. I am thankful to all members in Laboratory of Computational and Applied Polymer Science (LCAPS), and all graduate students at School of Chemistry, SUT for their support and encouragement which made my study a fun time. I would like to thank to the NSDTA for Thailand Graduated Institute of Science and Technology (TGIST) financial support. Last, but certainly not least, it is my pleasure to thank my beloved family for their support, believe, and encouragement.

Mantana Chansuna

CONTENTS

	Page
ABSTRACT IN THAI.....	I
ABSTRACT IN ENGLISH.....	III
ACKNOWLEDGMENTS.....	V
CONTENTS.....	VI
LIST OF TABLES.....	XI
LIST OF FIGURES	XIII
LIST OF ABBREVIATIONS AND SYMBOLS.....	XX
CHAPTER	
I INTRODUCTION.....	1
II LITERATURE REVIEW.....	21
2.1 Polymer micelle as drug delivery system.....	21
2.2 Triblock copolymer micelle as drug carrier.....	22
2.3 PLA-PEG-PLA triblock copolymer micelle as drug carrier.....	23
2.4 Mesoscale scale simulation of triblock copolymer micelle.....	25
2.5 Monte Carlo simulation of polymer brush and nanoparticle.....	27
2.6 References.....	29
III MONTE CARLO SIMULATION OF POLYMER BRUSHES AND NANOPARTICLE: A MODEL FOR THE CORONA AND CORE PART OF MICELLE.....	36

CONTENTS (Continued)

	Page
3.1 Abstract.....	36
3.2 Background of Monte Carlo simulation for molecular system.....	38
3.2.1 Monte Carlo simulation of polymer model on a high coordination lattice.....	41
3.2.2 Coarse-grained polymer chain to rotational isomeric state.....	43
3.2.3 Further coarse graining of RIS chain on 2nd lattice.....	44
3.2.4 Conventional RIS formalism.....	46
3.2.5 RIS formalism for 2nd chain.....	48
3.2.6 Long-range interaction.....	51
3.2.7 Chain move.....	53
3.2.8 Applications of the method.....	54
3.3 PE brush melt.....	54
3.3.1 Simulation detail.....	57
3.3.2 Results and discussion.....	59
3.3.3 Summary.....	67
3.4 Monte Carlo simulation of PEO brush on 2nd lattice.....	67
3.4.1 PEO model.....	67
3.4.2 Hamiltonian.....	68
3.4.3 RIS parameters of PEO model from electronic structure calculation.....	70

CONTENTS (Continued)

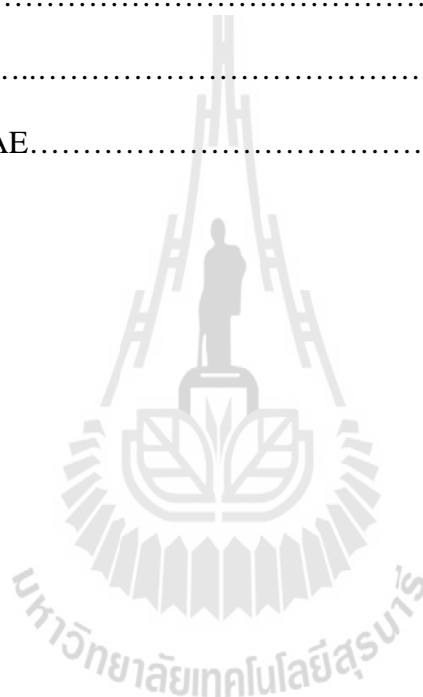
	Page
3.4.4 Long-range interaction of PEO model.....	72
3.4.5 The implicit model for solvent quality for PEO in solution.....	75
3.4.6 PEO chain move.....	77
3.5 PEO brush in melt and solvent state.....	79
3.5.1 Simulation detail.....	79
3.5.2 Results and discussion.....	79
3.5.3 Summary.....	96
3.6 PEO nanoparticle in solution.....	97
3.6.1 Simulation detail.....	97
3.6.2 Results and discussion.....	98
3.6.3 Summary.....	109
3.7 References.....	110
 IV MESOSCALE SIMULATION OF TRIBLOCK COPOLYMER	
MICELLE.....	116
4.1 Abstract.....	116
4.2 Introduction.....	117
4.3 Research methods.....	119
4.3.1 Mesoscopic Dynamics (Mesodyn).....	119
4.3.2 Dissipative Particle Dynamic (DPD).....	123

CONTENTS (Continued)

	Page
4.4 Mesoscale simulation result of ABA triblock copolymer model based on Pluronic [®] (PEO-PPO-PEO).....	124
4.4.1 Simulation detail.....	124
4.4.2 Results and discussion.....	126
4.4.3 Summary.....	134
4.5 Mesoscale simulation of PLA _x -PEG _y -PLA _x triblock copolymer.....	135
4.5.1 Simulation detail.....	135
4.5.2 Results and discussion.....	137
4.5.3 Summary.....	145
4.6 References.....	146
V POLYLACTIDE- POLYETHYLENE GLYCOL –POLYLACTIDE (PLA_x-PEG_y-PLA_x) TRIBLOCK COPOLYMER MICELLE.....	150
5.1 Abstract.....	150
5.2 Introduction.....	151
5.3 Materials and Methods.....	154
5.3.1 Materials.....	154
5.3.2 Analysis instrument.....	154
5.3.3 Research methods.....	155
5.4 Results and discussion.....	159
5.4.1 Triblock copolymer characterization.....	159

CONTENTS (Continued)

	Page
5.4.2 Triblock copolymer micelle characterization.....	163
5.5 Conclusions.....	171
5.6 References.....	172
VI CONCLUSIONS	177
CURRICULUM VITAE	180



LIST OF TABLES

Table	Page
3.1 Length of vectors connecting beads i and $i+2$ for coarse-grained PE model.....	51
3.2 Non-bonded energy parameters for coarse-grained PE model on 2nd lattice.....	53
3.3 Bidisperse PE brushes melts systems.....	58
3.4 Four states include the conformations on diamond lattice and lengths of segment connecting bead i and $i+2$ on the 2nd lattice.....	69
3.5 RIS model of PEO from <i>ab initio</i> calculation of DME model compound..	72
3.6 Non-bonded energy parameters for coarse-grained PEO model on 2nd lattice simulation.....	75
3.7 Investigated systems of PEO brush	80
3.8 The first three energies shell for the interaction of beads in the simulation.....	80
3.9 The average overall dimensions of PEO chains in nanoparticle and their standard deviations under each solvent quality.....	103
4.1 Designated Gaussian chain for ABA triblock copolymers.....	125
4.2 Interaction parameters for polymer, water and Haloperidol drug molecule.....	126

LIST OF TABLES (Continued)

Table	Page
4.3 Designated Gaussian chain for PLA _x -PEG _y -PLA _x triblock copolymers...	136
4.4 The interaction parameters for DPD.....	136
4.5 The interaction parameters for MesoDyn.....	136
4.6 The effect of polymer concentration on micelle size of LA _x -EG _y -LA _x triblock copolymer in term of end to end distance from DPD simulation..	141
4.7 The effect of drug content on micelle size of LA _x -EG _y -LA _x triblock copolymer in term of end to end distance from DPD simulation.....	143
5.1 Polymerization conditions used in the triblock copolymer synthesis.....	156
5.2 Characteristic of PLA _x -PEG _y -PLA _x triblock copolymers.....	163
5.3 Light scattering results for PLA _x -PEG _y -PLA _x in water at 298 K.....	168
5.4 Summarization of the PLA _x -PEG _y -PLA _x triblock copolymer properties...	171

LIST OF FIGURES

Figure	Page
1.1 Representation types of pharmaceutical carriers.....	3
1.2 The aggregation structures formed by block copolymers in solution.....	4
3.1 Model to represent the block copolymer micelle.....	37
3.2 Elementary moves based on Verdier-Stockmayer type model.....	42
3.3 Collective moves, reptative move, end-bridge move and concerted rotation.....	43
3.4 The mapping of a real chain into lattice.....	45
3.5 The 2nd lattice.....	46
3.6 The rotational states of a linear chain and corresponding statistical weights independent bond and interdependent bond.....	48
3.7 The coarse-grained of n-heptane with 4 rotors to a single rotor in 2nd lattice.....	50
3.8 Lennard-Jones potential energy as a function of distance.....	52
3.9 Evaluation the equilibrium by the mean-square displacement of the center-of-mass, $g_{cm}(t)$ and by the orientation autocorrelation functions (OACFS) as the end-to-end vector of the linear chain.....	60
3.10 Density profiles of bidisperse PE brush at fix long chain length.....	61
3.11 Density profiles of bidisperse PE brush at fix short chain length.....	61

LIST OF FIGURES (Continued)

Figure	Page
3.12 Average position of the i th monomer of each chain in bidisperse PE at fix long chain length.....	62
3.13 Average position of the i th monomer of each chain in bidisperse PE at fix short chain length.....	63
3.14 Plot of the projection $\langle \cos\theta_i \rangle$ of the local orientation chord vector versus the position of the i th bond along the chain of each chain in bidisperse PE at fix long chain length.....	64
3.15 Plot of the projection $\langle \cos\theta_i \rangle$ of the local orientation chord vector versus the position of the i th bond along the chain of each chain in bidisperse PE at fix short chain length.....	64
3.16 End bead distribution of each chain in bidisperse PE at fix long chain length.....	66
3.17 End bead distribution of each chain in bidisperse PE at fix short chain length.....	66
3.18 Comparison mean square radius of gyration $\langle R_g^2 \rangle$ of a single isolated PEO chain as a function of the numerical value of k and 100 coarse-grained PEO beads.....	77
3.19 Evaluation the equilibrium by the mean-square displacement of the center-of-mass, $g_{cm}(t)$ and by the orientation autocorrelation functions (OACFS) as the end-to-end vector of the linear chain.....	82

LIST OF FIGURES (Continued)

Figure	Page
3.20 Local density profile ($\rho(z)$) as a function of distance from solid interface of monodisperse PEO brush.....	82
3.21 The normalized mean height $\zeta(s)$ as a function of normalized bead coordinate along chain contour of monodisperse PEO brush.....	83
3.22 Bond orientation of i th monomer $\langle \cos\theta_i \rangle$ as a function of the position of the i th bond along the chain of monodisperse PEO brush.....	84
3.23 The middle ($\rho_m(z)$) and end ($\rho_E(z)$) bead distribution as a function of Z of monodisperse PEO brush.....	85
3.24 Local density profile ($\rho(z)$) as a function of distance from solid interface of PEO brush under different solvent.....	87
3.25 The normalized mean height $\zeta(s)$ as a function of normalized bead coordinate along chain contour of PEO brush under different solvent.....	87
3.26 The orientation of each i th monomer $\langle \cos\theta_i \rangle$ as a function of the position of the i th bond along the chain of PEO brush under different solvent.....	88
3.27 The middle ($\rho_m(z)$) and end ($\rho_E(z)$) bead distribution as a function of Z of PEO brush under different solvent.....	89
3.28 Local density profiles for mono- (B40n160) and bidisperse PEO brush (B30n80+B50n80) under solvent quality.....	91

LIST OF FIGURES (Continued)

Figure	Page
3.29 Local density profiles of bidisperse PEO brush under different solvent quality.....	94
3.30 The normalized mean height $\zeta(s)$ as a function of normalized bead coordinate of bidisperse PEO brush under different solvent quality.....	94
3.31 The orientation of each monomer $\langle \cos\theta_i \rangle$ as a function of the position of the i th bond along the chain of bidisperse PEO brush under different solvent quality.....	95
3.32 The end bead distribution ($\rho_E(z)$) as a function of z of bidisperse PEO brush under different solvent quality.....	95
3.33 The middle bead distribution ($\rho_m(z)$) as a function of z of bidisperse PEO brush under different solvent quality.....	96
3.34 The method to generate a new cohesive polymer structure from bulk (3D) \rightarrow thin film (2D) \rightarrow nanofiber (1D) \rightarrow nanoparticle (0D).....	98
3.35 The nanoparticle of 36 coarse-grained chains of $-(\text{CH}_2\text{CH}_2\text{O})_{33}-$ under difference solvent quality in (A) vertical and (B) horizontal direction.....	99
3.36 Radial density profiles as a function of distance from the center of mass of the nanoparticle in different solvent quality in poor region.....	100
3.37 The normalized radial density profiles for middle and end beads of the nanoparticles.....	102

LIST OF FIGURES (Continued)

Figure	Page
3.38 The center of mass distribution as a function of the displacement from the center of the nanoparticle.....	104
3.39 The ellipsoid shape defined by the principal components $L_1 > L_2 > L_3$ for the nanoparticle model.....	105
3.40 The change in the principal moment of the chains (normalized by R_g^2) as a function of the distance from the center of the nanoparticle.....	105
3.41 The change in chain shape (asphericity and acylindricity) as a function of the distance from the center of the nanoparticles.....	106
3.42 The orientation of chords (mid-, end- and all) as a function of the displacement from the center of the nanoparticle.....	108
3.43 The orientation of the largest and smallest principal moment to the reference vector connecting the center of particle to the center of each PEO chain in the nanoparticle.....	109
4.1 Phase morphology in aqueous solution at 298 K for $A_8B_8A_8$, $A_6B_{12}A_6$ and $A_4B_{16}A_4$	129
4.2 The isosurface of A and B species and the density slices for 12% v. of $A_4B_{16}A_4$ in aqueous solution at 298 K.....	130
4.3 The isosurface of B part and the order parameter plot simulation time step in aqueous solution at 298 K for 24% v. of $A_6B_{12}A_6$ and 12% v. of $A_4B_{16}A_4$	130

LIST OF FIGURES (Continued)

Figure	Page
4.4 The order parameter versus the simulation time for 12% v. of $A_4B_{16}A_4$ in water.....	131
4.5 Sketch morphology for 12% v. of $A_4B_{16}A_4$ in aqueous solution at 298 K.	132
4.6 Time evolution for 12% v. of $A_4B_{16}A_4$ in aqueous solution at 298 K.....	132
4.7 The isosurface of the hydrophobic part for 12% v. of $A_4B_{16}A_4$ and $A_4C_{16}A_4$	134
4.8 Phase morphology in aqueous solution at 298 K for $LA_4EG_5LA_4$, $LA_8EG_5LA_8$ and $LA_{12}EG_5LA_{12}$	139
4.9 The isosurface of LA and EG species in the spherical micelle for 8% v. of $LA_8B_5A_8$ in aqueous solution.....	139
4.10 Section view of one spherical micelle for 8% v. of $LA_8B_5LA_8$	140
4.11 Snapshot of spherical micelle for 8% v. of $LA_8EG_5LA_8$ and $LA_{12}EG_5LA_{12}$ in aqueous solution.....	142
4.12 The size of micelle as a function of polymer concentration in water.....	142
4.13 Aggregation morphologies for 8 % v. of $LA_8EG_5LA_8$ at various drug contents.....	144
4.14 The size of micelle as a function of drug concentration in aqueous solution.....	144
5.1 Molecular structure of polyethylene oxide - polypropylene oxide - polyethylene oxide (PEO-PPO-PEO) triblock copolymer.....	152

LIST OF FIGURES (Continued)

Figure	Page
5.2 Gel permeation chromatogram of PLA _x -PEG _y -PLA _x triblock copolymer	159
5.3 Chemical structure of PLA _x -PEG _y -PLA _x triblock copolymer.....	160
5.4 The ¹ H NMR spectra of TB1, TB2 and TB3 in CDCl ₃ at 298 K.....	161
5.5 Pyrene excitation spectra (at emission wavelength 390 nm) as a function of polymer concentration of TB1, TB2 and TB3.....	165
5.6 Plots of the intensity ratio I ₃₃₆ /I ₃₃₄ versus log c for TB2 and TB3.....	166
5.7 Relaxation spectra $A(\tau, k)$ spectra $A(\tau, k)$ at $\theta = 90^\circ$ for 0.01 g/L of TB2 (---) and TB3 (—).....	167
5.8 Hydrodynamic radius (R_H) plotted against the triblock copolymer concentration of TB2 and TB3.....	167
5.9 Static light scattering results for TB2 and TB3 in aqueous solutions.....	168
5.10 Plot of $[Py]_m/[Py]_w$ versus concentration of TB2 and TB3.....	171

LIST OF ABBREVIATIONS AND SYMBOLS

a_{meso}	=	Coarse-grained chain length
$A(\tau, k)$	=	Relaxation spectra
B	=	Bead number
cmc	=	Critical micelle concentration
D	=	Dimension
DDSs	=	Drug delivery systems
DPD	=	Dissipative particle dynamics
E	=	Potential energy
EG	=	Ethylene glycol
$E\sigma, E\omega$	=	The first-, second-order short-range interaction energies
f	=	Mayer f -function
F	=	Force
$g(g+, g-)$	=	Gauche (gauche plus, gauche minus)
g_{cm}	=	The center-of-mass
GPC	=	Gel permeation chromatography
k	=	Quality of solvent
k_B, k	=	Boltzmann constant ($\sim 1.38 \times 10^{-23} \text{ J K}^{-1}$)
K_v	=	The equilibrium partition coefficient
L	=	Principal axis
LJ	=	The Lennard-Jones potential
LS	=	Light scattering

LIST OF ABBREVIATIONS AND SYMBOLS (Continued)

LA	=	Lactide
MC	=	Monte Carlo
MCS	=	Monte Carlo step
MesoDyn	=	Mesosopic dynamics
Mn	=	Number average molecular weight
n	=	Number of site in 2nd
nm	=	Nanometer
NMR	=	Nuclear Magnetic Resonance
N_{meso}	=	Coarse-grained bead number
OACFS	=	Orientation autocorrelation functions
PE	=	Polyethylene
PEG	=	Polyethylene glycol
PEO	=	Polyethylene oxide
PLA	=	Poly lactide/polylactic acid
PPO	=	Polypropylene oxide
[Py]	=	Pyrene concentration
ROP	=	Ring opening polymerization
R_H	=	Hydrodynamic radius
R_g^2	=	Mean-square radius of gyration
S	=	Chord order parameter
t	=	Trans

LIST OF ABBREVIATIONS AND SYMBOLS (Continued)

T	=	Temperature
u	=	Statistical weight
U	=	Statistical weight matrix
Z	=	Partition function
2nd/ SNND	=	Second-nearest neighbor diamond
ϕ	=	Unperturbed state
Φ	=	Torsion angle
σ	=	(1) Zero point of Lennard-Jones potential, (2) Grafting density
δ_t	=	Time step of simulation
θ	=	(1) Bond angle, (2) Angle between chords
ε	=	Depth of the potential well
$v^{-1}\varepsilon_{ij}$	=	Interaction between beads in MesoDyn
ρ	=	Probability
$\rho(z)$	=	Density profile
ρ^o	=	Collective concentration field
$\langle \dots \rangle$	=	Ensemble average
ψ	=	Angle between the main axes of two chains
χ	=	Flory-Huggins interaction parameter
τ	=	Relaxation time
ζ	=	Rotational state
$\zeta(s)$	=	The normalized mean height

CHAPTER I

INTRODUCTION

The earliest pharmaceuticals have consisted of simple and fast-releasing chemical compounds that are dispensed oral, nasal, pulmonary, and ocular or as rectal administration (Khafagy *et al.*, 2007; Lang, 1995) which are usually exhibit specific problem. For examples, the partial degradation of drug is limit or may reduce the specifically affects a disease's pathway and potencies before they reach target in the body (Alekha *et al.*, 1998; Zimmer and Kreuter, 1995). Moreover, time-release medications deliver treatment continuously, rather than providing relief of symptoms (Huang and Brazel, 2001). Most problems are particularly dangerous to rapidly check for serious diseases or even to target cells that are relatively subtle. To gain the most effective therapy, understanding of the human body and the development of new and potential treatments are necessary. The pharmaceutical and science research are interest not only development of new curing method (Ding, 1998; Kearney, 1996; Koo *et al.*, 2005; Rothen-Weinhold *et al.*, 2000) but also mechanisms (Pettrak, 2005; Zignani *et al.*, 1995) to administrate them. Recently, drug delivery systems (DDSs) is using to solve pharmaceutical therapy problem based on the idea that the drug is released at the right site, in the right dose and for the required time without any side effect (Mishra *et al.*, 2010; Whittlesey and Shea, 2004). Biocompatible or biodegradable properties are required for especial for implantable drug delivery

systems (IDDS). The products from fragment must be eliminated harmlessly from the body (Kumari *et al.*, 2010; Nair and Laurencin, 2007; Winzenburg *et al.*, 2004). The success of pharmaceutical therapy by DDS is largely dependent on the delivery carrier and controlled release system. For examples, viruses fulfilled the first requirement as carrier, but their use in humans raised concerns over their safety (Lehn *et al.*, 1998; Manchester and Singh, 2006; Russell and Peng, 2007). Therefore, another carrier type will be further developed. In the past two decade, polymers have been most widely used as DDS to be effective in improving treatment absorption rates, providing protection for pharmaceuticals against biochemical degradation and also non toxicity carrier (Pillai and Panchagnula, 2001). A polymer is useful in solving drug delivery problems due to several properties. For examples, it can be designed to be more solubility, stability, permeability material thus affecting drug delivery (Chandra and Rustgi, 1998; Pillai and Panchagnula, 2001). After the present, modern research is interested at investigating biodegradable polymer (Jeong *et al.*, 1999; Tharanathan, 2003). Due to this polymer type can be easy degraded through hydrolysis reaction. The degradation process involves the breakdown of polymers into acid form which are eventually reduced by the Krebs's cycle to carbon dioxide and water. Both of natural and synthetic biodegradable polymers have been considered. Research in biodegradable systems originally concerned on natural polymers and has moved into the synthetic polymer later. Many natural polymers have the advantage of high biocompatibility and less immunogenicity, while synthetic polymers provide the most important ways for research which can be designed. Moreover, to obtain added advantage as carrier material some of composites of have been considered (Cascone *et al.*, 1995). There are several key factors to design more highly degradable polymers

such as polymer structure, architecture, radiation and chemical treatments and molecular weight (Amass *et al.*, 1998; Gunatillake *et al.*, 2003; Martina and Hutmacher, 2007). The desired polymer may be a hydrophilic, amorphous or low molecular weight polymer. Therefore, varying each of these factors in synthetic process should allow adjusting the rate of polymer degradation that subsequent control the rate of drug delivery.

Various polymer carriers, such as micro/nanospheres, micelles, liposomes, dendrimers, hydrogels or liquid crystals have been shown great capability in DDS. The sketch morphology of them was illustrated in Figure 1.1. The goal of developing these formulations is to obtain systems with the most efficiency therapy and the lowest toxicity. Nowadays, nanoscopic drug carriers evade recognition and uptake by mononuclear phagocyte system (MPS) (Ganta *et al.*, 2008; Sung *et al.*, 2007).

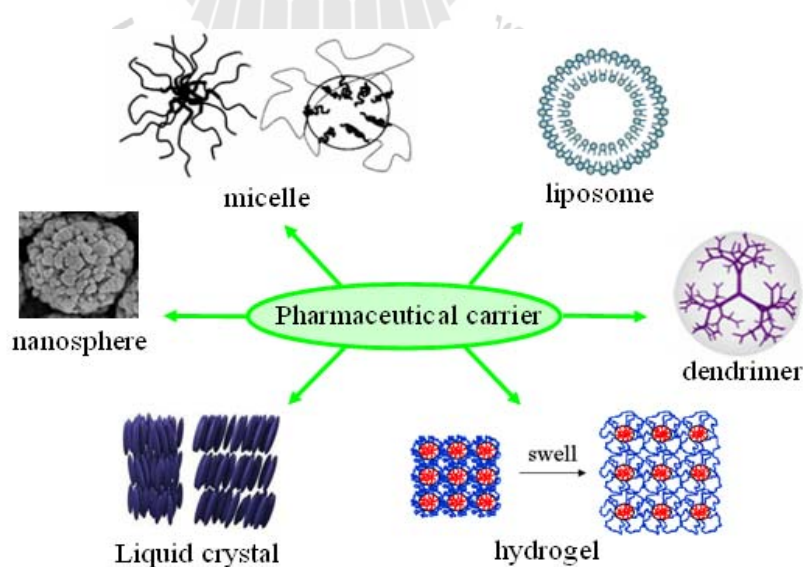


Figure 1.1 Representation types of pharmaceutical carriers.

Among nanoscopic carriers, polymer micelles with advances in the chemistry of amphiphilic, biocompatible and biodegradable polymer have been interested for effective drug deliver application due to their performance to self-organize at nanoscales in appropriate condition (Cho *et al.*, 2010; Gaucher *et al.*, 2005; Torchilin, 2007). Especially, their self-assembled in solution states have already been shown to be useful for many applications in gene therapy, nanotechnology and drug delivery. At appropriate solvent quality, which is good for one block but poor for other, the aggregation process of polymer micelle is taking place. The concentration at which first spherical micelle is appearing define as the critical micelle concentration (cmc).

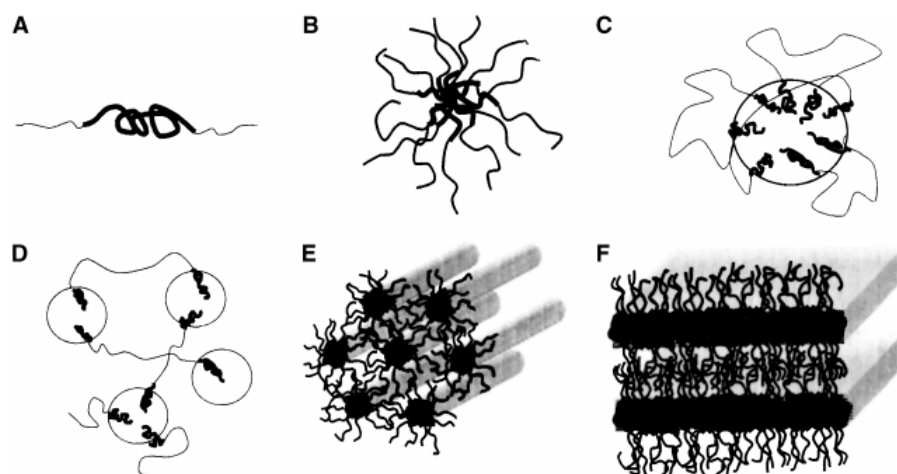


Figure 1.2 The aggregation structures formed by block copolymers in solution: (A) copolymer unimer, (B) spherical micelle in a solvent selective for the end-blocks, (C) spherical micelle in a solvent selective for the middle block, (D) network formation in solvent selective for the middle block, (E) hexagonal arrangement of cylindrical micelles, and (F) lamellar structure (Loh, 2002).

As present in Figure 1.2, the individual polymer form molecular solutions at concentration below than cmc. The aggregation of unimer molecules to form spherical micelle is occurring when the concentration reaches their cmc, this process is called 'micellization'. After that, another micelle structures are forming with increasing polymer concentration (Nakashima and Bahadur, 2006). The morphology of micelles can be spherical, rod-like and lamellar or another depends on their hydrophilicity, concentration and environmental surrounding as show in Figure 1.2. The spherical micelle play attractive role as carrier material. The hydrophilic corona part will be help protecting the micelle cores from chemical attack by the aqueous medium in which they must travel by formed hydrogen bonds with the aqueous surroundings and form a tight shell around the hydrophobic core.

Several of experimental techniques are used to characterize block copolymer micelle in solution in difference aspect *i.e.* the structure of the micelle as well as influence of micellization on solution properties. It has to be revealed that different methods give different kinds of information for the system under observe behavior. For examples, fluorescence probe technique is used to study micellization (Aguiar *et al.*, 2003), scattering technique is used to determine micelle dimensions and intra-micelle structure (Chu and Liu, 2000), transmission electron microscopy is used to image micelle structure (Won *et al.*, 2002).

Initially, most block copolymer micelle-based delivery systems studied are focus on polyethylene oxide - polypropylene oxide - polyethylene oxide triblock copolymer (PEO-PPO-PEO) (Batrakova and Kabanov, 2008; Kabanov *et al.*, 2002). Due to their specially properties, the micellization and aggregation behavior of pure and multicomponent in aqueous solutions and their application as drug delivery

carriers have been much consider (Alexandridis *et al.*, 1994; Mata *et al.*, 2004; Rapoport, 2004). The phase behaviors of Pluronic[®] micelle are effective by their concentration, polymer composition and surrounding environment such as temperature, salt and drug molecule. Due to achievement in use Pluronic[®] micelle as drug carrier, another block copolymer has been attention.

A vast majority of biodegradable polymer that was studied belongs to the polyester family. Biodegradable polyester was attractive in medical application because its degradation product nontoxic final product. Recent studied suggested that only lactic acid degrades to carbon dioxide and water which can be removed from the body via the respiratory system. Causing polylactide or polylactic acid (PLA) has proven to be the most attractive and useful class of biodegradable polyesters (Södergård and Stolt, 2002). The block copolymers made of PLA and PEG has evoked considerable interest as biodegradable drug carriers. PEG is a polymer of ethylene oxide which is the form of relatively low molecular weight. It is generally considered to be inert and possess a low order of toxicity in animals and humans. In addition, it has been widely investigated and often shows extended circulation through modification with other polymer (Gref *et al.*, 1995; Xiao *et al.*, 2010). The triblock copolymer of PLA and PEG can be synthesized as designed properties by varying chemical composition, molecular weight and block ratio, which allows control micelle properties in applications. Due to the perfect combination of these block copolymer, it has been intensively investigated in numerous medical and pharmaceutical applications *i.e.* sustained drug delivery systems, implants for orthopedic devices and absorbable fibers (He *et al.*, 2007; Ruan and Feng, 2003). With an amphiphilic polymer, their micelle is form self-assemble in selective solvent. The PLA part is

form the hydrophobic core of the micelles, while the PEG shell is form a dynamic molecular shield over the surface that provides interactions with the solvent and makes the nanoparticles can be stable in the medium. The hydrophobic drugs can be physically entrapped in the micelle core which can evade the immune system and circulate for longer periods of time after administrate without any takeover. Causing these structures is great interest for hydrophobic drug delivery applications. The polymer aggregation is effect by changing in polymer concentration, composition and surrounding environment. The efficient application of polymer micelles as drug carriers is considered by the loading capacity, size, circulation time, stability, release kinetics and biodistribution. The experiment is give many information about the aggregation, except for kinetic process of self-assembly of micelle is still not fully understood. Moreover, to develop new materials with designed new properties, it is essential to predict before preparation, characterization and further material processing. To solving problem as mention above, molecular modeling and simulation are necessary for the problem which is the limitation of experiment.

Molecular modeling and simulation combine methods that cover a range of size scales is use in order to give sufficiency information of material systems. Atomistic modeling is used to obtain thermodynamic information of the system. In any case for applications the degree of detail provided in which simulations may be unnecessary. Many important properties of polymers that involve large distance or time scales, for example, microphase separation in copolymers is exceed by fully atomistic simulations. So, another simulation technique in the use of so-called 'coarse grain' continuous space based on the bead-spring model of polymer have been developed (Clarke, 1998). There are various simulation method based coarse-

grained molecular models. A mesoscopic simulation technique provide a powerful approach to predict mesoscopic phenomena and kinetic process of complex fluids and soft materials *i.e.* surfactants, emulsions, colloids, block copolymers, and polymer blends (Fermeglia and Pricl, 2007). The models form a bridge between fast molecular kinetics and slow thermodynamic relaxation of macroscale properties. They treat the real polymer chains of a coarse-grained level by grouping atoms together up to the persistence length of polymer chain, which can be extended to length and time scales by several orders of magnitude as compared to all-atomistic simulations. So, mesoscopic regions of fluid material that show similar chemical properties are represented by fundamental particles called “beads”. Contrary to atomistic model, these particles do not have atomic properties since all degrees of freedom smaller than a bead radius are assumed to have been integrated out. Thus, coarse-grained interactions between beads are calculated, and all atomic details are lost. To model specify chemical nature of the system in mesoscopic simulation, there are two sets of parameters have to be defined (Lam *et al.*, 2004). The first parameter is Gaussian chain architecture that depends on the degree of coarsening of the original system. The second parameter is the interaction energy between the different chemical components, which also captures the hydrophilicity and hydrophobicity of the components. The interaction energy may obtain from atomistic simulation, empirical methods or experimental data. The Mesodyn method is based on idea that the free energy of an inhomogeneous liquid is a functional of the local density function. From the free energy, all thermodynamic functions can be derived. It has gained wide respect in literature and commercial circles with scientifically astute algorithms aimed at elucidating important mesoscale structure and kinetics *i.e.* polymer, polymer blend

and copolymer in pure and multicomponent system (Guo *et al.*, 2007; Jawalkar and Aminabhavi, 2006; Lam and Goldbeck-Wood, 2003). Another method developed for the simulation of complex fluids is DPD. It was introduced by Hoogerbrugge and Koelman for hydrodynamic simulation method (Hoogerbrugge and Koelman, 1992). This technique is based on the simulation of soft spheres, whose motion is governed by certain collision rules. By introducing bead-and-spring type particles, polymers can be simulated. The simulations are performed on a collection of particles interacting with Newton's equations of motion. There are three contributions to the overall force acting on the i th particle. These short-range inter-particle forces are a repulsive conservative force, a dissipative force and random force acting symmetrically between every pair of particles i and j . Applications of DPD to polymer problems are single-chain melt dynamics, polymer composites, copolymer microphase separation, binary blend compatibility and phase behavior of polymer solutions. In addition, mesoscopic simulation method is provide insight into the mechanism of mesoscopic structures, and also serve as a complement to experiments and more efficiently guide the experimental preparation with desired properties (Guo *et al.*, 2007).

There are another micelle-like polymer structures which considering in industrially application *i.e.* tethered chain. Tethered polymer is systems in which one or both ends of the chain are constrained in their motion because they are attached to a dimensional surface. This surface could be a point or small central core as in the case of a many-arm star polymer, a line as in the case of a comb polymer, or a flat surface as in the case of a polymer brush. Nowadays, tethered polymer is model system for many practical polymer systems such as block copolymers at fluid-fluid interfaces and polymer micelles due to there are similarly structure. Polymer brush or grafted-

polymer is a tethered polymer type which considers in many applications such as colloidal stabilization, lubrication and medical industry. Besides preparation, the determination of physical properties of the tethered polymer layer, such as the thickness and density distribution, is challenging as well. Numerous experimental methods to prepare and characterize polymer brush including neutron scattering and reflectivity, surface force apparatus, ellipsometry and atomic force microscopy. However, the experiments in the field of polymer brushes with well characterized systems lag behind the theoretical developments by several years. In the past decade several theoretical brush models of varying complexity have been presented in the literature. The approaches include scaling theories, analytical models, numerical statistical models and molecular modeling. Variation of parameters such as the grafting density, solvent quality and adsorption strength to the grafting plane results in a large variety of predicted behavior of polymer brushes. The theoretical approach have been particular important in picture our understanding of both static and dynamic properties of star polymers. Molecular modeling has been used to analyze desired physical properties of the system which may not perform by experiment. Monte Carlo (MC) simulations may provide an alternative choice for the dynamical simulation of realistic polymers. MC can argue faster motions only serve as the heat bath for the slower motions which make the torsion dynamics a category of random motion without memory of its past history. Thus, this slower motion can be modeled by a Markovian master equation, which virtually opens the door for the dynamic simulation of realistic polymers via MC algorithms. The dynamic MC itself is usually built upon stochastic nature of moves according to the Metropolis criterion, naturally containing the detailed balance principle. As a result, including the bond stretching

and bending into MC algorithms is no longer necessary, which greatly saves computing time. Furthermore, excluding bond stretching and bending results in fixed bond length and bond angle, which, combined with the symmetrical torsion angle of many realistic polymers, enables a lattice MC algorithm to use the fast integer computation. The elemental moves of MC can be very flexible for the sake of computing speed. A new MC simulation was introduced to study amorphous polymer. The model incorporates the rotational isomeric state (RIS) theory that gives the molecular detail depending on the level of coarse-graining and long-range interaction, which is essential to describe the cohesive properties of the system. The second-nearest neighbor diamond (2nd) lattice in combination with the short- and long-range interactions is used to simulate high molecular weight polymers at their bulk density. The simulation method has been validated in previous studies on polymer nanofibers (Vao-soongnern and Mattice, 2000a, b) and nanoparticles (Vao-soongnern *et al.*, 2001) producing reasonable static and dynamic properties with good agreement with theoretical observations.

Research objectives

Firstly, the 2nd lattice MC simulation in comparison with theory was employed to study structure and conformation properties of PEO brush and nanoparticle. Secondly, the micellization and aggregation behavior of amphiphilic triblock copolymer micelle were investigated by both experiment and molecular modeling. Lastly, the effect of LA/EG block ratio on pyrene drug model encapsulation efficiency was studied.

Scope and limitations

To gain more understanding about the polymer structure dependent properties at the mesoscopic level of triblock copolymer, the triblock copolymer solution system was simulated and data was tendency compared with experiment. The considered data were micellization and aggregation behavior of polymer. The interested factors *i.e.* LA/EG block ratio, concentration and hydrophobic drug effect. Moreover, this research was applied Monte Carlo techniques to study PEO brush and nanoparticle. This system were assumed as flexible PEG corona of micelle which was affected by surrounding environment *i.e.* solvent quality, polydispersity and grafting density.

Triblock copolymer synthesis

Triblock copolymer of PLA and PEG was synthesized by ring opening polymerization (ROP) of lactide monomer. The triblock copolymers were synthesized with different LA/EG block ratio at fixed EG block length.

Triblock copolymer and triblock copolymer micelle characterization

- Nuclear Magnetic Resonance (NMR) Spectroscopy was applied to characterize copolymer composition.
- Gel Permeation Chromatography (GPC) was employed to investigate polydispersity of block copolymer.
- Fluorescence Spectroscopy was used to determine critical micelle concentration (cmc) of block copolymer by pyrene-probe method.
- Light scattering (LS) was used to study size of polymer micelle.

Computational simulation

The simulation techniques were employed to study the aggregation behavior and micellization of triblock copolymer solution *i.e.* $PLA_x-PEG_y-PLA_x$ triblock copolymer in aqueous solution and also polymer brush. The techniques that are employed in this work include:

- **Mesosopic simulation**

Mesosopic simulation method *i.e.* Dissipative Particle Dynamics (DPD) and Mesoscopic Dynamics (MesoDyn) were used to study the effect of concentration, block ratio and third component addition on aggregation behavior of the amphiphilic triblock copolymer in aqueous solution.

- **Monte Carlo simulation**

A 2nd lattice based MC, which was developed by Vao-soongnern for coarse-grained model, was applied to study polymer brushes and nanoparticle. The systems used in this section were composed of mono- and bidisperse system with varying grafting density and solvent quality.

References

- Aguiar, J., Carpena, P., Molina-Bolívar, J. A. and Carnero Ruiz, C. (2003). On the determination of the critical micelle concentration by the pyrene 1:3 ratio method. **Journal of Colloid and Interface Science** 258(1): 116-122.
- Alekha, K., Dash, C., Greggery, C. and Cudworth, I. (1998). Therapeutic applications of implantable drug delivery systems. **Journal of Pharmacological and Toxicological Methods** 40(1): 1-12.
- Alexandridis, P., Holzwarth, J. F. and Hatton, T. A. (1994). Micellization of poly(ethylene oxide)-poly(propylene oxide)-poly(ethylene oxide) triblock copolymers in aqueous solutions: thermodynamics of copolymer association. **Macromolecules** 27(9): 2414-2425.
- Amass, W., Amass, A. and Tighe, B. (1998). A review of biodegradable polymers: uses, current developments in the synthesis and characterization of biodegradable polyesters, blends of biodegradable polymers and recent advances in biodegradation studies. **Polymer International** 47(2): 89-144.
- Batrakova, E. V. and Kabanov, A. V. (2008). Pluronic block copolymers: evolution of drug delivery concept from inert nanocarriers to biological response modifiers. **Journal of Controlled Release** 130(2): 98-106.
- Cascone, M. G., Sim, B. and Sandra, D. (1995). Blends of synthetic and natural polymers as drug delivery systems for growth hormone. **Biomaterials** 16(7): 569-574.
- Chandra, R. and Rustgi, R. (1998). Biodegradable polymers **Progress in Polymer Science** 23(7): 1273-1335.

- Cho, H., Cheong, I., Lee, J. and Kim, J. (2010). Polymeric nanoparticles, micelles and polymersomes from amphiphilic block copolymer. **Korean Journal of Chemical Engineering** 27(3): 731-740.
- Chu, B. and Liu, T. (2000). Characterization of nanoparticles by scattering techniques. **Journal of Nanoparticle Research** 2(1): 29-41.
- Clarke, J. H. R. (1998). Molecular modelling of polymers. **Current Opinion in Solid State and Materials Science** 3(6): 596-599.
- Ding, S. (1998). Recent developments in ophthalmic drug delivery. **Pharmaceutical Science & Technology Today** 1(8): 328-335.
- Fermeglia, M. and Priol, S. (2007). Multiscale modeling for polymer systems of industrial interest. **Progress in Organic Coatings** 58(2): 187-199.
- Ganta, S., Devalapally, H., Shahiwala, A. and Amiji, M. (2008). A review of stimuli-responsive nanocarriers for drug and gene delivery. **Journal of Controlled Release** 126(3): 187-204.
- Gaucher, G., Dufresne, M.-H., Sant, V. P., Kang, N., Maysinger, D. and Leroux, J.-C. (2005). Block copolymer micelles: preparation, characterization and application in drug delivery. **Journal of Controlled Release** 109(1-3): 169-188.
- Gref, R., Domb, A., Quellec, P., Blunk, T., Müller, R. H., Verbavatz, J. M. and Langer, R. (1995). The controlled intravenous delivery of drugs using PEG-coated sterically stabilized nanospheres. **Advanced Drug Delivery Reviews** 16(2): 215-233.

- Gunatillake, P. A., Martin, D. J., Meijs, G. F., Mc Carthy, S. J. and Adhikari, R. (2003). Designing biostable polyurethane elastomers for biomedical implants. **ChemInform** 56(6): 545-557.
- Guo, X. D., Zhang, L., Qian, Y. and Zhou, J. (2007). Effect of composition on the formation of poly(dl-lactide) microspheres for drug delivery systems: mesoscale simulations. **Chemical Engineering Journal** 131(1): 195-201.
- He, G., Ma, L. L., Pan, J. and Venkatraman, S. (2007). ABA and BAB type triblock copolymers of PEG and PLA: a comparative study of drug release properties and “stealth” particle characteristics. **International Journal of Pharmaceutics** 334(1): 48-55.
- Hoogerbrugge, P. J. and Koelman, J. M. V. A. (1992). Simulating microscopic hydrodynamic phenomena with dissipative particle dynamics. **EPL (Europhysics Letters)** 19(3): 155-161.
- Huang, X. and Brazel, C. S. (2001). On the importance and mechanisms of burst release in matrix-controlled drug delivery systems. **Journal of Controlled Release** 73(2): 121-136.
- Jawalkar, S. S. and Aminabhavi, T. M. (2006). Molecular modeling simulations and thermodynamic approaches to investigate compatibility/incompatibility of poly(l-lactide) and poly(vinyl alcohol) blends. **Polymer** 47(23): 8061-8071.
- Jeong, B., Choi, Y. K., Bae, Y. H., Zentner, G. and Kim, S. W. (1999). New biodegradable polymers for injectable drug delivery systems. **Journal of Controlled Release** 62(1): 109-114.

- Kabanov, A. V., Batrakova, E. V. and Alakhov, V. Y. (2002). Pluronic[®] block copolymers as novel polymer therapeutics for drug and gene delivery. **Journal of Controlled Release** 82(2): 189-212.
- Kearney, A. S. (1996). Prodrugs and targeted drug delivery. **Advanced Drug Delivery Reviews** 19(2): 225-239.
- Khafagy, E.-S., Morishita, M., Onuki, Y. and Takayama, K. (2007). Current challenges in non-invasive insulin delivery systems: A comparative review. **Advanced Drug Delivery Reviews** 59(15): 1521-1546.
- Koo, O. M., Rubinstein, I. and Onyuksel, H. (2005). Role of nanotechnology in targeted drug delivery and imaging: a concise review. **Nanomedicine: Nanotechnology, Biology and Medicine** 1(3): 193-212.
- Kumari, A., Yadav, S. K. and Yadav, S. C. (2010). Biodegradable polymeric nanoparticles based drug delivery systems. **Colloids and Surfaces B: Biointerfaces** 75(1): 1-18.
- Lam, Y.-M. and Goldbeck-Wood, G. (2003). Mesoscale simulation of block copolymers in aqueous solution: parameterisation, micelle growth kinetics and the effect of temperature and concentration morphology. **Polymer** 44(12): 3593-3605.
- Lam, Y.-M., Goldbeck-Wood, G. and Boothroyd, C. (2004). Mesoscale simulation and cryo-TEM of nanoscale drug delivery systems. **Molecular Simulation** 30(4): 239-247.
- Lang, J. C. (1995). Ocular drug delivery conventional ocular formulations. **Advanced Drug Delivery Reviews** 16(1): 39-43.

- Lehn, P., Fabrega, S., Oudrhiri, N. and Navarro, J. (1998). Gene delivery systems: Bridging the gap between recombinant viruses and artificial vectors. **Advanced Drug Delivery Reviews** 30(1): 5-11.
- Loh, W. (2002). Block copolymer micelles. **Encyclopedia of Surface and Colloid Science**: 802-813.
- Manchester, M. and Singh, P. (2006). Virus-based nanoparticles (VNPs): platform technologies for diagnostic imaging. **Advanced Drug Delivery Reviews** 58(14): 1505-1522.
- Martina, M. and Hutmacher, D. W. (2007). Biodegradable polymers applied in tissue engineering research: a review. **Polymer International** 56(2): 145-157.
- Mata, J., Joshi, T., Varade, D., Ghosh, G. and Bahadur, P. (2004). Aggregation behavior of a PEO–PPO–PEO block copolymer + ionic surfactants mixed systems in water and aqueous salt solutions. **Colloids and Surfaces A: Physicochemical and Engineering Aspects** 247(1): 1-7.
- Nair, L. S. and Laurencin, C. T. (2007). Biodegradable polymers as biomaterials. **Progress in Polymer Science** 32(8): 762-798.
- Nakashima, K. and Bahadur, P. (2006). Aggregation of water-soluble block copolymers in aqueous solutions: Recent trends. **Advances in Colloid and Interface Science** 123: 75-96.
- Petrak, K. (2005). Essential properties of drug-targeting delivery systems. **Drug Discovery Today** 10(23): 1667-1673.
- Pillai, O. and Panchagnula, R. (2001). Polymers in drug delivery. **Current Opinion in Chemical Biology** 5(4): 447-451.

- Rapoport, N. (2004). Combined cancer therapy by micellar-encapsulated drug and ultrasound. **International Journal of Pharmaceutics** 277(1): 155-162.
- Rothen-Weinhold, A., Gurny, R. and Dahn, M. (2000). Formulation and technology aspects of controlled drug delivery in animals. **Pharmaceutical Science & Technology Today** 3(7): 222-231.
- Ruan, G. and Feng, S.-S. (2003). Preparation and characterization of poly(lactic acid) – poly(ethylene glycol) – poly(lactic acid) (PLA–PEG–PLA) microspheres for controlled release of paclitaxel. **Biomaterials** 24(27): 5037-5044.
- Russell, S. J. and Peng, K.-W. (2007). Viruses as anticancer drugs. **Trends in Pharmacological Sciences** 28(7): 326-333.
- Södergård, A. and Stolt, M. (2002). Properties of lactic acid based polymers and their correlation with composition. **Progress in Polymer Science** 27(6): 1123-1163.
- Sung, J. C., Pulliam, B. L. and Edwards, D. A. (2007). Nanoparticles for drug delivery to the lungs. **Trends in Biotechnology** 25(12): 563-570.
- Tharanathan, R. N. (2003). Biodegradable films and composite coatings: past, present and future. **Trends in Food Science & Technology** 14(3): 71-78.
- Torchilin, V. P. (2007). Micellar nanocarriers: pharmaceutical perspectives. **Pharmaceutical Research** 24(1): 1-16.
- Vao-soongnern, V. and Mattice, W. L. (2000a). Dynamic properties of an amorphous polyethylene nanofiber. **Langmuir** 16(16): 6757-6759.
- Vao-soongnern, V. and Mattice, W. L. (2000b). Topological effects on static and dynamic properties in an amorphous nanofiber composed of cyclic polymers. **Macromol. Theory Simul.** 9(8): 570-577.

- Vao-soongnern, V., Ozisik, R. and Mattice, W. L. (2001). Monte carlo simulation of the structures and dynamics of amorphous polyethylene nanoparticles. **Macromol. Theory Simul.** 10(5): 553-563.
- Winzenburg, G., Schmidt, C., Fuchs, S. and Kissel, T. (2004). Biodegradable polymers and their potential use in parenteral veterinary drug delivery systems. **Advanced Drug Delivery Reviews** 56(10): 1453-1466.
- Won, Y.-Y., Brannan, A. K., Davis, H. T. and Bates, F. S. (2002). Cryogenic transmission electron microscopy (Cryo-TEM) of micelles and vesicles formed in water by poly(ethylene oxide)-based block copolymers. **The Journal of Physical Chemistry B** 106(13): 3354-3364.
- Xiao, R. Z., Zeng, Z. W., Zhou, G. L., Wang, J. J., Li, F. Z. and Wang, A. M. (2010). Recent advances in PEG-PLA block copolymer nanoparticles. **International Journal of Nanomedicine** 5(1): 1057-1065.
- Zignani, M., Tabatabay, C. and Gurny, R. (1995). Topical semi-solid drug delivery: kinetics and tolerance of ophthalmic hydrogels. **Advanced Drug Delivery Reviews** 16(1): 51-60.
- Zimmer, A. and Kreuter, J. (1995). Microspheres and nanoparticles used in ocular delivery systems. **Advanced Drug Delivery Reviews** 16(1): 61-73.

CHAPTER II

LITERATURE REVIEW

2.1 Polymer micelle as drug delivery system

Drug delivery systems are required an administered therapeutic agent needs to be protected against metabolic attack, or when there are absorption barriers or dosage limitations. The ideal delivery vehicle will ensure that the drug is released at the right site, in the right dose and for the required time. It will also be biocompatible or biodegradable such that the delivery system is transformed into non-toxic fragments that are eliminated harmlessly from the body. The importance of this field of research is growing as ever more complex drugs and biopharmaceuticals are being developed, many of which cannot be administered without a controlled dosage system.

Among varieties of drug delivery vehicle, micelle from biodegradable polymer has been considered. The unique properties of polymer micelle for drug delivery system is that it can self-assembly to spherical form which have a hydrophobic core and externally a hydrophilic surface with the diameter ranges from 10 to 100 nm. The hydrophobic drug or active molecules can be easily incorporated into the core of polymer micelles to overcome solubility problems. The hydrophilic shell and the nanoscopic size prevent mechanical clearance of micelles by filtration or in the spleen. This is beneficial for prolonging the blood circulation of drug. Moreover, the

shell stabilizes the micelle, interacts with the plasma proteins and cell membranes and its nature controls biodistribution of the carrier. Additionally, there is no need of modification of chemical structure of the drugs. Triblock copolymer micelles in a dilute solution under selective solvent for one block usually tend to form spherical micelles. Suitable amphiphilic block copolymers are obtainable via controlled synthesis by varying the hydrophobic and hydrophilic block ratio, the total molecular weight, and the chemical structure. By adjusting the structure of the amphiphilic copolymers, the size and morphology of the resulting polymer micelles can be easily controlled.

2.2 Triblock copolymer micelle as drug carrier

Recently, the polymer micelle prepared from di- or triblock copolymer mostly consists of polyethylene glycol (PEG) or polyethylene oxide (PEO) as a hydrophilic part because the PEO extends from the surface of the micelle into the aqueous environment. This PEO layer helps the carrier avoid recognition by the MPS by minimizing interactions with blood proteins, thus prolonging the residence time in blood circulation (Tan *et al.*, 1993). Polyethylene glycol (PEG) is defined as polyethylene oxides with hydroxyl end groups and a molecular weight not more than 20,000. PEG is nontoxic and cleared by the United State Food and Drug Administration for internal use in the human body. The treatment of PEG is easier and safer than those of PEO (Harris *et al.*, 1984). Amphiphilic triblock copolymers based PEO such as Pluronic® is the polymer that has a hydrophobic and a hydrophilic part on the same molecule. It is the amphiphilic triblock copolymer consists of PEO and polypropylene oxide (PPO) and can self-assemble to form micelle in aqueous

solutions. This kind of micelles has been widely attention for a long time (Almgren *et al.*, 1995; Linse, 1994; Svensson *et al.*, 1999; Zvelindovsky *et al.*, 1998). In addition, it was often used as drug carriers for controlled drug delivery systems (Batrakova and Kabanov, 2008; Kabanov *et al.*, 2002; Kadam *et al.*, 2011). However, there are major problem of using Pluronic® micelles as a drug delivery system *i.e.* low stability, efficiency in controlled drug releasing and high cmc. Hence, it is not easy and not healthy to maintain such high concentrations in the body (Pruitt *et al.*, 2000).

2.3 PLA-PEG-PLA triblock copolymer micelle as drug carrier

The triblock copolymer micelle composes of polylactide (PLA) and polyethylene glycol (PEG) (PLA-PEG-PLA) has dramatically researched for applied as carrier material. The triblock copolymer is an amphiphilic polymer with good stability *in vivo*. The PEG hydrophilic layer can increase the solubility of insoluble drugs, effectively prevent the protein absorbed on the nanoparticle surface make this nanoparticle is unrecognizable by the reticuloendothelial system as foreign bodies and thereby show a characteristic of long circulation. A common method of preparing triblock copolymers is polymerizing of lactide monomer onto a preformed PEO via ring-opening polymerization (ROP). A number of catalysts have been used for this purpose. Tin salts are the commonly used catalysts, especially stannous compounds with a higher catalytic efficiency (Lee *et al.*, 2002; Mai *et al.*, 2009; Zhu *et al.*, 1990). Besides, another catalyze also been used *i.e.* acetic acid bismuth (Kricheldorf and Meier-Haack, 1993), calcium hydride (Li *et al.*, 1996; Rashkov *et al.*, 1996), zinc compound (Wang *et al.*, 2006). Stannous octoate is the most frequently mentioned in literature because it leads to high yield and high molecular weights (Du *et al.*, 1995;

Kricheldorf and Meier-Haack, 1993). It was found that in the copolymerization system of L-lactide and PEG, the length of polymer chain could be controlled by changing the proportion of monomer and initiator, and copolymers with different molecular structures could be synthesized. Many researchers have been attempting to prepare and characterize PLA-PEO-PLA triblock copolymer micelle for application in drug delivery system. There are various kind of techniques are using to observe the micellization and its properties *i.e.* light scattering, cryo-transmission electron microscopy (Cryo-TEM), DSC, fluorescence, rheology, emission scanning electron microscopy (SEM) and surface tension (Hamley, 2005). It has to be revealed that different methods are given different kinds of information for the system under observing behavior. For examples, fluorescence probe technique is used to study micellization (Aguilar *et al.*, 2003), scattering technique is used to determine micelle dimensions and intra-micelle structure (Chu and Liu, 2000) and TEM is used to image micelle structure (Won *et al.*, 2002). Many factors are influence the micelle properties and drug releasing profile of PLA-PEO-PLA triblock copolymer micelle (Xiao *et al.*, 2010). For examples, the study about the effect of polymer types, solvent types and content of drug loading on paclitaxel releasing profile of PLA-PEO-PLA triblock copolymer (Ruan and Feng, 2003). The results showed that the faster release from PLA-PEG-PLA in comparison with the PLGA counterpart with a sustained release of paclitaxel within 1 month. That means the PLA-PEG-PLA microspheres were promising for the clinical administration of highly hydrophobic drugs. In comparison to this report, the study about drug release from similar block copolymer micelle system was performed (Venkatraman *et al.*, 2005). The release rate of paclitaxel drug was faster than data reported by Ruan. The main factor was the size of micelle that

causing in difference encapsulation efficiency. However, they results were in good agreement which Ruan's work that, lower drug loading appeared to have faster rate of release. Besides, they found that the micelle nanospheres shown good efficiency in encapsulation of anti-cancer drugs 5-FU. The release profile showed good control over the release of paclitaxel from these polymers. In 2006, the effect of PLA block length and their crystallinity on the drug release profiles was investigated (Agrawal *et al.*, 2006). They found that drug release was much faster for polymers with crystalline PLA blocks as compared to those amorphous. The releasing rate was also depended on the length of the PLA block at fixed PEO. Moreover, the sustained release profile of drug was affected by polymer–drug interactions. Moreover, they are many research groups are interesting study on PLA-PEO-PLA triblock copolymer micelle due to there are many effect that plays an important role in their properties which is relate to desired application (Dai *et al.*, 2004; He *et al.*, 2007; Lee *et al.*, 2002; Saffer *et al.*, 2011; Wang *et al.*, 2006).

2.4 Mesoscale simulation of triblock copolymer micelle

The experimental result can give details about the interested system, except for kinetic process of self-assembled amphiphilic molecules to micelle structures is still not fully understood. Moreover, to develop new materials and compositions with designed new properties, it is essential that these properties can be predicted before preparation, processing, and characterization.

For self-assembled aggregates, the patterns of nanostructures play a critical role in drug delivery applications. In order to facilitate a better understanding of the

pattern formation besides experimental efforts, computer simulation is a promising tool in offering efficient evaluation of aggregate formation and properties of nanostructures (Sevink *et al.*, 2001; Xiang *et al.*, 2005). The coarse-graining or mesoscopic simulations are reasonable level model to study of phase aggregation and morphology of at the mesoscale level. Mesoscopic simulations based on MesoDyn have been carried out to identify microphase transitions of block copolymer (Fraaije and Sevink, 2003; Guo *et al.*, 2011; Ludwigs *et al.*, 2005). Based on MesoDyn, the microphase separation dynamics and the morphology of the triblock copolymer can be investigated (van Vlimmeren *et al.*, 1999; Zhao *et al.*, 2007). The simulation can give more detail which is rarely obtained by the experiment. For examples, the application of the MesoDyn to image the phase behavior triblock polymer in aqueous solution (van Vlimmeren *et al.*, 1999). The simulation method is a valuable tool for describe morphology of the polymer which were in very good agreement with experiment. Moreover, the kinetics of polymer micelle can be monitored. Besides, DPD simulation is the useful technique to solve polymer problems *i.e.* single-chain melt dynamics, polymer composites, block copolymer microphase separation, binary blend compatibility and phase behavior of polymer solutions (Chen *et al.*, 2007; Guo *et al.*, 2007; Zhao *et al.*, 2009). The application of DPD is given valuable data for more understand and for further polymer designed. The phase behavior of drug loaded diblock copolymer of PLA and PEO in the mesoscopic region has been successfully studied using DPD method (Guo *et al.*, 2009). The observed morphology is including spherical, rod, hexagonal perforated layers, and lamella structures for pure polymer in water. When the drug was added, all ordered structures are bicontinuous, lamella and rod. Besides, the phase diagram as a function of concentration can be approximated.

2.5 Monte carlo simulation of polymer brush and nanoparticle

Polymer brush or grafted-polymer is a simple model for study polymer micelle structures in theoretical prediction. Polymer brush is a tethered polymer type which considers in many applications such as colloidal stabilization, lubrication and medical industry. Besides preparation, the determination of physical properties of the polymer layer, such as the thickness and density distribution, is challenging as well. However, the experiments in the field of polymer brushes with well characterized systems lag behind the theoretical developments by several years. Molecular modeling has been used to analyze desired physical properties of the system which may not perform by experiment. Monte Carlo (MC) simulations may provide an alternative choice for the dynamical simulation of realistic polymers. Recently, the second-nearest neighbor diamond (2nd) lattice in combination with the short- and long-range interactions is used to simulate high molecular weight polymers at their bulk density. The simulation method has been validated in previous studies on polymer nanofibers (Vao-soongnern and Mattice, 2000a, b) and polymer nanoparticles (Vao-soongnern *et al.*, 2001) which were produced reasonable static and dynamic properties with good agreement with theoretical observations.

Nowadays, an experimental technique was developed for creating very fine polymer particles of arbitrary composition and size. These particles in the nanometer size range provide many unique properties. However, the experiments to measure properties of these particles were very difficult. More efficient method to study the larger systems was a coarse grained MC simulation on a high coordination lattice was developed to explore the behavior of large polymer systems. In 2001, the structural

and dynamic properties of monodisperse polyethylene (PE) nanoparticle was reported (Vao-soongnern *et al.*, 2001). The density profiles were hyperbolic with end beads being more abundant than middle beads at the surface. The particles were orientated preferences at the surface on the scale of individual bonds and whole chains. While the different size of nanoparticle did not show any significant differences in the local and global equilibrium properties. Moreover, in 2004, the crystallization, melting and annealing of tetracontane nanoparticles via the same model was studied (Vao-Soongnern *et al.*, 2004). The obtained data indicates that the crystals form first in the region close to the surface. Each nanoparticle contains multiple crystalline domains. Annealing of the multiple domain crystal at 360 K can transform the structure to a more regular one without a grain boundary

As above mention, the PLA-PEG-PLA triblock copolymer micelles are very interesting for research and apply as drug delivery. They are various useful method to investigated the polymer micelle property *i.e.* experiment, mesoscale simulation and Monte Carlo simulation. In this research, the mesoscale simulation *i.e.* MesoDyn and DPD were used to study the effect of polymer concentration, block ratio and adding the third component on mesostructure of the triblock copolymer micelle before further experimental synthesis. The MC simulation on 2nd lattice will be employed to study the effects of grafting density, polydispersity and solvent quality on the properties of PE and PEO brush, a model for the corona part of the triblock copolymer micelle. In addition, the MC method was also applied to study effect of solvent quality on stability and structure properties of PEO nanoparticles, a model for the core part of the triblock copolymer micelle.

2.6 References

- Agrawal, S. K., Sanabria-DeLong, N., Coburn, J. M., Tew, G. N. and Bhatia, S. R. (2006). Novel drug release profiles from micellar solutions of PLA-PEO-PLA triblock copolymers. **Journal of Controlled Release** 112(1): 64-71.
- Aguiar, J., Carpena, P., Molina-Bolívar, J. A. and Carnero Ruiz, C. (2003). On the determination of the critical micelle concentration by the pyrene 1:3 ratio method. **Journal of Colloid and Interface Science** 258(1): 116-122.
- Almgren, M., Brown, W. and Hvidt, S. (1995). Self-aggregation and phase behavior of poly(ethylene oxide)-poly(propylene oxide)-poly(ethylene oxide) block copolymers in aqueous solution. **Colloid and Polymer Science** 273(1): 2-15.
- Batrakova, E. V. and Kabanov, A. V. (2008). Pluronic block copolymers: evolution of drug delivery concept from inert nanocarriers to biological response modifiers. **Journal of Controlled Release** 130(2): 98-106.
- Chen, S., Hu, G.-H., Guo, C. and Liu, H.-Z. (2007). Experimental study and dissipative particle dynamics simulation of the formation and stabilization of gold nanoparticles in PEO-PPO-PEO block copolymer micelles. **Chemical Engineering Science** 62(18): 5251-5256.
- Chu, B. and Liu, T. (2000). Characterization of nanoparticles by scattering techniques. **Journal of Nanoparticle Research** 2(1): 29-41.
- Dai, Z., Piao, L., Zhang, X., Deng, M., Chen, X. and Jing, X. (2004). Probing the micellization of diblock and triblock copolymers of poly(l-lactide) and poly(ethylene glycol) in aqueous and NaCl salt solutions. **Colloid and Polymer Science** 282(4): 343-350.

- Du, Y. J., Lemstra, P. J., Nijenhuis, A. J., Van Aert, H. A. M. and Bastiaansen, C. (1995). ABA type copolymers of lactide with poly(ethylene glycol). kinetic, mechanistic, and model studies. **Macromolecules** 28(7): 2124-2132.
- Fraaije, J. G. E. M. and Sevink, G. J. A. (2003). Model for pattern formation in polymer surfactant nanodroplets. **Macromolecules** 36: 7891-7893.
- Guo, X., Yuan, S., Yang, S., Lv, K. and Yuan, S. (2011). Mesoscale simulation on patterned core-shell nanosphere model for amphiphilic block copolymer. **Colloids and Surfaces A: Physicochemical and Engineering Aspects** 384(1): 212-218.
- Guo, X. D., Tan, J. P. K., Zhang, L. J., Khan, M., Liu, S. Q., Yang, Y. Y. and Qian, Y. (2009). Phase behavior study of paclitaxel loaded amphiphilic copolymer in two solvents by dissipative particle dynamics simulations. **Chemical Physics Letters** 473(4): 336-342.
- Guo, X. D., Zhang, L., Qian, Y. and Zhou, J. (2007). Effect of composition on the formation of poly(dl-lactide) microspheres for drug delivery systems: mesoscale simulations. **Chemical Engineering Journal** 131(1): 195-201.
- Hamley, I. (2005). Block copolymers in solution: fundamentals and applications. Chichester, John Wiley & Sons Ltd.
- Harris, J. M., Struck, E. C., Case, M. G., Paley, M. S., Yalpani, M., Van Alstine, J. M. and Brooks, D. E. (1984). Synthesis and characterization of poly(ethylene glycol) derivatives. **Journal of Polymer Science: Polymer Chemistry Edition** 22(2): 341-352.
- He, G., Ma, L. L., Pan, J. and Venkatraman, S. (2007). ABA and BAB type triblock copolymers of PEG and PLA: a comparative study of drug release properties

- and “stealth” particle characteristics. **International Journal of Pharmaceutics** 334(1): 48-55.
- Kabanov, A. V., Batrakova, E. V. and Alakhov, V. Y. (2002). Pluronic[®] block copolymers as novel polymer therapeutics for drug and gene delivery. **Journal of Controlled Release** 82(2): 189-212.
- Kadam, Y., Yerramilli, U., Bahadur, A. and Bahadur, P. (2011). Micelles from PEO–PPO–PEO block copolymers as nanocontainers for solubilization of a poorly water soluble drug hydrochlorothiazide. **Colloids and Surfaces B: Biointerfaces** 83(1): 49-57.
- Kricheldorf, H. R. and Meier-Haack, J. (1993). Polylactones, 22 ABA triblock copolymers of L-lactide and poly(ethylene glycol). **Die Makromolekulare Chemie** 194(2): 715-725.
- Lee, S.-H., Kim, S. H., Han, Y.-K. and Kim, Y. H. (2002). Synthesis and characterization of poly(ethylene oxide)/polylactide/poly(ethylene oxide) triblock copolymer. **Journal of Polymer Science Part A: Polymer Chemistry** 40(15): 2545-2555.
- Li, S. M., Rashkov, I., Espartero, J. L., Manolova, N. and Vert, M. (1996). Synthesis, characterization, and hydrolytic degradation of PLA/PEO/PLA triblock copolymers with long poly(l-lactic acid) blocks. **Macromolecules** 29(1): 57-62.
- Linse, P. (1994). Adsorption and phase behaviour of pluronic block copolymers in aqueous solution. **Colloids and Surfaces A: Physicochemical and Engineering Aspects** 86: 137-142.

- Ludwigs, S., Krausch, G., Magerle, R., Zvelindovsky, A. V. and Sevink, G. J. A. (2005). Phase behavior of ABC triblock terpolymers in thin films: mesoscale simulations. **Macromolecules** 38: 1859-1867.
- Mai, S.-m., Abbot, A., Norton, D., McKean, R. and Ryan, A. J. (2009). Synthesis and characterization of block copolymers of polyoxyethylene and polylactide with different architectures. **Macromolecular Chemistry and Physics** 210(10): 840-851.
- Pruitt, J. D., Husseini, G., Rapoport, N. and Pitt, W. G. (2000). Stabilization of Pluronic[®] P-105 micelles with an interpenetrating network of N,N-diethylacrylamide. **Macromolecules** 33(25): 9306-9309.
- Rashkov, I., Manolova, N., Li, S. M., Espartero, J. L. and Vert, M. (1996). Synthesis, characterization, and hydrolytic degradation of PLA/PEO/PLA triblock copolymers with short poly(l-lactic acid) chains. **Macromolecules** 29(1): 50-56.
- Ruan, G. and Feng, S.-S. (2003). Preparation and characterization of poly(lactic acid) – poly(ethylene glycol) – poly(lactic acid) (PLA–PEG–PLA) microspheres for controlled release of paclitaxel. **Biomaterials** 24(27): 5037-5044.
- Saffer, E. M., Tew, G. N. and Bhatia, S. R. (2011). Poly(lactic acid)-poly(ethylene oxide) block copolymers: new directions in self-assembly and biomedical applications. **Current Medicinal Chemistry** 18(36): 11.
- Sevink, G. J. A., Zvelindovsky, A. V., Fraaije, J. G. E. M. and Huinink, H. P. (2001). Morphology of symmetric block copolymer in a cylindrical pore. **J. Chem. Phys.** 115: 8226-8230.

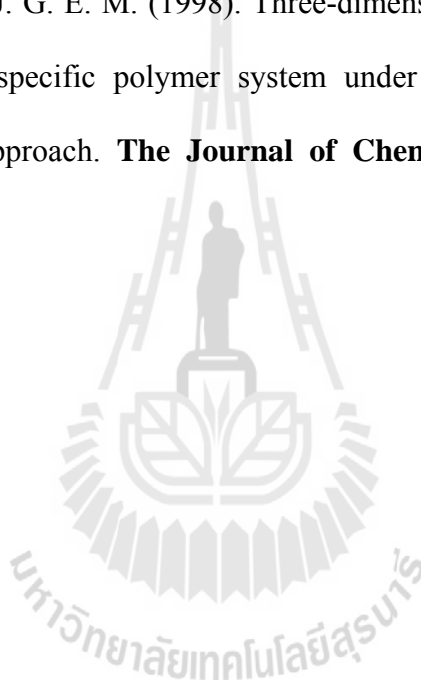
- Svensson, M., Alexandridis, P. and Linse, P. (1999). Phase behavior and microstructure in binary block copolymer/selective solvent systems: experiments and theory. **Macromolecules** 32(3): 637-645.
- Tan, J. S., Butterfield, D. E., Voycheck, C. L., Caldwell, K. D. and Li, J. T. (1993). Surface modification of nanoparticles by PEO/PPO block copolymers to minimize interactions with blood components and prolong blood circulation in rats. **Biomaterials** 14(11): 823-833.
- van Vlimmeren, B. A. C., Maurits, N. M., Zvelindovsky, A. V., Sevink, G. J. A. and Fraaije, J. G. E. M. (1999). Simulation of 3D mesoscale structure formation in concentrated aqueous solution of the triblock polymer surfactants (ethylene oxide)₁₃(propylene oxide)₃₀(ethylene oxide)₁₃ and (propylene oxide)₁₉(ethylene oxide)₃₃(propylene oxide)₁₉: application of dynamic mean-field density functional theory. **Macromolecules** 32(3): 646-656.
- Vao-soongnern, V. and Mattice, W. L. (2000a). Dynamic properties of an amorphous polyethylene nanofiber. **Langmuir** 16(16): 6757-6759.
- Vao-soongnern, V. and Mattice, W. L. (2000b). Topological effects on static and dynamic properties in an amorphous nanofiber composed of cyclic polymers. **Macromol. Theory Simul.** 9(8): 570-577.
- Vao-soongnern, V., Ozisik, R. and Mattice, W. L. (2001). Monte carlo simulation of the structures and dynamics of amorphous polyethylene nanoparticles. **Macromol. Theory Simul.** 10(5): 553-563.
- Vao-Soongnern, V., Xu, G. and Mattice, W. L. (2004). Structure formation in the crystallization and annealing of tetracontane nanoparticles. **Macromol. Theory Simul.** 13(6): 539-549.

- Venkatraman, S. S., Jie, P., Min, F., Freddy, B. Y. C. and Leong-Huat, G. (2005).
Micelle-like nanoparticles of PLA-PEG-PLA triblock copolymer as
chemotherapeutic carrier. **International Journal of Pharmaceutics** 298(1):
219-232.
- Wang, Z.-Y., Zhao, Y.-M. and Wang, F. (2006). Syntheses of poly(lactic acid)-
poly(ethylene glycol) serial biodegradable polymer materials via direct melt
polycondensation and their characterization. **Journal of Applied Polymer
Science** 102(1): 577-587.
- Won, Y.-Y., Brannan, A. K., Davis, H. T. and Bates, F. S. (2002). Cryogenic
transmission electron microscopy (Cryo-TEM) of micelles and vesicles
formed in water by poly(ethylene oxide)-based block copolymers. **The
Journal of Physical Chemistry B** 106(13): 3354-3364.
- Xiang, H. Q., Shin, K., Kim, T., Moon, S., Mccarthy, T. J. and Russell, T. P. (2005).
The influence of confinement and curvature on the morphology of block
copolymers. **Polym. Sci., Part B: Polym. Phys.** 43: 3377-3383.
- Xiao, R. Z., Zeng, Z. W., Zhou, G. L., Wang, J. J., Li, F. Z. and Wang, A. M. (2010).
Recent advances in PEG-PLA block copolymer nanoparticles. **International
Journal of Nanomedicine** 5(1): 1057-1065.
- Zhao, Y., Chen, X., Yang, C. and Zhang, G. (2007). Mesoscopic simulation on phase
behavior of Pluronic[®] P123 aqueous solution. **The Journal of Physical
Chemistry B** 111(50): 13937-13942.
- Zhao, Y., You, L.-Y., Lu, Z.-Y. and Sun, C.-C. (2009). Dissipative particle dynamics
study on the multicompartment micelles self-assembled from the mixture of
diblock copolymer poly(ethyl ethylene)-block-poly(ethylene oxide) and

homopolymer poly(propylene oxide) in aqueous solution. **Polymer** 50(22): 5333-5340.

Zhu, K. J., Xiangzhou, L. and Shilin, Y. (1990). Preparation, characterization, and properties of polylactide (PLA)–poly(ethylene glycol) (PEG) copolymers: A potential drug carrier. **Journal of Applied Polymer Science** 39(1): 1-9.

Zvelindovsky, A. V. M., van Vlimmeren, B. A. C., Sevink, G. J. A., Maurits, N. M. and Fraaije, J. G. E. M. (1998). Three-dimensional simulation of hexagonal phase of a specific polymer system under shear: The dynamic density functional approach. **The Journal of Chemical Physics** 109(20): 8751-8754.



CHAPTER III

MONTE CARLO SIMULATION OF POLYMER BRUSHES AND NANOPARTICLE: A MODEL FOR THE CORONA AND THE CORE PART OF MICELLE

3.1 Abstract

MC simulations of PE and PEO brushes and PE nanoparticle have been performed on the 2nd lattice for model as the corona and the core part of triblock copolymer micelle. The model to represent polymer micelle structure was shown in Figure 3.1. A polymer was mapped onto a coarse-grained model in which each bead represents series of linked vector connecting the $-\text{CH}_2\text{CH}_2-$ or $-\text{CH}_2\text{O}-$ unit. Both short-range interactions based on the RIS model and long-range interactions from a discretized form of the LJ potential energy were included. The lattice model was applied to investigate the effect of grafting density, solvent quality and polydispersity on the structural, conformational and orientation properties of PE and PEO brush. The simulation was model the polydispersity polymer comprises of a mixture of short and long grafted PE melts. The results revealed that, as NS increase at constant NL, both short and long chains were affected. On other hand, as NL increased, the short chains were more compressed in the inner layer whereas the long chains were more stretched to the outer layer. Strong difference in bead distribution causing the two main features of the bimodal brushes: vertical segregation and the difference of the local degree of

stretching between long and short chains. In addition, the end bead distribution revealed of interpenetration of the short chain ends into the outer layer. Moreover, the effect of solvent quality on the mono- and bisdisperse PEO brush were also investigated. The results show that both quality of solvent and polydispersity were affected to the brush properties. Due to difference in an interaction between polymer-polymer and polymer-solvent, the brush under poor solvent was more compressed as confirmed by the density profile, the bond orientation and the beads distribution. In addition, the model was additional modified and employed to study the effect of solvent quality on the stability and structure properties of the PEO nanoparticle, a model the core part of polymer micelle. The observation properties were shown the denser packing of the nanoparticle and the density in bulk region was increased. The shape of nanoparticle was nearly ellipsoid when the quality of solvent becomes poorer. The distribution of middle beads in nanoparticle had no significant affected by any solvent quality, while the end beads distribution are strongly depended. All results were in good agreement with the previous simulation that most bond orientation in the nanoparticle was relatively random.

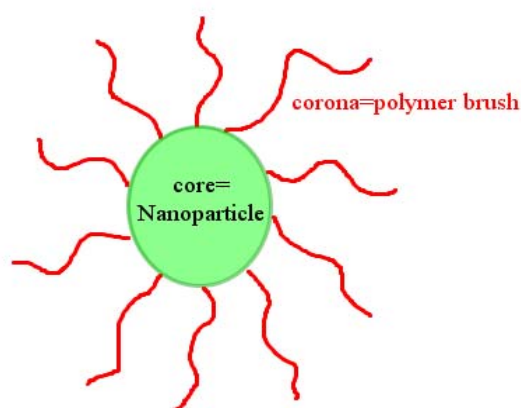


Figure 3.1 Model to represent the triblock copolymer micelle.

3.2 Background of Monte Carlo simulation for molecular system

Base on the Metropolis algorithm, Monte Carlo (MC) sampling has become a widely used tool of computer simulation. It is a useful method to solve the problem both for the problem of statistical mechanics of condensed matter in general and also for polymers. As the name of MC implies, the simulation uses random numbers for making decision during the simulation. In terms of molecular mechanics, the MC provides another way to explore a conformational space, by generating random numbers. With a given potential like Equation (3.1), the simulation involves a successive energy evaluation to make a decision for acceptance of a move attempt which is chosen randomly.

$$\begin{aligned}
 V_{total} = & \underbrace{V(r)_{bond} + V(\theta)_{angle} + V(\phi)_{torsion} + V(\chi)_{out-of-plane}}_{V_{bonded}} \\
 & + \underbrace{V(r)_{vwd} + V(r)_{elec}}_{V_{non-bonded}}
 \end{aligned} \tag{3.1}$$

To simulate polymer based on MC, the transition between different states or configurations are achieved by: (a) generating a random trial configuration; (b) evaluating an “acceptance criterion” by calculating the change in energy as equation (3.1) and other properties in the trial configuration; (c) comparing the acceptance criterion to the random number and either accepting or rejecting the trial configuration. To accurately determine the properties of the system in the finite time available for simulation, it is important to sample those states that make the most significant contributions this is achieved by generating a Markov chain (Hastings, 1970). A Markov chain is a sequence of trials which outcome successive trials which depends only on the immediate predecessor. In a Markov chain, a new state will only

be accepted if it is more “favorable” than the existing state. It usually means that the new trial state is lower in energy.

MC simulation can sampling from $3N$ -dimensional space represented by the position of particles. It is not necessary to know particle momenta to calculate thermodynamic properties because the momentum contributes only to the ideal gas term. Deviations from an ideal behavior are caused by the interaction between particles which can be calculated from the potential energy function (Equation (3.1)). The potential energy depends only on the position of atoms and not their momenta. In effect, a MC simulation calculates excess thermodynamics properties that result in a deviation from an ideal gas behavior. The appropriate ideal gas term can be simply added at the conclusion of the simulation to obtain total thermodynamic property. The average of any thermodynamic property $\langle A(r^N) \rangle$ can be obtained by evaluating the multidimensional integral over $3N$ degrees of freedom on N particles in system.

$$\langle A(r^N) \rangle = \int A(r^N) \rho(r^N) dr^N \quad (3.2)$$

where $\rho(r^N)$ is the probability of the obtaining configuration r^N which is depends on the potential energy V_{total} of the configuration.

$$\rho(r^N) = \frac{\exp[-\beta E(r^N)]}{\int \exp[-\beta E(r^N)] dr^N} \quad (3.3)$$

These integral cannot be evaluated analytically and any conventional methods are also not feasible. For example to apply either Simpson’s rule or the Trapezium rule to evaluate $3N$ -dimensional integral would require m^{3N} function evaluations, where m is the number of points required to determine the integral in each dimension. The MC simulation generates a large number of trial configurations r^N and replacing

the integral by summation over a finite number of configurations. If the configurations are chosen randomly, Equation (3.2) becomes:

$$\langle A(r^N) \rangle = \frac{\sum_{i=1}^{N_{\text{trial}}} A_i(r^N) \exp[-\beta E_i(r^N)]}{\sum_{i=1}^{N_{\text{trial}}} \exp[-\beta E_i(r^N)]} \quad (3.4)$$

However, in practice, this simple approach is not feasible because random sampling yields many configurations which have very small Boltzmann factor. Such configurations make very little contribution to the average. Therefore, a prohibitively large number of configurations are required to obtain the correct number. This is a philosophy behind Metropolis sampling (Metropolis *et al.*, 1953) that is based on the generation of configurations towards those that make the most significant contribution to the integral. Metropolis sampling generates a Markov chain which satisfies the condition in following criteria.

$$\begin{aligned} \Delta E = V(r)_{\text{new}} - V(r)_{\text{old}} \leq 0 & \quad \text{accepted} \\ \Delta E = V(r)_{\text{new}} - V(r)_{\text{old}} > 0 \text{ and } \exp(-\Delta E / kT) \geq \text{rand}(0,1) & \quad \text{accepted} \end{aligned} \quad (3.5)$$

$$\Delta E = V(r)_{\text{new}} - V(r)_{\text{old}} > 0 \text{ and } \exp(-\Delta E / kT) < \text{rand}(0,1) \quad \text{rejected}$$

If the new state is in a lower energy state, the new state replaces the previous state. If the new state is in a higher energy state, the decision is based on the energy difference between two states. For the decision procedure, the simulation allows a system to move to higher energy state, the probability depends on the energy difference between the new and the current conformation. By doing so, MC finds the conformational space to calculate the ensemble averaged properties. Much effort has

drawn attention to increasing the computational efficiency. One of the efforts is simulating on a lattice, which reduces the floating number calculation. Another way is to use an efficient move algorithm that allows the faster relaxation or equilibration.

There is considerable interest in the application of MC algorithm to determine the properties of large molecules such as polymers (Binder and Paul, 1997). One representative MC simulation is the bond fluctuation model (Baschnagel and Binder, 1995; Baschnagel *et al.*, 1998; Deutsch and Binder, 1991; Paul *et al.*, 1991). The model is a more efficient method which allows a better flexibility for the bond length and bond angle. Another way to give more flexibility to span a conformational space is to use a high coordination lattice (Rapold and Mattice, 1995a). In a lattice based MC simulation, the computational cost can be largely reduced by using large-scale moves. There are several elementary moves such as kink jump, crank shaft rotation, and end rotation as pictured in Figure 3.2 (Verdier and Stockmayer, 1962). In addition, the reptative move (Fried and Binder, 1991), the end-bridging move and the concerted rotation move (Pant and Theodorou, 1995) can be useful for the faster relaxation and can deal with a more delicate situation, as illustrated in Figure 3.3.

3.2.1 Monte Carlo simulation of polymer model on a high coordination lattice

A coarse-grained model in a lattice has the computational efficiency that comes from two reasons; the first one is the reduction of the evaluation of energy terms and the other one is that the positions of particles during simulation can be stored as integers. As a result of the efficiency, the method enables running a simulation in a large scale. As often is the case, the pros come with the cons. This

coarse grained model has a drawback in understanding the chemical details and the conformation of a chain. Therefore, an understanding by the MC simulation is limited to the phenomenological level. For example, the density is generally arbitrarily chosen in a MC simulation for polymer. Considering that the density is represented by the thermodynamic equilibrium of a system, the understanding of thermodynamics obtained from MC simulation is also quite incomplete. The drawbacks observed in MC simulations have motivated to develop a compromising model. The model should be able to simulate a relatively long and large system, but not lose much detail of the chemical nature and conformational information of polymer model.

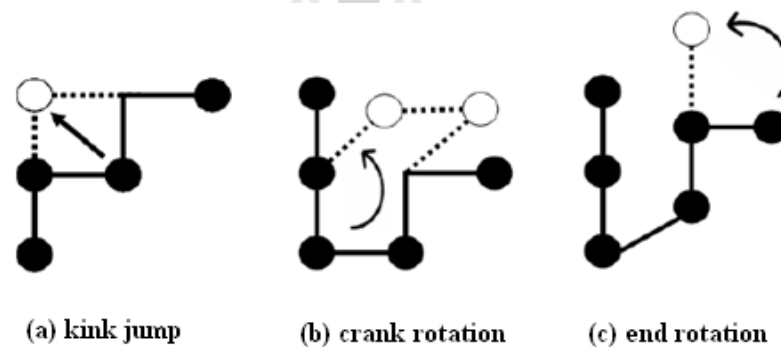


Figure 3.2 Elementary moves based on Verdieer-Stockmayer type model.

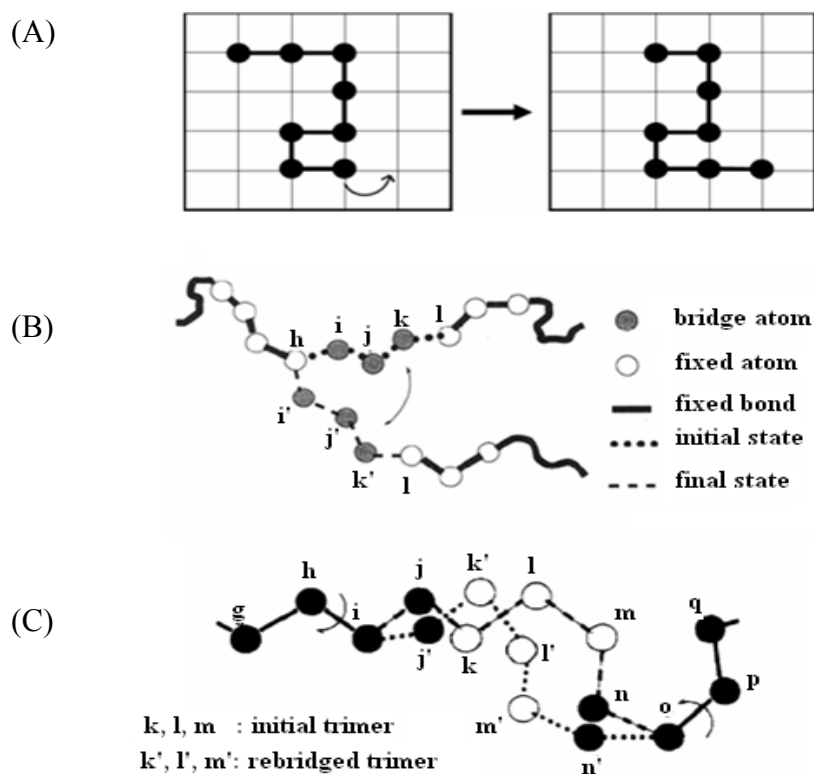


Figure 3.3 Collective moves (A) reptative move (B) end-bridge move (C) concerted rotation.

3.2.2 Coarse-grained polymer chain to rotational isomeric state

Energy state of a molecule is usually describing by a sum of energetic contributions of internal coordinates and non-bonded interactions. Among them, the bond stretching and angle bending terms are so strong. Since computational efficiency is indispensable for a polymer simulation, these two terms can be neglected in most cases. Therefore, the property of polymer chains cannot be only dependent on the remaining energy terms, torsional energy and non-bonded energy. Furthermore, if polymer chains are not perturbed by the existence of others, an importance of the long range interaction is diminished. In that case, the partition function of a single chain

can be expressed by only torsional partition function or conformational partition function as follows.

The continuous torsional states can be grouped to have several discrete states. This assumption is reasonable because discrete torsional states are separated by an activation barrier. This torsional state is called “rotational isomeric state (RIS)”. With the discrete torsional states, the conformational partition functions can be rewritten as the summation over the discrete conformational space.

$$Z = \sum_{\phi_1} \dots \sum_{\phi_n} \exp\left(\frac{-E_{\phi_1 \dots \phi_n}}{kT}\right) \quad (3.6)$$

The RIS model is a coarse-grained polymer model, which only considers the discrete rotational isomeric states with other internal coordinates frozen. For examples, the mapping from a realistic polyethylene (PE) chain to the RIS chain is illustrated in Figure 3.4. The model was established to present the RIS model with three torsional states of CC-CC = 180° (*trans*; *t*), 60° (*gauche plus*; *g+*), and -60° (*gauche minus*; *g-*) at the fixed bond length l_{CC} and bond angle $\hat{C}CC = 1.54 \text{ \AA}$ and 112°, respectively (Abe *et al.*, 1966). Based on the model, a PE chain can be mapped onto the tetrahedral lattice very successfully except for the very small bond angle mismatch. Each occupied lattice site of the tetrahedral lattice represents a single $-\text{CH}_2-$ group of the PE chain. The bond between two neighboring occupied lattice sites can be one of three rotational states; *trans* (*t*), *gauche+* (*g+*) or *gauche-* (*g-*).

3.2.3 Further coarse-grained of RIS chain on 2nd lattice

A further coarse-grained lattice PE chain can be obtained by discarding every second site from the tetrahedral lattice. This process is well represented in

Figure 3.4 (A)-(B). The coarse-grained generates a declined cubic cell whose length is 2.5 \AA in all directions with angles between two units vectors = 60° . The modification produces has a coordination number of twelve (or $10i^2 + 2$ sites in shell i), which is identical to the closest packing of uniform hard spheres provides a flexibility to define a rotational state in the lattice. This lattice is called as the “second nearest neighbor diamond (2nnd) lattice”. Each occupied site in the model represents an ethylene ($-\text{CH}_2-\text{CH}_2-$) group. The lattice provides a better computational efficiency due to a reduction in the number of particles and conformational states as illustrated in Figure 3.5. More detailed information can be found elsewhere (Balijepalli and Rutledge, 1998).

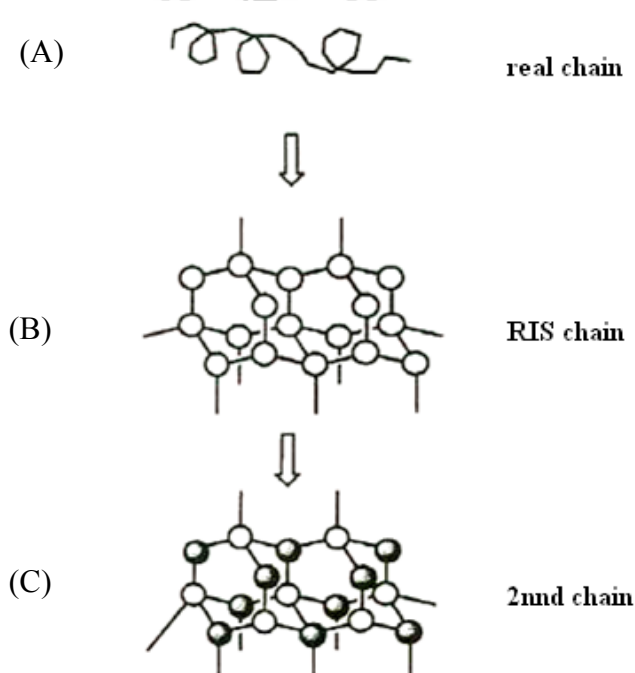


Figure 3.4 The mapping of a real chain into lattice. The degree of coarse-grained increases from (A) continuous space to (B) space available with a single bond length, tetrahedral bond angle, $\phi = 180^\circ, \pm 60^\circ$ and to (C) rejection of alternate sites from (B).

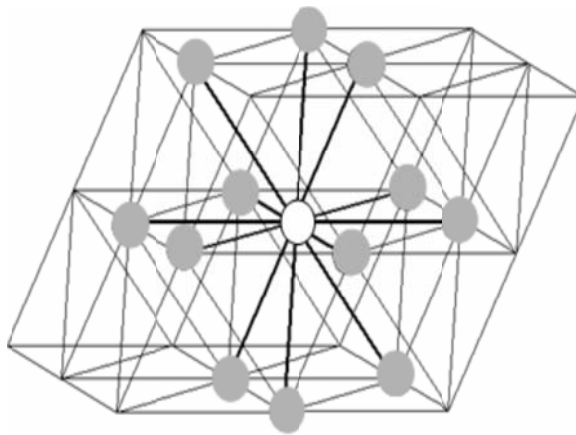


Figure 3.5 The 2nd lattice. The gray spheres represent the possible twelve coordination lattice sites around a central bead (open circle).

3.2.4 Conventional RIS formalism

In the RIS scheme for n-alkane homolog, the first approximation is to handle the rotatable bonds independently. On the assumption that a rotational state of a bond is not affected by other bonds and defined solely by the first order interaction, the conformational energy of a chain will be

$$E\{\phi\} = \sum_i E_i(\phi_i) = \sum_i E_{\xi;i} \quad (3.7)$$

where ξ denotes the rotational state of bond i . The statistical weights $u_{\xi;i}$ can be defined by the Boltzman probability, which means the relative population of the ξ state in the i th bond.

$$u_{\xi;i} = \exp(-E_{\xi;i} / RT) \quad (3.8)$$

Then, the conformational partition function of a chain Z as a whole is given by

$$Z = \prod_i \sum_{\xi} u_{\xi;i} = \prod_i z_i \quad (3.9)$$

If the rotor has three rotational states as shown in Figure 3.6 (A), which is a proper choice for the n-alkane homologs, the Z is given by $(1+2\sigma)^{n-2}$ for a linear alkane or PE chain with n carbon, where 1 and σ correspond to the statistical weights of trans and gauche states, respectively.

The first approximation, independent bonds approximation, is invalid in real situation because of the second order interaction known as pentane effect. The interdependence of bonds destroys the degeneracy of the energy state of the *gauchegauche* (gg) conformation and splits into $g+g+$ and $g+g-$ or $g-g$ and $g+g-$. As a result, the total energy of a chain with the interdependent bonds given by

$$E\{\phi\} = \sum_i E_i(\phi_{i-1}, \phi_i) = \sum_i E_{\xi\eta;i} \quad (3.10)$$

where $\xi_{\eta;i}$ means the $(i-1)$ th bond is in ξ state and i th bond is in η state. The statistical weights corresponding to $E_{\xi\eta;i}$ can be written as a matrix form as

$$U_i = (u_{\xi\eta})_i \quad (3.11)$$

The conventional RIS model for PE of (Abe *et al.*, 1966) is defined by the statistical weight for two successive rotatable internal bonds,

$$U_i = \begin{bmatrix} 1 & \sigma & \sigma \\ 1 & \sigma & \sigma\omega \\ 1 & \sigma\omega & \sigma \end{bmatrix} \quad (3.12)$$

where σ and ω are the first- and second-order interaction parameters and the rows are indexed by the states of $(i-1)$ th bond and the columns are indexed by the states of i th bond. The orders of indexing are t , $g+$, and $g-$. Then, the total conformational partition function will be

$$Z = \prod_i U_i \quad (3.13)$$

For RIS scheme in MC, a move attempt can change the rotational states of the chain which is affected by the move. The change enters the Metropolis evaluation (Metropolis *et al.*, 1953) to decide to accept or reject the move attempt. This decision can be done by obtaining bond probabilities from the statistical weights.

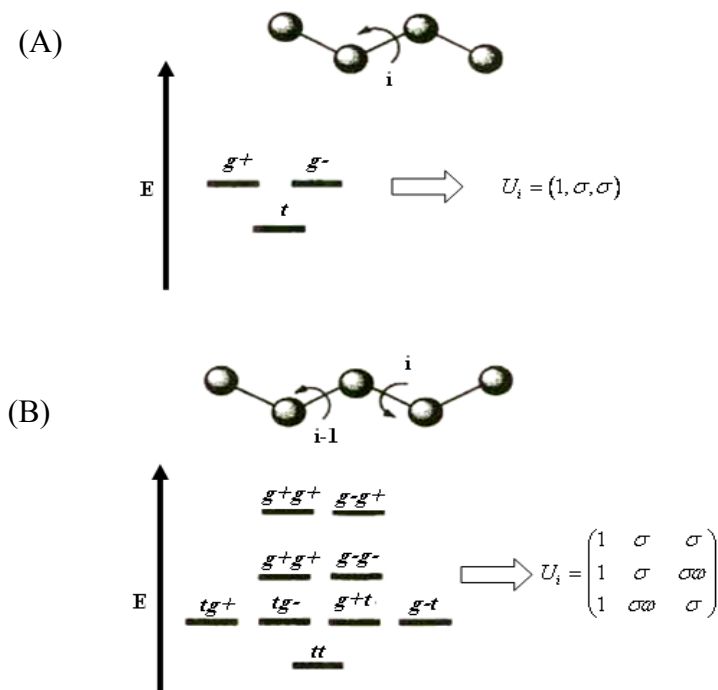


Figure 3.6 The rotational states of a linear chain and corresponding statistical weights (A) independent bond and (B) interdependent bond.

3.2.5 RIS formalism for 2nd chain

The two successive bonds are contracted into one virtual bond between two neighboring beads in the 2nd lattice. The formalism of the model of the virtual bonds for the coarse-grained chain should be modified. A virtual rotor in the 2nd frame, as shown in Figure 3.7, contains four successive rotors corresponding to n-

heptane in the original RIS frame. The detailed description of n-heptane at the sameplace, which requires a 9×9 statistical weight matrix, is given by

$$U = \begin{bmatrix} 1 & \sigma & \sigma & \sigma & \sigma & \sigma^2 & \sigma^2 & \sigma^2\omega & \sigma^2\omega \\ 1 & \sigma & \sigma & \sigma & \sigma\omega & \sigma^2 & \sigma^2\omega & \sigma^2\omega & \sigma^2\omega^2 \\ 1 & \sigma & \sigma & \sigma\omega & \sigma & \sigma^2\omega & \sigma^2 & \sigma^2\omega^2 & \sigma^2\omega \\ 1 & \sigma & \sigma & \sigma & \sigma & \sigma^2 & \sigma^2 & \sigma^2\omega & \sigma^2\omega \\ 1 & \sigma & \sigma & \sigma & \sigma & \sigma^2 & \sigma^2 & \sigma^2\omega & \sigma^2\omega \\ 1 & \sigma & \sigma & \sigma & \sigma\omega & \sigma^2 & \sigma^2\omega & \sigma^2\omega & \sigma^2\omega^2 \\ 1 & \sigma & \sigma & \sigma\omega & \sigma & \sigma^2\omega & \sigma^2 & \sigma^2\omega^2 & \sigma^2\omega \\ 1 & \sigma & \sigma & \sigma\omega & \sigma & \sigma^2\omega & \sigma^2 & \sigma^2\omega^2 & \sigma^2\omega \\ 1 & \sigma & \sigma & \sigma & \sigma\omega & \sigma^2 & \sigma^2\omega & \sigma^2\omega & \sigma^2\omega^2 \end{bmatrix} \quad (3.14)$$

The row represents 1 and 2 rotors and the column represents 3 and 4 rotors in Figure 3.7 (A). The order of the rotational states of the rows and columns are tt , tg^+ , tg^- , $g+t$, $g-t$, $g+g^+$, $g-g^-$, $g+g^-$, $g-g^+$. By the nature of the coarse graining, several details of conformational information are missing in such a way that some torsional states are no longer distinguishable in the coarse-grained chain. Then, Equation (3.14) can be modified into a simpler form with the modified statistical weights a , b , and c which are obtained from the geometric mean ($a = \sigma\omega^{1/8}$, $b = \sigma\omega^{1/4}$ and $c = \sigma^2\omega^{1/2}$).

$$U = \begin{bmatrix} 1 & \sigma & \sigma & \sigma & \sigma & \sigma^2 & \sigma^2 & \sigma^2\omega & \sigma^2\omega \\ 1 & a & a & a & a & b\sigma & b\sigma & b\sigma\omega & b\sigma\omega \\ 1 & a & a & a & a & b\sigma & b\sigma & b\sigma\omega & b\sigma\omega \\ 1 & a & a & a & a & b\sigma & b\sigma & b\sigma\omega & b\sigma\omega \\ 1 & a & a & a & a & b\sigma & b\sigma & b\sigma\omega & b\sigma\omega \\ 1 & b & b & b & b & c & c & cb\omega & cb\omega \\ 1 & b & b & b & b & c & c & cb\omega & cb\omega \\ 1 & b & b & b & b & c & c & cb\omega & cb\omega \\ 1 & b & b & b & b & c & c & cb\omega & cb\omega \end{bmatrix} \quad (3.15)$$

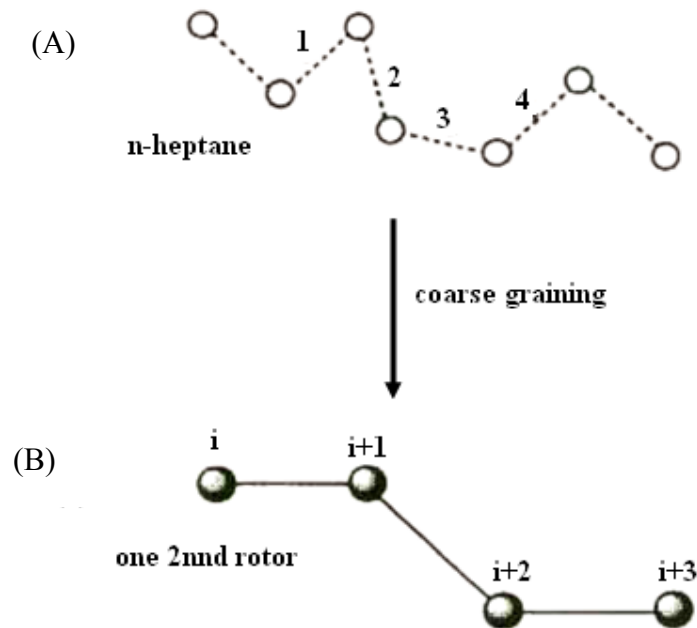


Figure 3.7 The coarse-grained of n-heptane with 4 rotors to a single rotor in 2nnd lattice: (A) n-heptane and (B) 2nnd chain equivalent to n-heptane.

Equation (3.15) can be reduced further because of the symmetry of the torsional potential energy (Rapold and Mattice, 1996).

$$U_{2nnd} = \begin{bmatrix} 1 & 4\sigma & 2\sigma\sigma & 2\sigma\sigma\omega \\ 1 & 4a & 2\sigma b & 2\sigma\omega b \\ 1 & 4b & 2c & 2c\omega \\ 1 & 4b & 2c & 2c\omega \end{bmatrix} \quad (3.16)$$

Here, the rows define the lengths of the vectors connecting beads i and $i+2$ in Figure 3.6 (B) and the columns define the lengths of the vectors connecting beads $i+1$ and $i+3$. This reduction means that the rotational isomeric states in 2nnd lattice can be categorized into four groups. The distances of 5.00 Å, 4.33 Å, 3.53 Å and 2.50 Å, which correspond to the local conformations of A: tt , B: $(tg+, tg-, g+t, g-t)$, C: $(g+g+, g-g-)$, and D: $(g+g-, g-g+)$, respectively show in Table 3.1. Equation

(3.16) can be condensed further to a 3×3 matrix with the modified indexing, A, B, and (C+D).

$$U_{2nd} = \begin{bmatrix} 1 & 4\sigma & 2\sigma^2(1+\omega) \\ 1 & 4a & 2b\sigma(1+\omega) \\ 1 & 4b & 2c(1+\omega) \end{bmatrix} \quad (3.17)$$

Table 3.1 Length of vectors connecting beads i and $i+2$ for coarse-grained PE model.

Category	Length in nm	Detailed conformation
A	0.500	tt
B	0.433	tg^+, tg^-, g^+t, g^-t
C	0.353	g^+g^+, g^-g^-
D	0.250	g^+g^-, g^-g^+

3.2.6 Long-range interaction

The incorporation of the rotational isomeric state model is not enough to describe the energetic of the melt system because the RIS model is a single chain model in the unperturbed state, ϕ state. The model only accounts for the short-range intermolecular interaction up to next nearest neighbor bonds on the 2nd lattice. For the remaining long-range intra molecular and intermolecular interaction, the Lennard-Jones pair potential, $u(r)$, seems to be a reasonable choice since there are only dispersive interactions in a polyethylene melt. Including the long-range interaction, the total energy which will be used in Metropolis evaluation will be

$$E_{total} = E_{RIS} + E_{LJ} \quad (3.18)$$

The continuous Lennard-Jones potential at the i th shell, u_i , is obtained from an averaged Mayer f -function which is used for describing the second virial coefficient of a non-ideal gas. The interaction parameter at the i th shell is defined through Equation (3.19)

$$\exp\left(-\frac{u_i}{k_B T}\right) - 1 \equiv \bar{f}_i \quad (3.19)$$

The average Mayer f -function at the i th shell, f_i , is obtained by integrating $u(r)$ over the cells in the i th shell.

$$\bar{f}_i = \frac{\int_{cell} f dr}{\int_{cell} dr} \quad (3.20)$$

$$f = \exp\left(-\frac{u(r)}{k_B T}\right) - 1 \quad (3.21)$$

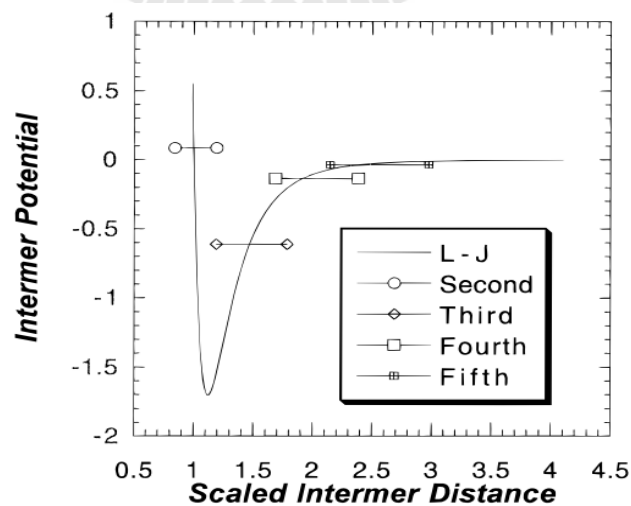


Figure 3.8 Lennard-Jones potential energy versus distance (Cho and Mattice, 1997b).

The set of the interaction parameters for 2nd beads is derived from the Lennard-Jones potential for an ethylene molecule ($\text{CH}_2=\text{CH}_2$). Table 3.2 gives a set of interaction parameters obtained by the averaging method.

Table 3.2 Non-bonded energy parameters for coarse-grained PE model on 2nd lattice.

E/K (K)	185
σ (nm)	0.44
u_1 (kJ/mol)	16.214
u_2 (kJ/mol)	0.731
u_3 (kJ/mol)	-0.623

3.2.7 Chain move

The single bead move is always employed in this study with the restriction that a chain cannot pass through itself, as in a self-avoiding random walk. A randomly chosen bead can move to a vacant site in the first shell when the attempt does not change the bond length to its two bonded neighbors. Local bead moves on the 2nd lattice are accepted according to the Metropolis MC algorithm which the probability of bead moving within a chain is given by

$$P_{move} = \min[1, P_{LR} / P_{new} / P_{old}] \quad (3.22)$$

where $P_{LR} = \exp(-\Delta E_{LR} / RT)$ is the probability from the change in the long-range interaction energy ΔE_{LR} , and P_{new} / P_{old} is the ratio of the probabilities for the new and old local conformations according to the short-range interaction. After

mapping the chains on this coarse-grained lattice, Dynamic MC Simulations were performed. One Monte Carlo step (MCS) is defined as a series of single bead move, in which all the beads in the system are randomly attempted once on average. A moving on lattice corresponds to displacement of two or three backbone atoms on the real PE chain. Even though the system equilibration is quite slow with the single bead move, the move provides the reliable dynamic properties at the time scale of MCS.

3.2.8 Applications of the method

The MC simulation on the high coordination lattice has proven to be quite successful to visit many polymer questions which show a large scale chain behavior based on the computational efficiency that comes from the lattice characteristic and the chemical details that come from the RIS characteristic. These include the successful mapping of the restoring of PE chains to the fully atomistic chains (Doruker and Mattice, 1997), the simulation of the dynamics of PE in the bulk state, the simulation of PE thin film (Doruker and Mattice, 1998a, b), the simulation of PE nanofibers (Vao-soongnern *et al.*, 2000), the structure formation in the crystallization and annealing of nanoparticles (Vao-Soongnern *et al.*, 2004) and the nanostructure of the grafted polymers (Vao-soongnern, 2006).

3.3 PE brush melt

Polymer brush is a molecule which attached one end of the chain to a solid interface or surface (de Gennes, 1980; Milner, 1991a; Zhao and Brittain, 2000). The ends can either be chemically attached (quite high binding energy) or physi-adsorbed

(binding energy of the order of $10 k_B T$) (Auroy *et al.*, 1992; Taunton *et al.*, 1990). The adsorbing, functional end could be a reactive group, or the immiscible block of a copolymer. In polymer brush, the chains are stretched away from the interface due to the high density of attachment points and any environment quality. In recent years, this polymer brush has been considerable interest in a number of technological applications such as lubricants, adhesives, biosensors and steric stabilization of colloidal suspensions (Lindberg and Elvingson, 2001).

Polymer brush has been interest of many experimental (Baker *et al.*, 2000; Kent *et al.*, 1996; Scheutjens and Fler, 1979; Schwartz *et al.*, 1992) and theoretical investigations (Kritikos and Terzis, 1976; Lai and Zhulina, 1992; Milner *et al.*, 1988a). However, there are some differences between the theoretical and experimental results. Because there are differences in assumptions, the theoretically assume strong stretching of the polymer chains in the brush, while it is hard for an experiment to achieve densities high enough for this strong stretching. Polydispersity is main factor in difference results (Amoskov and Birshtein, 2001; Chakrabarti and Toral, 1990; Lai and Zhulina, 1992). It is impossible to produce a perfectly monodisperse polymer brush in an experiment, almost no theoretical work has been done on the effect of polydispersity with a realistic size distribution.

Earliest theoretical study, most of the work mainly focus on the monodisperse brush (Murat and Grest, 1989; Zhao and Brittain, 2000), the simplest system to understand structure of polymer brush. However, in experimental situations, polydispersity has a great effect to the brush structure. This fact is an important motivation for theoretical studies of a polydisperse brush. The structure of the polydisperse brush has been theoretical studied (Birshtein *et al.*, 1990; Milner *et al.*,

1988b, 1989). Moreover, computer simulation also has used to study effect of polydispersity in polymer brush. A bimodal molecular weight distribution of short and long chain has often been used in simulations as a model system for polydispersity. The lattice MC simulation was carried out to study both monodisperse and bidisperse polymer brushes (Chakrabarti and Toral, 1990). However, only monomer density profile of one set of chain length and brush composition system was presented. Subsequently, the bidisperse brush have been studied by a bond-fluctuation model and compared with analytical self-consistent field (SCF) theory (Lai and Zhulina, 1992). The simulation results were fair agreed with SCF theory that the structural properties of the short chain depend very little on the length of the longer chain. The segregation structure of short and long chain leads to kink in the monomer density profile. Besides, the bidisperse system using a numerical self-consistent model in good solvent have been studied (Dan and Tirrell, 1993). The simulation results show that the longer chains were stretched more than the shorter chains. The segment density profiles of each system compressed together. A new numerical mean field theory was applied to investigate polydisperse polymer brushes both in dense and solution state (Kritikos and Terzis, 1976, 2005; Terzis, 2002). This new numerical mean-field theory gives very good agreement in prediction with experimental result. Moreover, it was applied with great success in similar polymer system. Recently, similar numerical self-consistent field theory that performed by Dan and Tirrel to study the structural properties of polydisperse polymer brush were widely used (Devos and Leermakers, 2009). The polydispersity of brush play an important role in brush properties. The average brush height was increased with increasing polydispersity, while the average

stretching decreased. This result affected the compression of shorter chain and the flower-like distribution of the longer chain fraction.

In this work, MC simulation of coarse-grained polymer model was applied to investigate bidisperse PE brush melt, the model for polydispersity polymer brush. The model comprises of a mixture of short and long chains and can be divided into two regions: the inner and the outer layer. The inner layer was contiguous to the surface and contains both short and long chain segments, while the outer layer was contained only segments of the long chains. Previously, this model has been used to study the structure of the monodisperse PE brush grafted onto a flat surface (Vao-soongnern, 2006). The agreement between simulations and the theoretical results was fine but there were some disagreement comparing the theory and the simulation of a realistic polymer chain.

3.3.1 Simulation detail

To model the PE chain in this section, bidisperse PE brush melts were performed on 2nnd, which was first introduced in 1995 (Rapold and Mattice, 1995b). One coarse-grained bead is representing by $-\text{CH}_2\text{CH}_2-$ repeating units of PE which is the number of site (n) in shell i th is $n = 10i^2 + 2$. This lattice was constructed by eliminating every second carbon atoms of the diamond lattice; making it is similar to the distorted cubic lattice with the same box angle in all three dimensions ($\alpha = \beta = \gamma = 60^\circ$) and step length is 0.25 nm. The coordination number increase is 12 which are identical to the closest packing of uniform hard sphere. In procedure, the brushes are randomly grafted or placed on plat surface. The grafting locations remain fixed during the simulation. Both short-range interactions based on the modified rotational

isomeric state (RIS) model and long-range interactions from a discretized form of the Lennard-Jones (LJ) potential energy function are included (Cho and Mattice, 1997a; Doruker and Mattice, 1997). The RIS formalism is used to model the local chain conformation for an unperturbed chain as the short-range intra molecular interactions of PE. The RIS model only considering the discrete rotational isomeric states with other internal coordinates frozen. So, it is not enough to describe the energetic of the melt system because it is a single chain model which only accounts for the short-range intermolecular interaction up to next nearest neighbor bonds on the 2nd lattice. This model consists of only two usual statistical weights (σ and ω) in statistical weight matrix with the step length of 0.25 nm on the 2nd lattice. The regular 9×9 statistical weight matrix can be reducing to the 3×3 extended statistical weight matrix. Length of vectors connecting beads i and $i + 2$ for coarse-grained PE model are presented in Table 3.1. In order to mimic the cohesive nature of realistic polymer in the bulk, long-range interactions between non-bonded building blocks of polymer chains are needed to incorporate by using the Lennard-Jones potential.

Table 3.3 Bidisperse PE brushes melts systems (N = chain length, n = chain number).

system	N_S	N_L	n_S	n_L
1	30	40	80	80
2	30	50	80	80
3	30	60	80	80
4	40	60	80	80
5	50	60	80	80

The bidisperse PE brush melt, each chain contain N ethylene units, with $30 < N_S < 50$ and $40 < N_L < 60$ detail in Table 3.3. The grafting density (σ) is fixed (1.85 nm^{-2}) and temperature was set at 509 K for all cases. The solid substrate was located at $z = 0$. Beads were not allowed to move from $z = 0$ to -1 . The total number of available surface sites is 40×40 (surface area = 86.6 nm^2). We choose periodic boundary conditions in the x and y directions, while the two boundaries in z direction are treated as hard impenetrable walls. Analysis is obtained as an ensemble average of the subsequent 10^7 MCS after equilibration. A snapshot is taken every 10,000 MCS for data analysis.

3.3.2 Results and discussion

Equilibration of the system was determined by evaluating the mean-square displacement of the center-of-mass, $g_{\text{cm}}(t)$ or the orientation autocorrelation functions (OACFS) using the end-to-end vector of the linear chain, $\langle R(t) \cdot R(0) \rangle$. The time for equilibration is the time required for the OACFS to fall to a constant value within a few million MCS. Besides, the $g_{\text{cm}}(t)$ reaches the mean-square radius of gyration $\langle R_g^2 \rangle$, $1,305.12 \text{ \AA}$. So, 10 million MCS were used to ensure equilibration and system properties were analyzed with an additional 10 million MCS.

- Density profile

The variation of the local melt density with distance from the solid interface for bidisperse PE brushes show in Figure 3.10 for an equimolar (50/50) mixtures of $N_S = C_{60}, C_{80}, C_{100}$ and $N_L = C_{120}$ and Figure 3.10(B) for $N_S = C_{60}$ mixed with $N_L = C_{80}, C_{100}, C_{120}$, respectively. Throughout this study, grafting density (σ) is

fixed at 1.85 nm^{-2} . From Figure 3.10, as N_S increases, the amplitude of $\rho_S(z)$ decrease and the distribution curves become broader. $\rho_L(z)$ are broader with lower density in the outer layer while there is little change for $\rho_L(z)$ in the inner region. The overall density decreased in the region closed to the wall and increased in the outer, resulting from the distribution of short chain is exposed more to the outer region of long chain profile. As N_L increases in Figure 3.11, $\rho_S(z)$ were slightly decreased while $\rho_L(z)$ were located away from the grafting point with higher and boarder profile. The outer regions are purely coexisting with long chains as had been pointed by other works (Dan and Tirrell, 1993; Kritikos and Terzis, 2005). This confirms the results from SCF prediction that the increase in N_L does not affect the short chains. The overall density becomes higher and flatter. This is due to the alignment of shorter chain in the inner layer and the long chains are stretched to the outer layer.

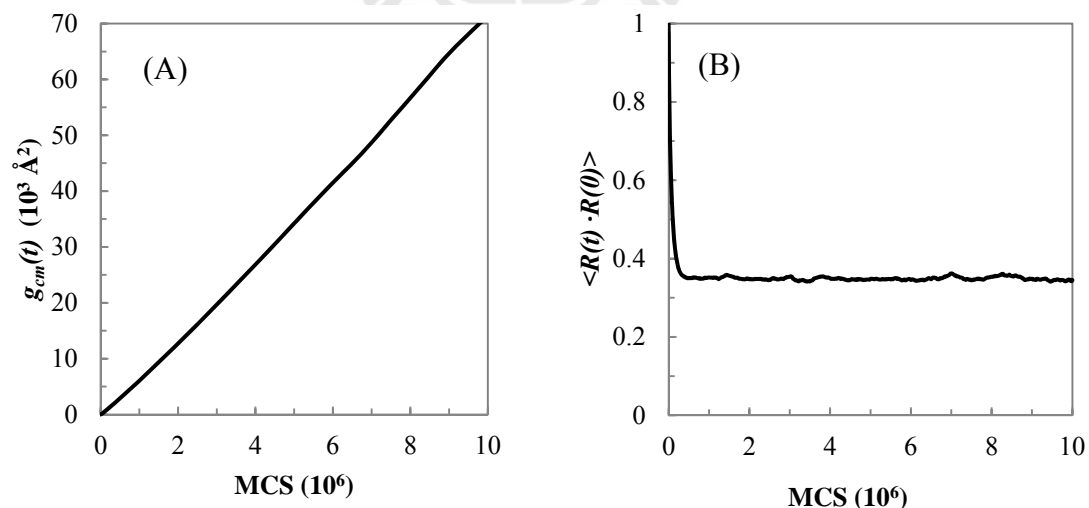


Figure 3.9 Evaluation the equilibrium; (A) by the mean-square displacement of the center-of-mass, $g_{cm}(t)$ and (B) by the orientation autocorrelation functions (OACFS) as the end-to-end vector of the linear chain, $\langle R(t) \cdot R(0) \rangle$.

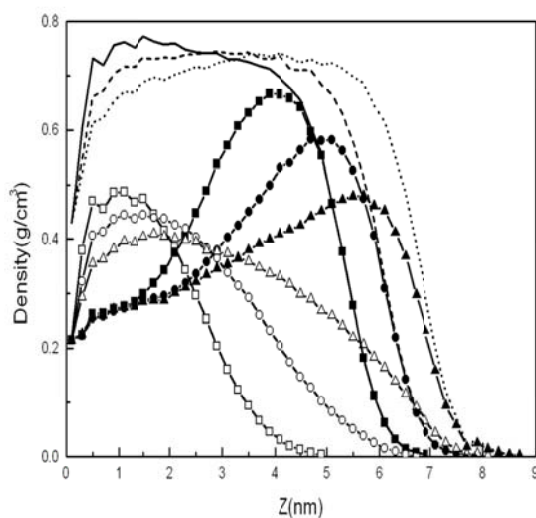


Figure 3.10 Density profiles of bidisperse PE brush at fixed long chain length. The density profile for short chains ($\rho_L(z)$) = (\square), (\circ), (\triangle), long chains ($\rho_S(z)$) = (\blacksquare), (\bullet), (\blacktriangle) and total ($\rho(z)$) = ($-$), ($--$), (\cdots) of $C_{60}+C_{120}$, $C_{80}+C_{120}$ and $C_{100}+C_{120}$, respectively.

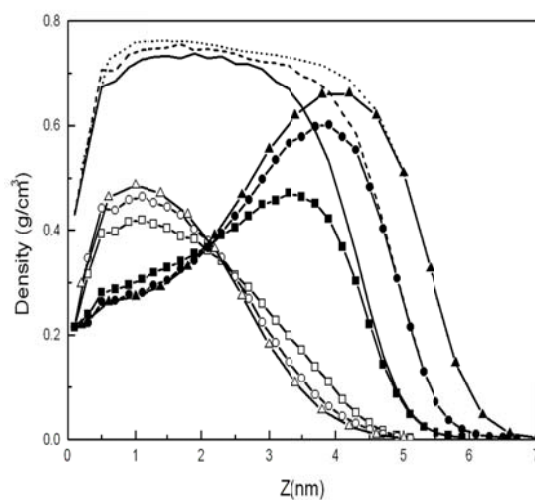


Figure 3.11 Density profiles of bidisperse PE brush at fixed short chain length. The density profile for short chains ($\rho_L(z)$) = (\square), (\circ), (\triangle), long chains ($\rho_S(z)$) = (\blacksquare), (\bullet), (\blacktriangle) and total ($\rho(z)$) = ($-$), ($--$), (\cdots) of $C_{60}+C_{80}$, $C_{60}+C_{100}$ and $C_{60}+C_{120}$, respectively.

- Conformational properties

The average trajectories $\langle z(i) \rangle$ *i.e.* the position of bead i above the wall in z direction are shown. The profiles for the short and long chains are changed, but in a different direction. From Figure 3.12 when N_S is varied, both shorter and longer chain trajectories were more extended. In contrast, if N_L is varied in Figure 3.13, the trajectories of the long chains were stretched whereas the short chains were compressed. This result confirms that in the presence of longer chains, the short chains are compressed. The bidisperse of not much different between the short and long chains length, the chains were interacted each other making both short and long chains were stretched together.

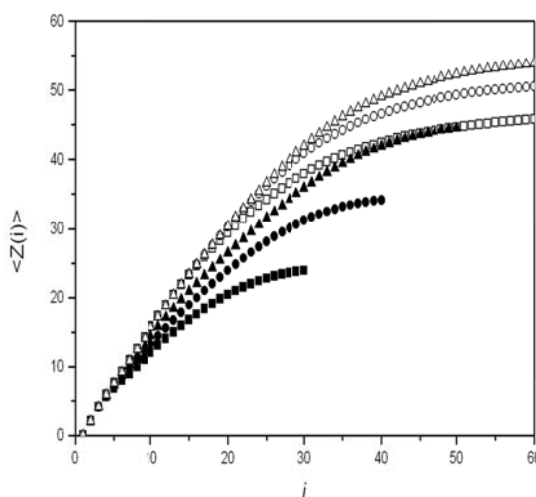


Figure 3.12 Average position of the i th monomer of each chain in bidisperse PE at fix long chain length. The filled (■), (●), (▲) and opened (□), (○), (△) symbols refer to short and long chains of $C_{60}+C_{120}$, $C_{80}+C_{120}$ and $C_{100}+C_{120}$, respectively.

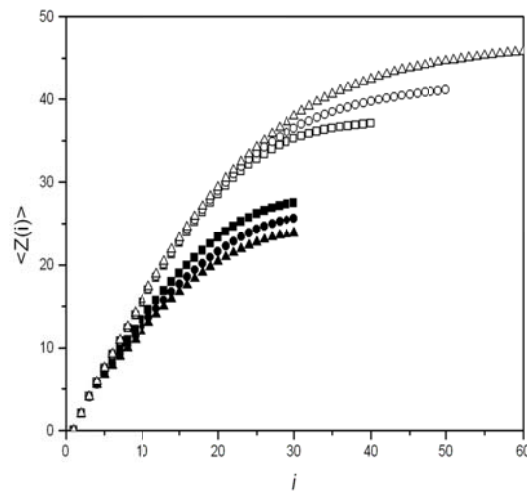


Figure 3.13 Average position of the i th monomer of each chain in bidisperse PE at fixed short chain length. The filled (■), (●), (▲) and open (□), (○), (△) symbols refer to short and long chains of $C_{60}+C_{80}$, $C_{60}+C_{100}$ and $C_{60}+C_{120}$, respectively.

- Bond orientation

Figure 3.14 and 3.15 show the bond orientation of the brush with varying chain composition. From Figure 3.14, as N_S increases, the short chains are more stretched. The long chains are stretched only the middle portion ($15 < i < 45$). Figure 3.15 shows compression of the short chains with increasing N_L . That means the local stretching of the short chains was resided in the inner layer and greatly affected by an enhanced stretching of the long chain in the outer layer. The long chains are more favorable to locate in the outer layer. Thus the portion of longer chain in the inner layer is more stretching, making more room for shorter chain to alignment.

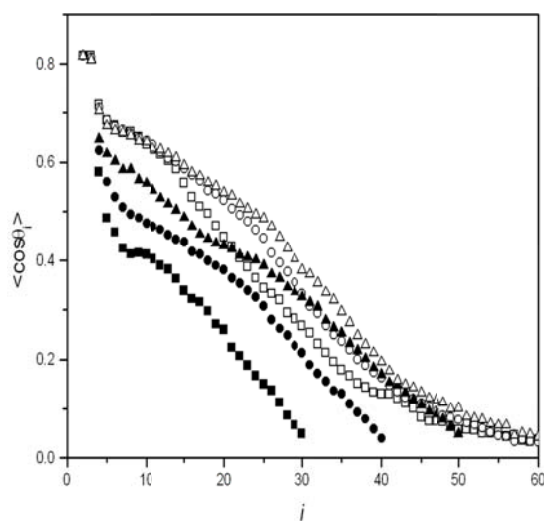


Figure 3.14 Plot of the projection $\langle \cos\theta_i \rangle$ of the local orientation chord vector versus the position of the i th bond along the chain of each chain in bidisperse PE at fix long chain length. The filled (■), (●), (▲) and opened (□), (○), (△) symbols refer to short and long chains of $C_{60}+C_{120}$, $C_{80}+C_{120}$ and $C_{100}+C_{120}$, respectively.

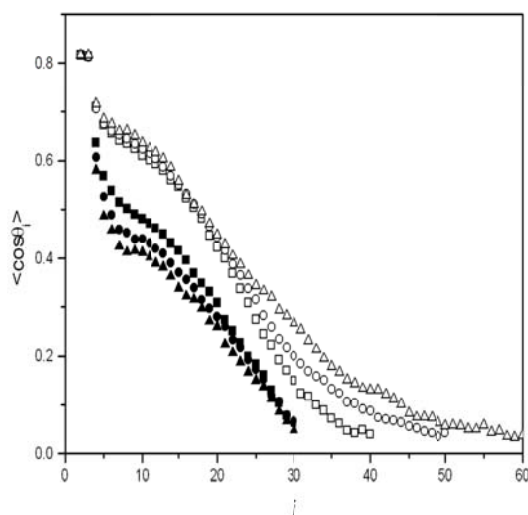


Figure 3.15 Plot of the projection $\langle \cos\theta_i \rangle$ of the local orientation chord vector versus the position of the i th bond along the chain of each chain in bidisperse PE at fix short chain length. The filled (■), (●), (▲) and opened (□), (○), (△) symbols refer to short and long chains of $C_{60}+C_{80}$, $C_{60}+C_{100}$ and $C_{60}+C_{120}$, respectively.

- **Bead distribution**

The bead distribution $\rho_{E(z)}$ plays an important role in polymer brush theory. This property shows large fluctuation which is proportional to the chain length. Therefore, it is of interest to investigate how the end beads are distributed in the bidisperse polymer brush. Figure 3.16 and 3.17 display the end bead distribution for varying short and long chain length, respectively. As shown in Figure 3.16, as N_S increases, $\rho_{E,S(z)}$ and $\rho_{E,L(z)}$ become broader and the peak maxima are shifted to larger z indicating more end beads from both short and long chain to segregate at the free surface. As N_L increases with fixed N_S in Figure 3.17, the situation is similar, except for distribution of the end beads of short chains increase while for the long chains decrease near the grafting point. SCF theory predicts that $\rho_{E,S(z)}$ should be identical with varying N_L . The agreement with the SCF results for $\rho_{E,L(z)}$ is quite good but is less satisfactory for short chains. The simulation result revealed chain end interpenetrations, by that, the penetration of the short chain ends into the outer layer is larger than that of the long chain ends in the inner layer. This is because the maximum of end bead distribution profile for short chains $\rho_{E,S(z)}$ is located close to the boundary between the two layers. Hence a considerable amount of shorter chain ends are able to penetrate into the outer layer. On the contrary, end bead distribution of long chains $\rho_{E,L(z)}$ is far from this boundary and only a small fraction of longer chain ends is located in the vicinity of the boundary. Hence penetration of long chains into the inner layer is less probable and decreases with increasing chain length.

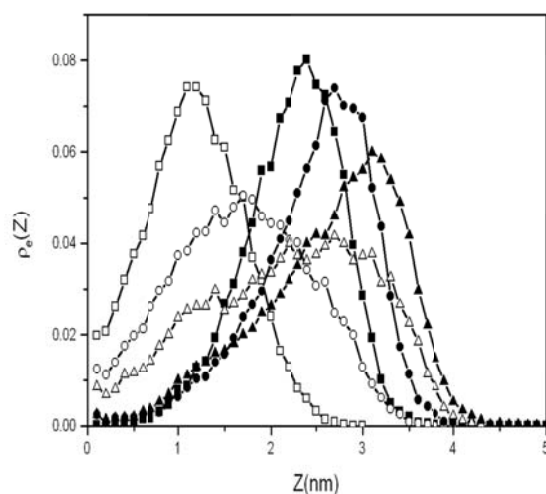


Figure 3.16 End bead distribution of each chain in bidisperse PE at fixed long chain length. The opened (\square), (\circ), (Δ) and filled (\blacksquare), (\bullet), (\blacktriangle) symbols refer to short and long chains of $C_{60}+C_{120}$, $C_{80}+C_{120}$ and $C_{100}+C_{120}$, respectively.

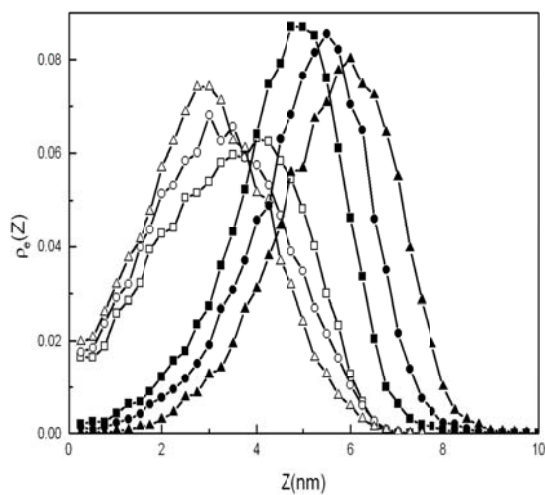


Figure 3.17 End bead distribution of each chain in bidisperse PE at fixed short chain length. The opened (\square), (\circ), (Δ) and filled (\blacksquare), (\bullet), (\blacktriangle) symbols refer to short and long chains of $C_{60}+C_{80}$, $C_{60}+C_{100}$ and $C_{60}+C_{120}$, respectively.

3.3.3 Summary

The MC simulation was applied to study the effect of polydispersity on bidisperse polymer brush which is composed of a mixture of short and long chains. The simulation results reveal that, as N_S increases at constant N_L , both short and long chains are affected. On other hand, as N_L is increased, the short chains are more compressed in the inner layer whereas the long chains are more stretched to the outer layer. Strong difference in bead distribution can cause two main features of the bimodal brushes *i.e.* vertical segregation and the difference of local degree of stretching between long and short chains. In addition, end bead distribution show an interpenetration of the short chain ends into the outer layer.

3.4 Monte Carlo simulation of PEO brush on 2nd lattice

3.4.1 PEO Model

MC technique was performed build on the Metropolis algorithm of a coarse-grained PEO chains ($\text{CH}_3\text{O}-[\text{CH}_2\text{CH}_2\text{O}]_n\text{CH}_3$) on a high coordination lattice. Each occupied site contains either $-\text{CH}_2\text{CH}_2-$ or $-\text{CH}_2\text{O}-$ units connected by coarse-grained bonds of length 2.39 Å. In this case, either one of CH_2 groups is represented as a single united atom as well as O atoms. Every second bead on the main backbone, regardless of C or O, is taken out, and the remainder of united atoms is connected. Every single bead has to be treated identically. There is no difference between C-O and C-C contacts in terms of the long-range interactions, but there exist a bit of ambiguity regarding the short-range interactions. On this lattice, the angle between any two axes along the sides of the unit cell is 60° , and the lattice sites are identical to

the hexagonal packing of hard spheres. When the melt density of PEO is simulated at 373 K, the lattice has occupancy only about 20%. The torsional angles are restricted to *trans* and two *gauche* states.

3.4.2 Hamiltonian

The Hamiltonian of the system contains of both short-range intra molecular interactions and long-range intra- and intermolecular interactions that were introduced into the current simulations. The short-range intra molecular interactions resulting from the local chain conformation are based on a RIS model for the unperturbed chain, which incorporates the influence of partial charges. The RIS model for poly(A-A-B) chains with A = -CH₂- and B = -O-, in which all bonds are subject to a symmetric 3-fold torsion potential with the nearest neighbor interdependence, is given by the following three statistical weight matrices for three successive bonds of type A-A, A-B, and B-A.

$$U_{AA} = \begin{bmatrix} 1 & \sigma_{BB} & \sigma_{BB} \\ 1 & \sigma_{BB} & \sigma_{BB}\omega_{AB} \\ 1 & \sigma_{BB}\omega_{AB} & \sigma_{BB} \end{bmatrix} U_{AB} = \begin{bmatrix} 1 & \sigma_{AA} & \sigma_{AA} \\ 1 & \sigma_{AA} & \sigma_{AA}\omega_{AB} \\ 1 & \sigma_{AA}\omega_{AB} & \sigma_{AA} \end{bmatrix} U_{BA} = \begin{bmatrix} 1 & \sigma_{AA} & \sigma_{AA} \\ 1 & \sigma_{AA} & \sigma_{AA}\omega_{AA} \\ 1 & \sigma_{AA}\omega_{AA} & \sigma_{AA} \end{bmatrix} \quad (3.23)$$

In the matrices, the rows and columns define the states of bonds $i - l$ and i , respectively. The three accessible rotational isomeric states for each bond are t , $g+$, and $g-$. The σ_{AA} and σ_{AB} are the statistical weights for the C-C and C-O type first-order interactions, which result from the rotational degree of freedom of the middle bond in a three-bond unit, and ω_{AA} and ω_{AB} represent the C-C and C-O type

second-order interactions for $g^{\pm}g^{\mp}$ state in the middle of a four-bond unit with two rotational degrees of freedom.

Four distinct states on the 2nd lattice for PEO can be defined by considering the length of the segment between every other bead on this lattice. The average bond length of PEO is closer to 1.47 Å. The states of the detailed chain that cannot be distinguished on the 2nd lattice are grouped together and their statistical weights are averaged in order to obtain 4×4 matrix, where the rows and columns represent the four states of the segments connecting beads (i and $i+2$) and ($i+1$ and $i+3$). These four states include the conformations on diamond lattice and lengths of segment connecting bead i and $i+2$ on the 2nd lattice are presented in Table 3.4.

Table 3.4 Four states include the conformations on diamond lattice and lengths of segment connecting bead i and $i+2$ on the 2nd lattice

State on 2nd lattice	Conformations on diamond lattice	Lengths of segment connecting bead i and $i+2$ on the 2nd lattice*
A	tt	4.80
B	$tg^+, tg^-, tg^+, g^+t, g^-t$	4.15
C	g^+g^+, g^-g^-	3.40
D	g^+g^-, g^-g^+	2.40

*The average bond length for PEO is closer to 1.47 Å.

Geometric averaging of statistical weights of indistinguishable states leads to the following coarse-grained statistical weight matrix, with $\sigma = (\sigma_1\sigma_2)^{1/2}$, $\omega_1 = \omega_{AA}$ and $\omega_2 = \omega_{BB}$.

$$U_{2nd}^G = \begin{bmatrix} 1 & 4\sigma & 2\sigma^2 & 2\sigma^2\omega_2 \\ 1 & 4\sigma\omega_1^{1/8} & 2\sigma^2\omega_1^{1/4} & 2\sigma^2\omega_1^{1/4}\omega_2 \\ 1 & 4\sigma\omega_1^{1/4} & 2\sigma^2\omega_1^{1/2} & 2\sigma^2\omega_1^{1/2}\omega_2 \\ 1 & 4\sigma\omega_1^{1/4} & 2\sigma^2\omega_1^{1/2} & 2\sigma^2\omega_1^{1/2}\omega_2 \end{bmatrix} \quad (3.24)$$

The geometric mean has led to more satisfactory results than the arithmetic average. These 4x4 matrices can be further reduced in dimensions to 3×3 , by suitable combination of the last two rows and columns.

3.4.3 RIS parameters of PEO model from electronic structure calculation

The geometries and conformational energies of model segment of PEO can be obtained from electronic structure calculations and used to determine the statistical weight parameters in a RIS chain. Dimethylethane (DME) was selected as a representative model for PEO. The energy of *gauche* conformation of the O-C-C-O bond relative to the *trans* conformation depends strongly not only on the basis set size but also on electron correlation effects. Geometries and conformational energies of nine rotamers of DME compound were optimized at HF/6-311+G* and D95** level. The energies for electron correlation effect for each conformer were estimated by MP2 calculation with the same basis set. Statistical weights (Boltzman populations) of each conformer are readily calculated based on the relative electronic energy and degeneracy of each conformation. *Ab initio* calculation yield 70 energetic relative to the *ttt* conformer and the *tgg* and *tgg'* energies are relative to *tgt* energies. The *tgg'*

state is much more favorable, which is indicated by the RIS model, and thereby accounting for the prediction of a relatively high population of $tgg+$, tgg' state. The tgg' conformer appears to be the result of strong attractive interactions between an O atom and a hydrogen on the opposite methyl group. One may introduce the effect of the O-H attractions in the second-order RIS model by changing the second-order interaction parameter E_ω . The second-order model takes into account interactions between atoms or groups separated by a maximum of four bonds and hence two consecutive torsions. Using values of $E_\sigma = 100$, $E_\rho = 1400$, $E_\omega = -1300$ and $E_{\omega\omega} = 1300$ cal/mol for example, one can represent the energies of eight of the ten DME conformers, including tgg' reasonably well as indicated in Table 3.5. The ggg conformer cannot be successfully described by the second-order RIS model, due probably to attractive interactions between the oxygen lone pair electrons and methyl hydrogen atoms and alleviation of repulsive lone pair interactions. These considerations point to the necessity of including the interactions between atom and groups separated by five bonds and hence three consecutive torsions into the RIS model. Nevertheless, such a third-order RIS model contributes insignificant difference for the conformational characteristics for the coarse-grained PEO chains. The simplification of the two-state RIS model adopted in the current simulation should thus be justified for the purpose at hand.

Table 3.5 RIS model of PEO from *ab initio* calculation of DME model compound.

Conformer	RIS Representation	<i>Ab initio</i> energy (kcal/mol)	RIS Energy
<i>ttt</i>	0	0.00	0.0
<i>tgt</i>	σ_{OO}	0.14	0.1
<i>ttg</i>	σ_{CC}	1.43	1.4
<i>tgg</i>	$\sigma_{OO} + \sigma_{CO}$	1.51	1.5
<i>tgg'</i>	$\sigma_{OO} + \sigma_{CO} + \omega_{CO}$	0.23	0.2
<i>gtg</i>	$2\sigma_{CC}$	3.13	2.8
<i>gtg'</i>	$2\sigma_{CC}$	3.08	2.8
<i>ggg'</i>	$\sigma_{OO} + 2\sigma_{CC} + \omega_{CO}$	1.86	1.6
<i>g'gg'</i>	$\sigma_{OO} + 2\sigma_{CC} + 2\omega_{CO}$	2.41	0.3
<i>ggg</i>	$\sigma_{OO} + 2\sigma_{CC}$	1.64	2.9

Parameter set are $\sigma_{OO} = 0.1$, $\sigma_{CC} = 1.4$ and $\omega_{CO} = -1.3$ kcal/mol.

3.4.4 Long-range interaction of PEO model

The local chain conformation for an unperturbed chain is determined by the short-range interactions as detailed above similar to PE model. In order to mimic the cohesive nature of realistic polymer in the bulk, long-range interactions between non-bonded building blocks of polymer chains are needed. For the remaining long-range intramolecular and intermolecular interaction, the Lennard-Jones (LJ) pair potential, $u(r)$, seems to be a reasonable choice. Including the long-range interaction, the total energy which will be used in Metropolis evaluation will be

$$E_{total} = E_{RIS} + E_{LJ} \quad (3.25)$$

The long-range interactions are obtained from a discretized form of the Lennard Jones (LJ) potential, in which the second virial coefficient (B_2) for polymers is evaluated similar to a nonideal gas using the Mayer f function according to the imperfect gas theory as follows:

$$B_2 = \frac{1}{2} \int \{\exp[-\beta u(r)] - 1\} d\mathbf{r} = \frac{1}{2} \int f d\mathbf{r} \quad (3.26)$$

where $\beta = 1/kT$, f is the Mayer function and $u(r)$ is the interparticle LJ potential of the form

$$u = \begin{cases} \infty & r < 2.39 \text{ \AA} \\ u_{LJ} = 4\varepsilon \left[\left(\frac{\sigma}{r}\right)^{12} - \left(\frac{\sigma}{r}\right)^6 \right] & r \geq 2.39 \text{ \AA} \end{cases} \quad (3.27)$$

where ε and σ are known as the well depth and the collision diameter, respectively as point in Figure 3.8. R is the spacing between two interacting beads, and the cut-off distance for PEO is 2.39 Å. On the 2nd lattice, B_2 is written in a discretized form by separating the intergral into the subintergrals for each lattice cell and regrouping them for each neighbor.

The LJ parameters for two backbone atoms of PEO are not available since the pairs of two backbone atoms are not always same. Two different methods were used to estimate the ε and σ values. The σ value is obtained by first noting that for propane is within 1% of $(3/2)^{1/3} \sigma_{ethane}$. Therefore, the required value for a PEO coarse-grained bead can be estimated from the data for methyl ether ($\text{CH}_3\text{-O-CH}_3$, $\sigma = 4.307 \text{ \AA}$) as

$$\sigma_{PEO} = (2/3)^{1/3} \sigma_{methyl\ ether} \quad (3.28)$$

which $\sigma_{\text{PEO}} = 3.76 \text{ \AA}$. The ϵ for two backbone atoms of PEO were estimated by fitting the experimental bulk density of PEO at a suitable temperature from a series of simulations of free-standing PEO thin films that have different values. Thin film is formed by increasing the periodic length of the simulation box in one direction about three times the original size. The image of each parent chain that is retained for the subsequent film simulation is the one with the most beads lying within original box along the z axis. This procedure eliminates the interaction of the parent chains with their images in the z direction; *i.e.*, the periodic boundary conditions are effective only in the remaining two directions. With this method, LJ parameters at the simulated temperature 373 K are: $\sigma_{\text{PEO}} = 3.76 \text{ \AA}$ and $\epsilon/kB = 154 \text{ K}$. Discretization of this LJ potential produces the long-range interaction energies. For example, the parameters for the first five shell of PEO at 373 K are 8.113, -0.213, -0.339, -0.067 and -0.017 kJ/mol. The first shell has a strongly repulsive interaction because the distance between two beads on the lattice, 2.39 \AA , is smaller than the value of σ in the LJ potential. The second and third shell has large attractive interaction, which leads to the cohesive nature of the bulk. Shells beyond the third have a weaker attraction, which plays little effect. Hence, only the first three shells are generally applied to speed up the simulation. These parameters yield a cohesive structure with a bulk density that most closely matches the experimental density of 1.06 g/cm^3 . The Non-bonded energy parameters for coarse-grained PEO model on 2nnd lattice simulation are summarized in Table 3.6.

Table 3.6 Non-bonded energy parameters for coarse-grained PEO model on 2nd lattice simulation.

Category	Length (nm)
ϵ (K)	154
σ (nm)	3.76
u_1 (kJ/mol)	8.113
u_2 (kJ/mol)	-0.213
u_3 (kJ/mol)	-0.339

3.4.5 The implicit model for solvent quality for PEO in solution

In order to study the effect of solvent quality on the structural and conformational properties of PEO system, the attractive portion of LJ potential which describes the pair-wise interaction of the coarse-grained PEO beads were adjusted. Generally, to define the energy shell in simulation the first three discretized shell energy of LJ potential were used. This first three energy values at 373 K are 8.113 kJ/mol, -0.213 kJ/mol and -0.339 kJ/mol, which were denoted as u_1 , u_2 and u_3 , respectively. The u_1 is strongly repulsive because the step length on the high coordination lattice. The higher energy shells have attractive value.

In this simulation, we assume only attractively energy can be affected by changing the solvent quality. Making the u_1 value is retained at 8.113 kJ/mol⁻¹ in all simulation, while the higher energy shells were changed with the quality of solvent. So, the effect of solvent on PEO structure can be studied by reassigned the

energies shell according to following equation as has been pointed in the previous report (Xu *et al.*, 2004)

$$u_{s1} = u_{1m}, \quad (3.29)$$

$$u_{s2} = ku_{2m}, \quad (3.30)$$

$$u_{s3} = ku_{3m}, \quad (3.31)$$

The assignment of mimic solvent quality in this simulation called “implicit solvent”. The subscriptions “*s*” and “*m*” are the shell energy assigned for polymer in the implicit solvent and the shell energy for the PEO melt, respectively. The “*k*” value is a designed number to define solvent to good, theta (θ) or poor. To calibrate the value, Flory’s hypothesis that the mean square dimension of polymer in the melt and in the dilute solution in theta state are the same. Base on above hypothesis, Xu and his co-worker have simulated a single isolated PEO chain, represented by 100 coarse-grained beads, as a function of the numerical value of *k* and 100 coarse-grained beads in the melt at 373 K in the absence of solvent. They was compared the mean square radius of gyration of that two systems. The vertical arrow in the figure shows the value of $k = 0.63$ that causes the isolated chain to have the same dimensions as the chains in the dense melt as shown in Figure 3.18.

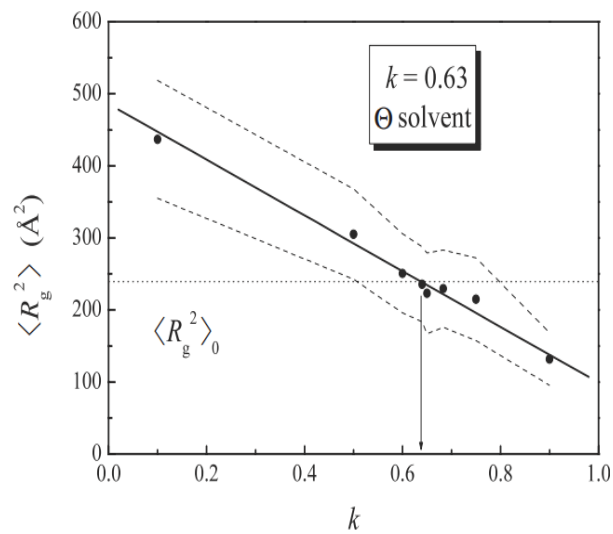


Figure 3.18 Comparison mean square radius of gyration $\langle R_g^2 \rangle$ of a single isolated PEO chain as a function of the numerical value of k (point data) and 100 coarse-grained PEO beads (horizontal dashed line) (Xu *et al.*, 2004).

The k value has been validated by the relation $\langle R_g^2 \rangle \sim (N-1)^{2\nu}$, the obtained ν values were quite close to the expectation for good, θ and poor solvent. So, the k value is corresponding to the quality of solvent are:

- Dilute solution in θ solvent when $k = 0.63$,
- Dilute solution in good solvent when $k > 0.63$ and
- Dilute solution in poor solvent when $k < 0.63$.

3.4.6 PEO chain move

Single bead and pivot move were used in order to improve the simulation efficiency. In a pivot move, bond vectors for a subchain of the original conformation were reversed to create a new configuration. A subchain with two to six

beads was applied for pivot moves. The moves are accepted or rejected according to the Metropolis criterion:

$$P_{move} = \min(1, P_{LR} P_{new} / P_{old}) \quad (3.32)$$

where $P_{LR} = \exp(-\Delta E_{LR} / RT)$ is the probability from the change in the long-range interaction energy (ΔE_{LR}), and P_{new} / P_{old} is the ratio of the probabilities for the new and old local conformations according to the short-range interaction. In this simulation, one MCS is defined as a series of single bead move, in which all the beads in the system are randomly attempted once on average. A moving on lattice corresponds to a displacement of two or three backbone atoms on the real PEO chain. The moves are accepted if they are generating a lower energy configuration. Otherwise, a move is accepted with the probability of P_{new}/P_{old} *i.e.* with Boltzman factor representing the degree of increase in the conformation energy. Details on the calculations of conditional probabilities and the application of the Metropolis algorithm have been described in previous publication. For every Monte Carlo step (MCS), single bead moves and multiple bead moves were performed randomly. Every bead was tried once, on average, in both single and pivot moves. Therefore, a move of every bead was attempted twice, on average, within one MCS. Moves that cause double occupancy and collapses, which were caused by the overlap of backbone atoms after reverse-mapping to the fully atomistic description, have been prohibited. The Metropolis criteria were applied to determine whether the move is made or not.

3.5 PEO brushes in melt and solution state

3.5.1 Simulation detail

In the simulations of PEO brush on a flat wall, random configuration of PEO chains were generated by mapping PEO beads on 2nd lattice with an application of periodic boundary conditions in all three directions (xyz). The solid substrate was located at $z = 0$ and $z = M$, where $M > N$ (N was denoted as chain length of polymer brush). The beads were not allowed to move from $z = 0$ to -1 . The total number of available surface sites is 40×40 lattice units (surface area = 86.6 nm^2). We choose periodic boundary conditions in the x and y directions, while the two boundaries in z direction are treated as hard impenetrable walls. The systems were equilibrated for 10^7 MCS and the latest conformation was run additional 10^7 MCS for subsequent data analysis.

The systems of PEO brushes are shown in Table 3.7. The effect of both grafting density and solvent quality were studied for mono- and bidisperse brushes. The qualities of solvent are classified to good, theta (θ) or poor by reassigned the shell energies u_2 and u_3 with difference k values, while the u_1 was fixed. The used energies for each shell were described in Table 3.8.

3.5.2 Results and discussion

The effect of grafting density on monodisperse PEO brush

In order to study the effect of grafting density on the brush properties of monodisperse PEO, the B40n80, B40n120 and B40n160 were simulated. When B

and n are the number of bead and chain length, respectively. The data analyses of final conformation were obtained as an ensemble average.

Table 3.7 Investigated systems of PEO brush (N = chain length, n = chain number).

system	N_S	N_L	n_S	n_L
1	20	30	80	80
2	20	40	80	80
3	30	50	80	80
4	40	-	80	-
5	40	-	120	-
6	40	-	160	-
7	40	60	80	80

Table 3.8 The first three energies shell (kJ/mol) for the interaction of beads in the simulation.

Solvent quality	u_1	u_2	u_3
Good ($k=0.20$)	8.113	0.043	0.068
Theta ($k=0.63$)	8.113	-0.134	-0.214
Poor ($k=0.80$)	8.113	-0.170	-0.271

- Equilibration

MC simulation for the largest system *i.e.* B40n160 brush on 2nd lattice was performed. Equilibration of the systems was determined in the same way

as described in the previous PE brush system. From Figure 3.19, the $g_{cm}(t)$ reaches their $\langle R_g^2 \rangle$ at 1,261.54 (± 582.63) Å within 6×10^6 MCS, the molecules have translated away from their initial positions. Moreover, the result demonstrated constant OACF was found within 6×10^6 MCS due to constrain effect of the grafting point. In this work, 10^7 MCS were used to ensure the equilibration.

- Local density profile

Figure 3.20 illustrates the variation of local density profile ($\rho(z)$) as a function of the distance from the solid wall for monodisperse PEO brushes for each grafting density (σ) at constant chain lengths $N = 40$. The filled square, filled triangle and filled circle symbol in graph represent the density profile of PEO brush at $\sigma = 0.92$ (80 chains), 1.39 (120 chains) and 1.85 nm^{-2} (160 chains), respectively. From this figure, the maximum ($\rho(z)$) are appeared near the grafting wall for all values of σ , this phenomena is the same as previous report (Chakrabarti and Toral, 1990; Milner, 1991b). Shape of curves can be approximated by a parabolic form for lower σ whereas the profiles are grown in step away from the solid wall as a function of σ as proposed by the scaling theory and SCF theory. The $\rho(z)$ were increased from 1.13 to 1.18 g/cm^3 and become broader with increasing σ from 0.92 to 1.85 nm^{-2} . It was good agreement with other works that the $\rho(z)$ of brushes is depended on σ . At high σ , the profiles become flatter rather than a parabola shape (Murat and Grest, 1989). This implies that more portions of monomer are sit near the grafting wall and the polymer brush height increase. These results are difference from previous study (Vao-soongnern, 2006) which was found that the bulk region of brush was independent

with σ . However, some works were said that the depletion zone close to the surface is except for the large molecules (Lindberg and Elvingson, 2001).

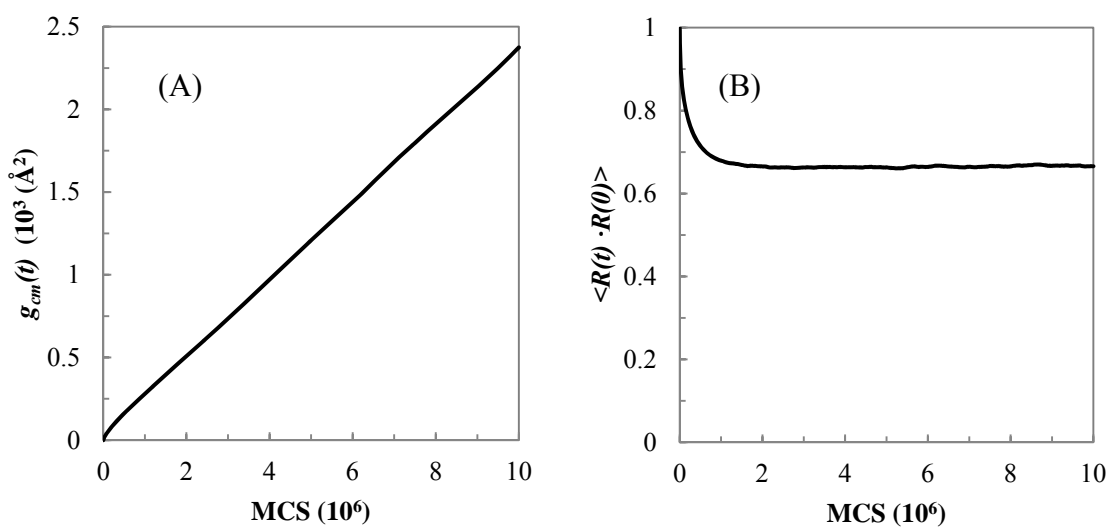


Figure 3.19 Evaluation the equilibrium; (A) by the mean-square displacement of the center-of-mass, $g_{cm}(t)$ and (B) by the orientation autocorrelation functions (OACFS) as the end-to-end vector of the linear chain, $\langle R(t) \cdot R(0) \rangle$.

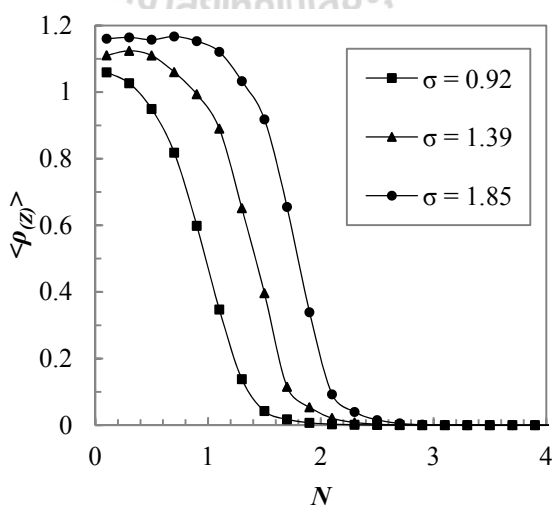


Figure 3.20 Local density profile ($\rho(z)$) as a function of distance from solid interface of monodisperse PEO brush.

- Conformation properties

Figure 3.21 shows the average chain conformational in term of the reduced mean height $\zeta(s) = \langle z(i) \rangle / \langle z(N) \rangle$ as a function of coordinate i/N for the effect of grafting density on PEO brush properties, where $\langle z(i) \rangle$ is average height of backbone atom i . The straight line is the data point from SCF prediction. The analytical brush theories proposed that σ should not affect conformation properties of all case. In the figure, all curves are grouped to a single curve under relation of $\zeta(s)$ a function of i/N . Chain trajectories of PEO brushes are more extended as a function of σ similar previous work (Vao-soongnern, 2006). The difference between simulation result and analytical theory is due to the fact that an analytical theory is based on the most probability trajectories, while the simulation base on the ensemble average over all conformation of the chains. Moreover, there is more chemical detail in this molecular model of simulation method than that in SCF or scaling theory.

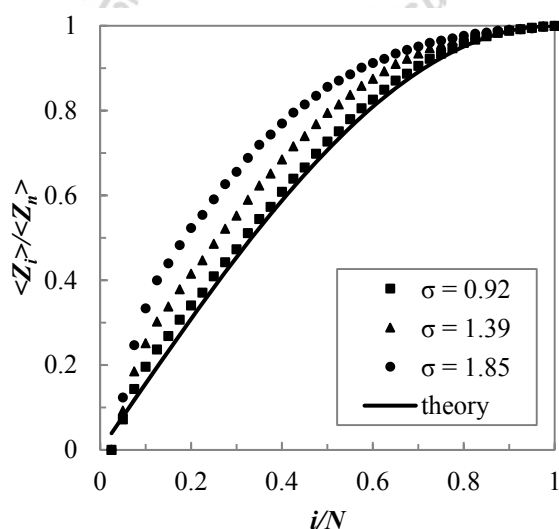


Figure 3.21 The normalized mean height $\zeta(s)$ as a function of normalized bead coordinate along chain contour of monodisperse PEO brush.

- Bond orientation

Figure 3.22 presents the local stretching of each i th monomer designed by $\langle \cos\theta_i \rangle$ as a function of the position of the i th bond along the chain, for PEO brush system of varying σ . The obtained results are in contrast with the SCF theory in which predicts σ was no effect to the bond stretching, except for near the solid substrate ($i < 5$) and the free surface region ($i > 35$). From the figure, as σ increases, the brushes are increasingly more stretched along the interface in the portion $5 < i < 35$ of the chain. This observation implies that the local stretching for the middle part of PEO chains through the outer region is greatly affected by an enhancing of chain numbers in brush due to no more space for chain to align.

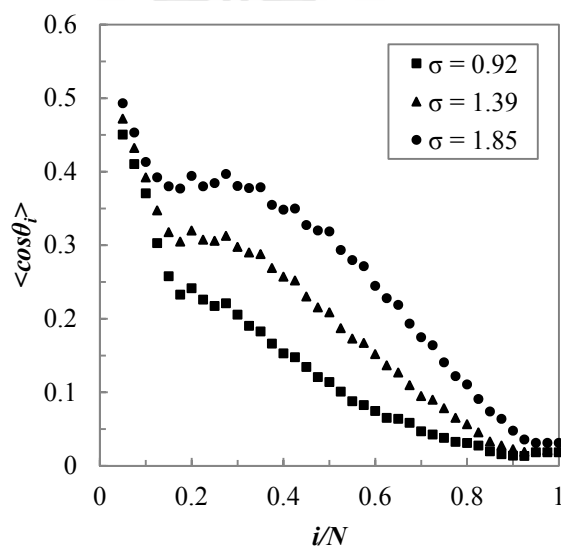


Figure 3.22 Bond orientation of i th monomer $\langle \cos\theta_i \rangle$ as a function of the position of the i th bond along the chain of monodisperse PEO brush.

- Bead distribution

An important property as predicted in polymer brush theory is the bead distribution $\rho(z)$. This property shows large fluctuation which is proportional to the chain length. Therefore, it is of interest to investigate how the beads are distributed in the system with different grafting coverage. Figure 3.23 displays the middle ($\rho_m(z)$) and end ($\rho_E(z)$) bead distribution for each σ . Both middle and end beads were found everywhere in the brush. The distributions look like the uniformly Gaussian distribution for low σ , but they exhibit a decreasing of peak amplitude and were shifted away from the wall at larger z as σ was increased. This indicated more beads segregation at the free surface with increasing σ .

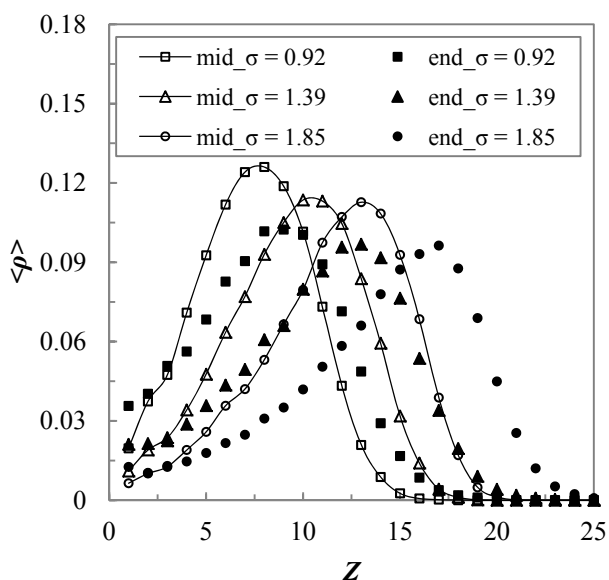


Figure 3.23 The middle ($\rho_m(z)$) and end ($\rho_E(z)$) bead distribution as a function of Z of monodisperse PEO brush.

The effect of solvent quality on monodisperse PEO brush

- Local density profile

Figure 3.24 illustrates the local density profile ($\rho(z)$) as a function of the distance from solid wall of PEO brush (B40n160) under different quality of solvent. Three different solvent qualities as poor, theta and good solvent were assigned. In the course of simulation, the density profiles were strongly depended on the solvent quality which a maximum peak shown very close to the grafted wall in all solvent conditions. The profiles are grown in step away from the solid wall as a function of chain length and the chains are fully stretched with changing solvent quality from poor to good. The brush under poor solvent is showing the highest density profile at 1.00 g/cm^3 but is dropping at very short distance. That means the polymer chains are more compressed near the solid substrate because polymer-polymer interactions are more favorable to each other than polymer-solvent interaction. The thickness of brush, which is defined from SCF theory as $z = h_{max}$ for which $\rho(z) = 0$, in poor and theta state have no significant difference, about 35 \AA . However, the profiles of density for polymer chains under the theta state are decreased slightly slower than those in the poor state. The profiles of chains in good solvent are flatter and have the highest thickness at about 40 \AA .

- Conformation properties

Figure 3.25 shows the reduced mean height $\zeta(s)$ as a function of normalized bead coordinate along chain contour for PEO brush under different solvent quality. It is very remarkable because all curves are not superimposed; the

chains in theta and poor solvent were deviated from the theoretical prediction whereas it was quite closed to the theoretical prediction for the brush in good solvent. The deviations are larger especially in the middle portion of the chains. The most deviation are found in brushes under the poorer quality of solvent indicating that chains are less stretched which is according to density profile as described before.

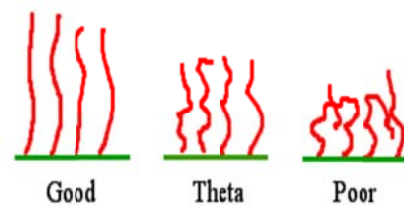


Figure 3.24 Local density profile ($\rho(z)$) as a function of distance from solid interface of PEO brush under different solvent.

Figure 3.25 The normalized mean height $\zeta(s)$ as a function of normalized bead coordinate along chain contour of PEO brush under different solvent.

- Bond orientation

Figure 3.26 presents the bond orientation for each i th monomer $\langle \cos\theta_i \rangle$ as a function of the position of the i th bond along the PEO chain in brushes (B40n160) under the different quality of solvent. It is clearly seen from the figure that the grafted PEO chains in good solvent are more stretched than those in other solvent quality and the chains are compressed as the quality of solvent is worsen. The stretching of brushes in poor and theta are not much different especially the segment near grafting wall and free end.

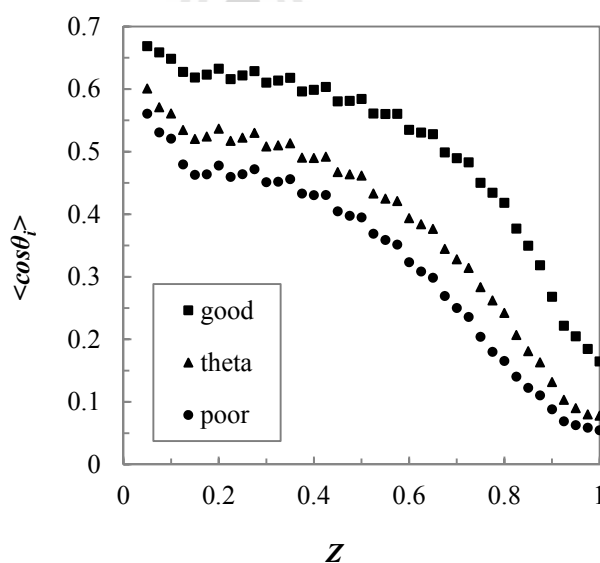


Figure 3.26 The orientation of each i th monomer $\langle \cos\theta_i \rangle$ as a function of the position of the i th bond along the chain of PEO brush under different solvent.

- Bead distribution

To get some more information on the structure of the brush, the distribution of monomers both for the middle- and end point as a function of distance from the grafting wall are shown in Figure 3.27. These distributions indicate quite

clearly that the chain stretching is distributed throughout the brush. The bead would be close to the interface and are stronger stretched while the solvent quality becomes better. The end-beads are not only distributed over a larger Z as the peak height increases, but also the bead localization becomes sharper at the end of the brush. The middle bead distribution has a similar trend to the distribution of the end bead in that they are located far away from the grafting wall with higher peak amplitude and sharper distribution.

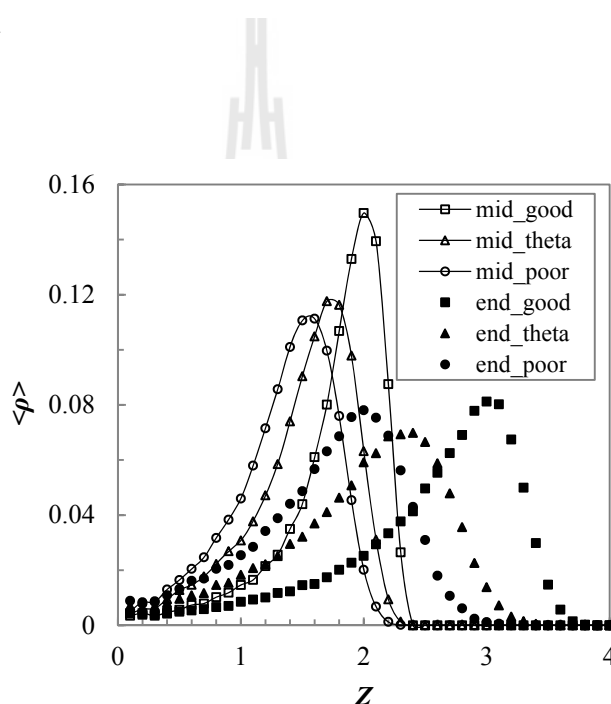


Figure 3.27 The middle ($\rho_m(z)$) and end ($\rho_E(z)$) bead distribution as a function of Z of PEO brush under different solvent.

The effect of solvent quality on bidisperse PEO brushes

Polydispersity, which is usually represented by the bidisperse system in theoretical and computational simulation, plays an important role on both chain conformation and brush structure. These effects have also been apparent to the interface between the grafted polymer and a matrix of free polymers (Laub and

Koberstein, 1994). So, studying bidisperse polymer brush is necessary. Before investigating the effect of solvent quality on properties of bidisperse PEO brushes, a comparison of the density profile of mono- (B40N160) and bidisperse (B30N80+B50N80) PEO brush in poor, theta and good solvent is first presented to clearly show the effect of polydispersity on the brush properties.

Figure 3.28 demonstrates a comparison for the effect of polydispersity under different solvent qualities on $\rho(z)$ of mono- and bidisperse PEO brush. The circle with dark line and filled square symbols are denoting to the density profile for mono- and bidisperse systems, respectively. Simulation results have shown that polydispersity affects to $\rho(z)$ of brush in all solvent quality but it is in difference region. For poor solvent system, the $\rho(z)$ of both mono- and bidisperse are broader with the distance away from grafting surface. The brushes in this condition are compressed making no more space for polymer chain to align far away from the grafting point. Near the solid wall, $\rho(z)$ of monodisperse is a parabolic profile with higher amplitude than that in the bidisperse case and it became lower with the distance. The profile is quickly dropped as the effect of different chain composition. This behavior is in contrast to the brushes in theta solvent. The amplitude of the $\rho(z)$ in bidisperse system is higher and it became lower as a function of Z . Moreover, $\rho(z)$ has a slightly kink profile for the bidisperse system as previously observed. In good solvent condition, the polymer chains were regarded to interact with the solvent molecules more strongly than with other polymer molecules. Polymer chains cannot get closer to each other due to the presence of the solvent layer surrounding polymer chains. So, the chains are more stretched under this condition both in mono- and bidisperse brush. However, the changes of density profile are clearly distinguished,

especially near the interface. Similarly to the profile under theta solvent that has a kink pattern. This behavior indicated a strong different chain stretching within the brush under different solvent quality. Polymer - polymer and polymer - solvent interactions manifest a strong influence on the stretching of polymer brush layers. In order to investigate the above effect, broad ranges of solvent quality were simulated.

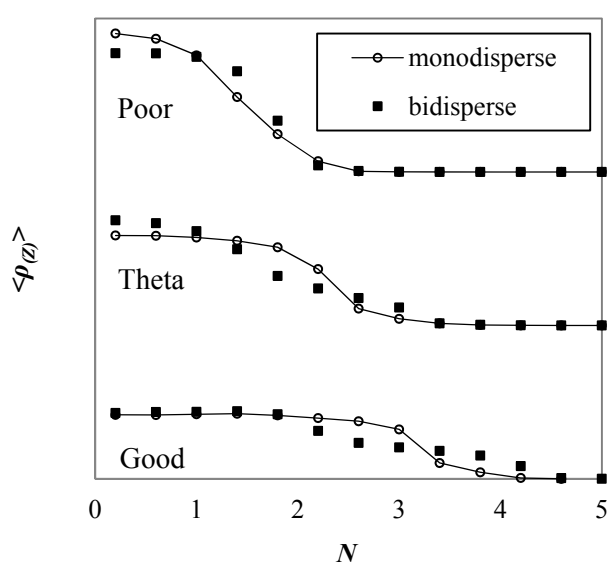


Figure 3.28 Local density profiles for mono- (B40n160) and bidisperse PEO brush (B30n80+B50n80) under solvent quality.

- Density profile

Figure 3.29 depicts the density profile of bidisperse PEO brushes, the mixture between short and long PEO chain under different solvent quality. Simulation results are present either the profile for total or separated to short and long chain composition denote by a line, opened and filled symbol, respectively. The total profile was changed from parabolic to flat line with kink when solvent quality become better affinity to PEO. In all solvent condition, the long chains are pushed away from

the grafting point and dominate at the top region of the brush, while the short chains are predominantly occupied at the bottom of the brush and do not reach the outer region. As mentioned above, the profile is changed with variable solvent quality. The kinks are found in both theta and good solvent which is the result from strong distinguished distribution between short and long chain composition.

- **Conformation properties**

Figure 3.30 shows the reduced mean height $\zeta(s)$ as a function of normalized bead coordinate along chain contour for PEO brushes under different solvent quality. It is very remarkable because all most curves of brush in poor and good solvent are not superimposed with theoretical prediction (solid line in Figure 3.29, except for the brush near the wall and free end. Conformation of the brush under theta solvent is quite well superimposed with theory. The brushes are most stretched under good solvent condition and the most compressed under poor solvent condition. This behavior is in good according with the density profile as discussed previously.

- **Bond orientation**

Figure 3.31 presents the orientation of each monomer $\langle \cos\theta_i \rangle$ as a function of the position of the i th bond along the chain of bidisperse PEO brush under different solvent quality. It is clearly seen for both short and long chains from the figure that the brushes in good solvent are the most stretched, and the chains are more compressed as the solvent quality become worsen. The stretching of brushes in poor and theta are not much different especially for the segment near the grafting wall and free ends. Under good solvent condition, the short chains are most stretched compared

with the brush in theta and poor condition. That means in this situation the long chains are completely spanned toward the free surface and causing free space of the short chain to be more aligned, especially for the free ends.

- **Bead distribution**

The brush dimensions can be also investigated by the analysis of the distribution of bead at different solvent conditions. Figure 3.32 and 3.33 presents the distributions of the middle- and end-beads of PEO brush under different solvent quality, respectively. One can notice that the curves for all cases are different in both amplitude and location. As can be seen in Figure 3.32, the end bead distribution of long chains is located away from the grafting wall as the better solvent quality. The end bead is completely absented at the wall in theta and good solvent, except for poor solvent condition that some end beads can be in the region $z < 10$. On the other hand, end-bead distribution of short chains can stay in everywhere at around $z < 30$. The distribution become broader when the brushes are immersed in poor and theta solvent, while the distribution is sharper and has the highest amplitude far away from grafting wall for the case of good solvent. These distributions are in agreement with the density profile that the brushes form a rather compact structure under poor solvent condition and they are swelled as solvent quality is better. The kink appeared in the density profile is resulting from the large different distribution between the short and long chains. Whereas, the compression in poor solvent is forcing the density profile to parabolic. Moreover, there are show some penetration of short chain to long chains and it make long chains to stretched away as illustrated by the shaper shape of its distribution *i.e.* brush in poor solvent.

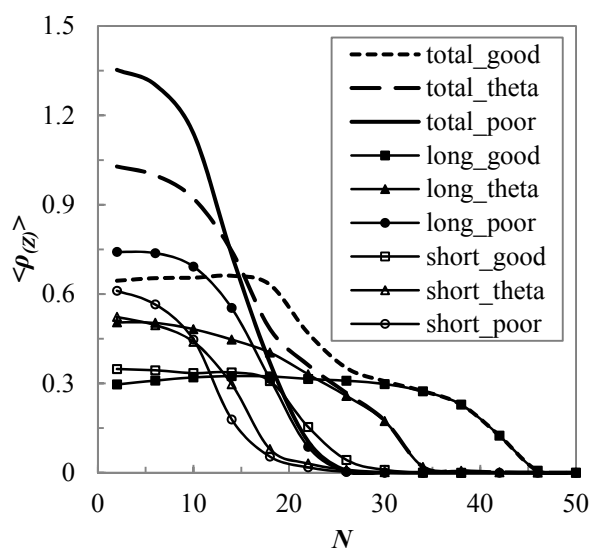


Figure 3.29 Local density profiles of bidisperse PEO brush under different solvent quality.

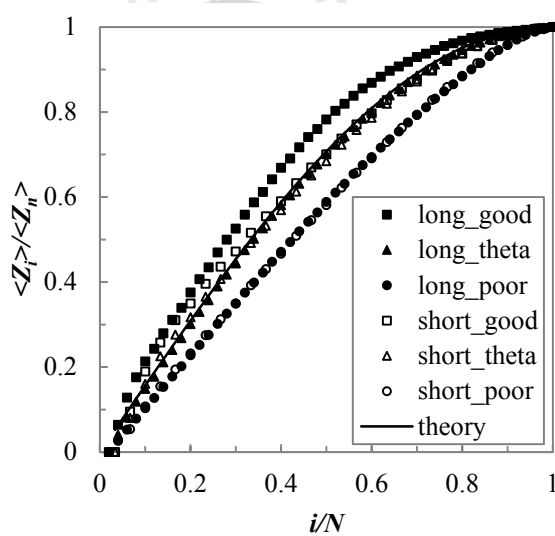


Figure 3.30 The normalized mean height $\zeta(s)$ as a function of normalized bead coordinate of bidisperse PEO brush under different solvent quality.

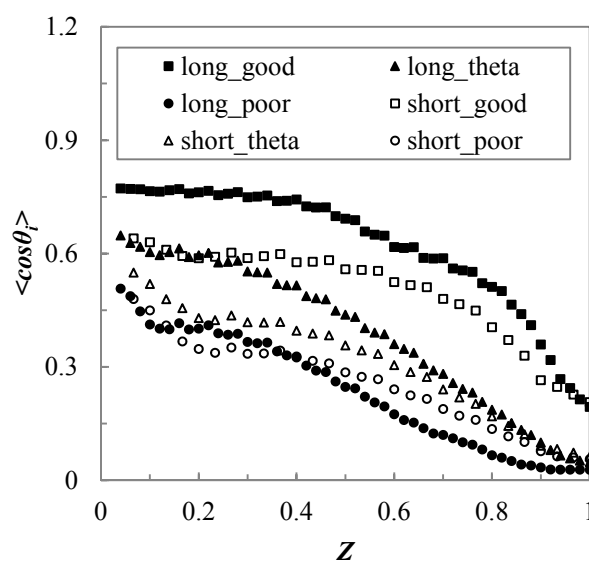


Figure 3.31 The orientation of each monomer $\langle \cos\theta_i \rangle$ as a function of the position of the i th bond along the chain of bidisperse PEO brush under different solvent quality.

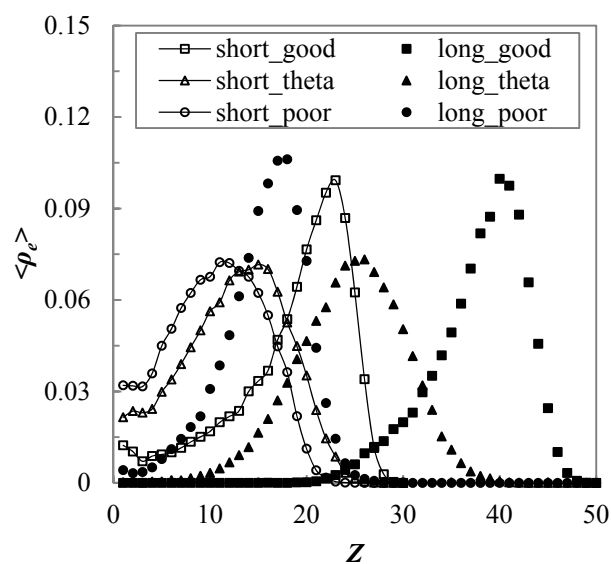


Figure 3.32 The end bead distribution ($\rho_E(z)$) as a function of z of bidisperse PEO brush under different solvent quality.

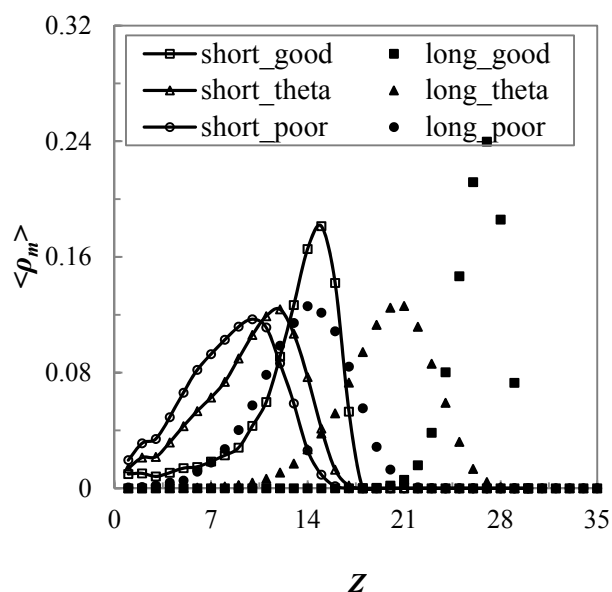


Figure 3.33 The middle bead distribution ($\rho_m(z)$) as a function of z of bidisperse PEO brush under different solvent quality.

3.5.3 Summary

The effect of solvent quality on mono- and bidisperse PEO brush were investigated as a model of the corona part of micelle. The results show that both polydispersity and solvent quality were affect to the brush properties. Due to different interaction between polymer-polymer and polymer-solvent interaction, the brush under poor solvent was more compressed as confirmed by the density profile, the orientation of bond and the polymer bead distribution.

3.6 PEO nanoparticle in solution

3.6.1 Simulation detail

The 36 chains of 50 PEO beads on the 2nd lattice were constructed to study the effect of solvent quality on the stability and structure of their nanoparticle as a conceptual model for the core part of polymer micelle. The steps to generate nanoparticle in this study can be described as illustrated in Figure 3.34. The method started from extending the x axis of the periodic box of the bulk system in three dimensions about 3 times which was large enough to ensure that there was no interaction between the parent chains and their images. Then the system was equilibrated to give polymer thin film first and it was employed as an initial structure of the polymer fiber. The nanofiber can be obtained by again extending the y axis of this initial conformation about 3 times and the system was carried out in the same way as done before. Finally, polymer nanoparticle can be obtained in a similar way to nanofiber by extending the z axis of the latest conformation of the fiber about 3 times. After equilibration stage the PEO nanoparticle was obtained. At less 10^6 MCS was run for each equilibration stage for thin film, fiber and nanoparticle. The latest conformation was run for an additional 10^6 MCS for subsequent data analysis.

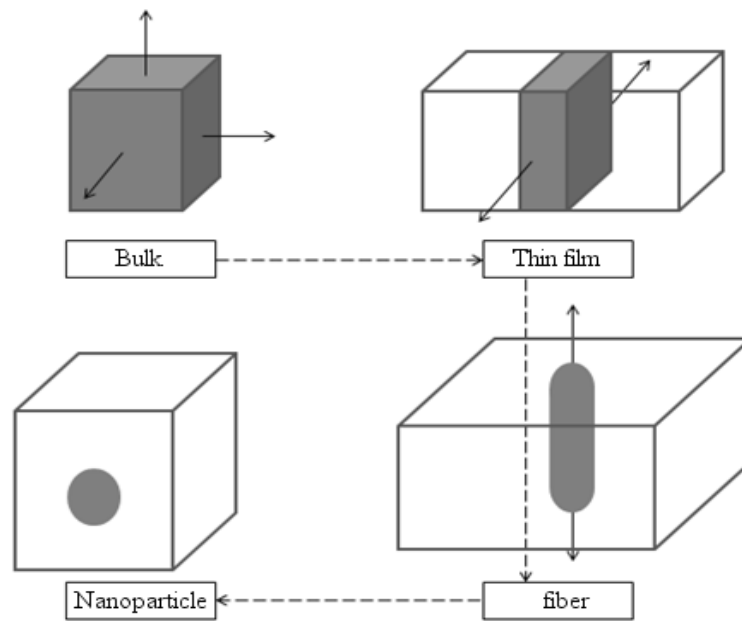


Figure 3.34 The method to generate a new cohesive polymer structure from bulk (3D) → thin film (2D) → nanofiber (1D) → nanoparticle (0D).

3.6.2 Results and discussion

The effect of solvent quality on PEO nanoparticle

Figure 3.35 presents the snapshot of an equilibrated coarse-grained PEO nanoparticle on 2nd lattice. The chains under different solvent quality from theta ($k = 0.63$) to poor condition ($k = 0.80, 1.00$ and 1.40) presents in both horizontal and vertical planar. Under the theta state the chains are disaggregated as individual chains freely distribute. The structures are aggregated and denser packed with changing the solvent quality from theta to poor solvent. The shape of nanoparticles are transformed to an ellipsoid for poorer solvent which is corresponding with Huang *et al.* that the shape of the polymer chain is more deviated from spherical shapes (Huang *et al.*, 2001).

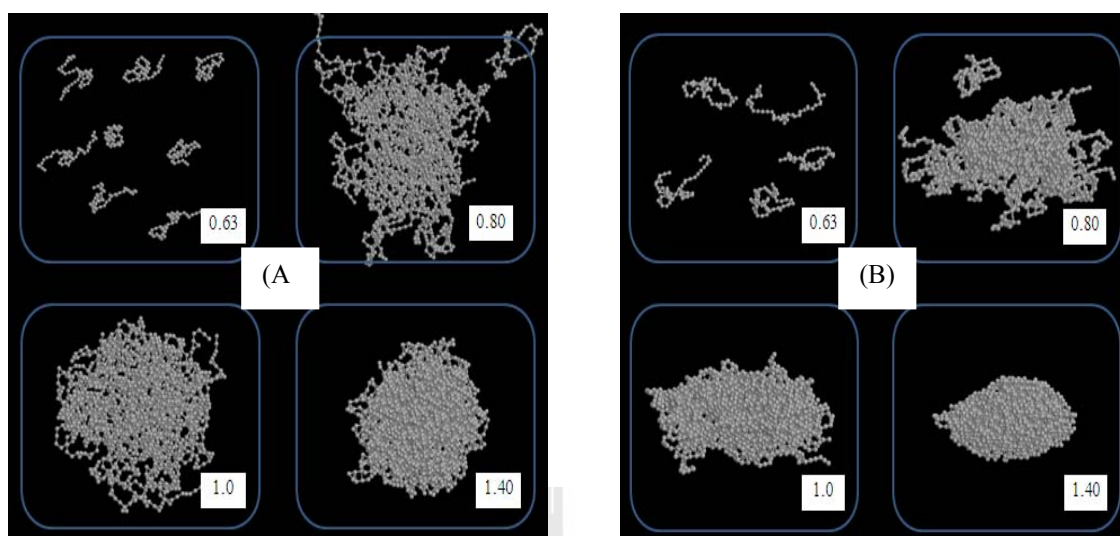


Figure 3.35 The nanoparticles of 36 coarse-grained chains of $-(\text{CH}_2\text{CH}_2\text{O})_{33}-$ under difference solvent quality in (A) vertical and (B) horizontal direction.

- Radial density profile

In this work, the radial density profiles is defined as the number of beads that fall in the shell centered on the center of mass of the PEO nanoparticle. Figure 3.36 shows the radial density profile for each nanoparticle in different solvent quality. The results show the density of particles are reached a bulk density at about 0.8, 0.9 and 1.1 g/cm^3 for nanoparticle which was immersed under solvent with increased poorer quality from $k = 0.80$, 1.00 and 1.40, respectively. The density of particles is resembles to the parabolic shape at $k = 0.80$. It is presented as the flat region in the density profile at higher distance and the density is slower decayed to the free surface for the chains under poorer solvent. At the beginning, the density is dropped at the distance around 1.0, 1.5 and 2.0 nm for $k = 0.80$, 1.00 and 1.40, respectively. The diameter of nanoparticle, define as the distance over which the density decrease from 90% to 10% of its bulk value, is increased from 3.5 to 5.0 nm

when the solvent quality become poorer *i.e.* from $k = 1.40$ to $k = 0.80$. $k = 1.40$ is the worst solvent quality which the interaction between polymer - polymer are the most strongest compared to polymer - solvent interaction. This make the nanoparticles are preferred to pack themselves denser, causing their density in bulk region are increased accordingly.

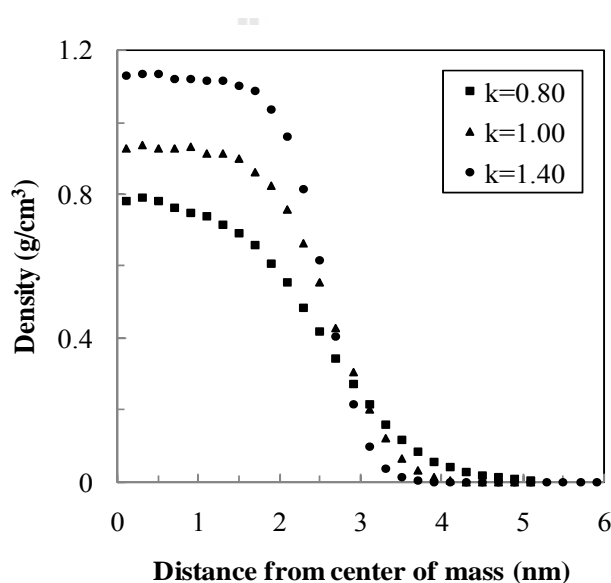


Figure 3.36 Radial density profiles as a function of distance from the center of mass of the nanoparticles in different solvent quality in poor region.

- Bead distribution and segregation of chain end

Figure 3.37 presents the density profile of the end (the first or the last carbon atom of the chain) and middle carbon atoms across the PEO nanoparticle. The segregation of bead distributions at the surface are clearly observed when the data is normalized by the total bead density profiles. In the interior region, both middle and end bead density are approached the bulk density which was divided by the total

number of carbon atoms in each chain. The middle bead is preferred at the center of particle, while the end bead is found anywhere especially around the center to the free surface. The profiles are in good agreement with those observed in thin film and free surface amorphous PE nanoparticle (Vao-Soongnern *et al.*, 2004) and nanofiber melts (Doruker and Mattice, 1998a, b; Vao-soongnern *et al.*, 2000) as have been reported in previous simulations. The distribution of middle bead in nanoparticle is no significant changed by any solvent quality, while the end bead distribution is strongly changed. It is little increased in middle bead density close to the center of the particles. This indicated an oscillatory behavior of the profile, which was also observed in MD simulation of a short alkane melt surface (Harris, 1992) and thin film (Doruker and Mattice, 1998b; Vao-soongnern *et al.*, 2000). The end bead density under $k = 0.80$ is lower than that of other solvent conditions. The profile is changed smoothly as a function of distance from the center of particle which can be distinguishable from the profile of particle under the poorer solvent $k = 1.00$ and $k = 1.40$ that show more bead profile fluctuation. This behavior is mainly determined by the entropic effect in contrast to an enrichment of the center of mass in the interface layer which was depended on the energetic situation.

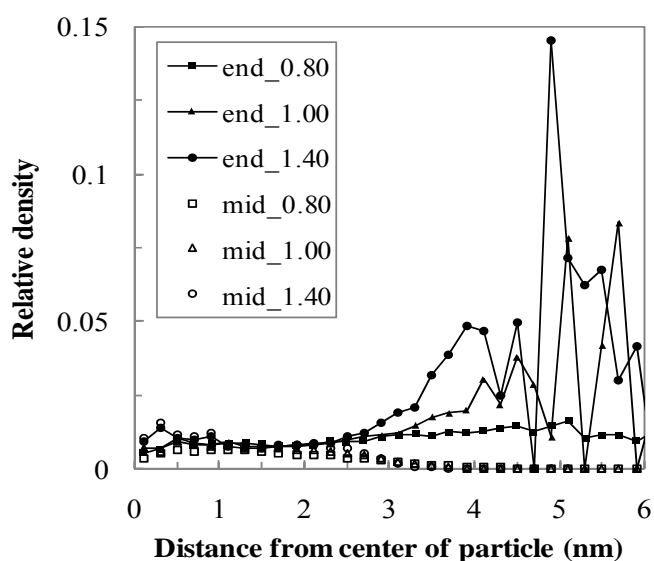


Figure 3.37 The normalized radial density profiles for middle and end beads of the nanoparticles.

- Chain and segment properties

The average overall molecular dimensions and its deviation of the PEO nanoparticles under each solvent quality summarize in Table 3.9. $\langle R_g^2 \rangle$ and $\langle R^2 \rangle$ of PEO chains in the nanoparticle under $k = 0.80, 1.00$ and 1.40 are present. The ratio of $\langle R^2 \rangle / \langle R_g^2 \rangle$ are 5.05, 4.98 and 4.67, respectively. It clearly sees that the ratios are large deviation from 6 with improving poor solvent quality.

The spatial distribution of the center of mass of PEO chains in the particles with respect to the distance from the particle center illustrates in Figure 3.38 to characterize the structure at the level of an entire chain. The center of mass profiles of the chains are expressed as the number of chains per volume of bin (0.25 nm width (\AA^3)). The region < 1 nm is shown random distribution of chain in the particle, this result indicates an oscillatory behavior is existed in the simulation. The results shown

in region between 1.00 - 2.25 nm that an increasing of the center of mass number per volume are strongly depended on the solvent quality. The values are higher increased close to the surface region when the quality of solvent become poorer, but the distribution is quickly dropped. Hence, the particles are compressed and denser packed as confirmed by snapshot present in Figure 3.35. Moreover, the profiles in the surface region (> 4 nm) are almost identical for the nanoparticles under all solvent condition, this position rather closely to the particle at which the density assumes a constant value as show before in Figure 3.36.

Table 3.9 The average overall dimensions of PEO chains (50 units) in nanoparticle and their standard deviations under each solvent quality.

	k=0.80	k=1.00	k=1.40
$\langle R_g^2 \rangle$	2.54±1.03	2.48±1.00	2.26±0.93
$\langle R^2 \rangle$	12.65±5.39	12.16±5.18	10.54±4.37
$\langle R^2 \rangle / \langle R_g^2 \rangle$	5.05	4.98	4.67

$\langle R_g^2 \rangle$ and $\langle R^2 \rangle$ denote as the mean square radius of gyration and the mean square end to end distance.

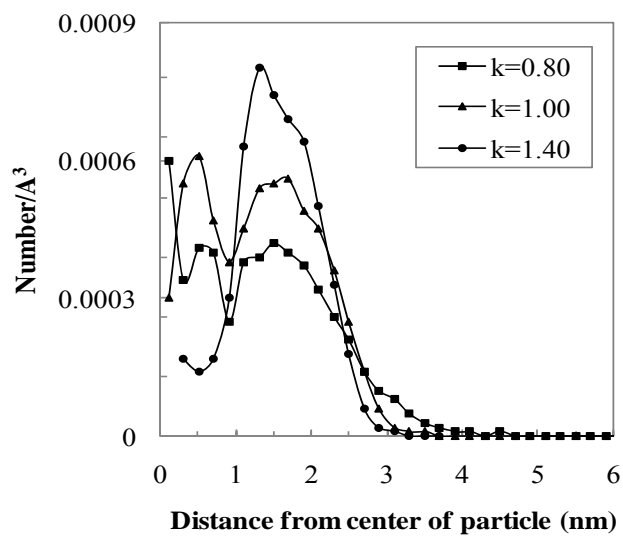


Figure 3.38 The center of mass distribution as a function of the displacement from the center of the nanoparticle.

The shapes of the polymer chains are approximated by an equivalent ellipsoid (Solc, 1971), which defined by the principal components $L_1 > L_2 > L_3$ of the radius of gyration tensor for an individual configuration taken along the principal axes as show in Figure 3.39. Figure 3.40 shows a comparison of the eigenvalue (principal moments) normalized by their square radius of gyration as a function of the distance of the center of mass for the nanoparticles under poor solvent. The worst solvent quality at $k = 1.40$ is higher degree of eigenvalue change in all principle component, most of which is occurs close to the vacuum side. All principal moments under less poor solvent quality at $k = 0.80$ system is not changed near the center of the nanoparticle, while is depicted little fluctuation at free surface. On the other hand, they are changed in all three eigenvalues at the surface region for $k = 1.40$ system. The first principle moment is decreased whereas the second and the third are increased.

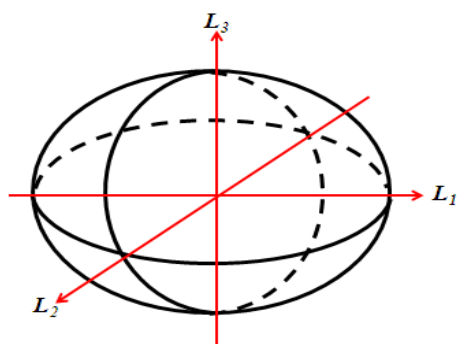


Figure 3.39 The ellipsoid shape defined by the principal components $L_1 > L_2 > L_3$ for the nanoparticle model.

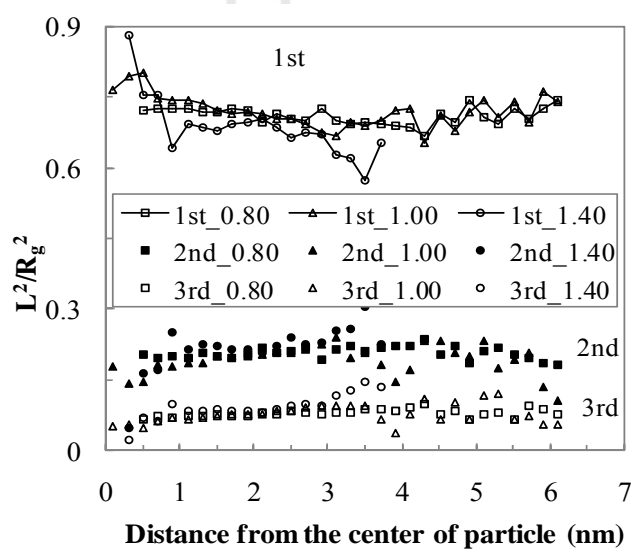


Figure 3.40 The change in the principal moment of the chains (normalized by R_g^2) as a function of the distance from the center of the nanoparticle.

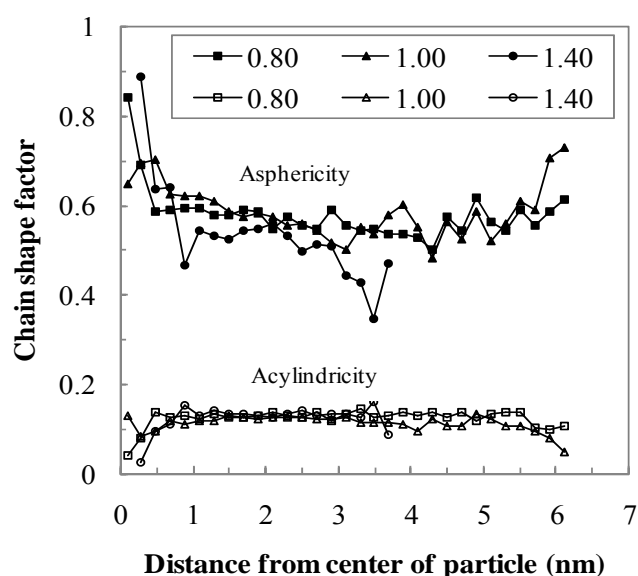


Figure 3.41 The change in chain shape (asphericity and acylindricity) as a function of the distance from the center of the nanoparticles.

The chain shapes are investigated using the acylindricity and the asphericity, which are defined by $c = L_2^2 - L_3^2$ and $b = L_1^2 - \frac{1}{2}(L_2^2 + L_3^2)$, respectively (Theodorou and Suter, 1985). These values are divided by the squared radius of gyration to determine the extent of deviation from cylindrical and spherical shapes in the range of 0 to 1. From Figure 3.41, the chain shape is changed as a function of the distance from the nanoparticle center. The acylindricity for all systems is not affected much by solvent quality. In contrast, the asphericity is clearly changed. The nanoparticle under $k = 0.80$ and 1.00 (less poor solvent) are shown an increasing in asphericity toward the surface, whereas the worst solvent $k = 1.40$ is decreased value as a function of the distance from the center of nanoparticle. These results are simply manifested of the flattening of chains into ellipsoid shape look like the nanoparticle snapshot in Figure 3.31.

– Local Orientation

Local orientation of chords (from carbon atom i to carbon atom $i+2$) order parameter defined as

$$S_b = \frac{1}{2} \langle 3 \cos^2 \theta - 1 \rangle \quad (3.34)$$

where θ is the angle formed between a chord and the referent vector (the vector connecting the center of mass of the particle to the center of the chord). S was perpendicular, random, and parallel orientation with respect to the reference vector by a value corresponding to -0.5, 0.0 or 1.0, respectively.

Figure 3.42 illustrates S for all of the chords. Comparison this parameter with the density profiles in Figure 3.36 shows that the number of observations for all bond vectors is approached to zero in all poor solvent cases. This indicates the orientation of chord is randomly in the inner region up to the free surface within the reliable data point between 0.5 - 4.0 nm. All results are in good corresponded with the previous simulations that most bond orientations of the nanoparticle are relatively random (Vao-soongnern, 2006). Beyond 4 nm, however, the middle bonds of particle under $k = 0.80$ are preferred perpendicular with small negative parameter whereas the end bonds are tended to parallel orientation. These two opposite effects are averaged in the orientation of all bonds to random orientation. On the other hand, both middle and end chords are preferred to parallel orientation for the particle under $k = 1.00$ (Doruker and Mattice, 1998a, b).

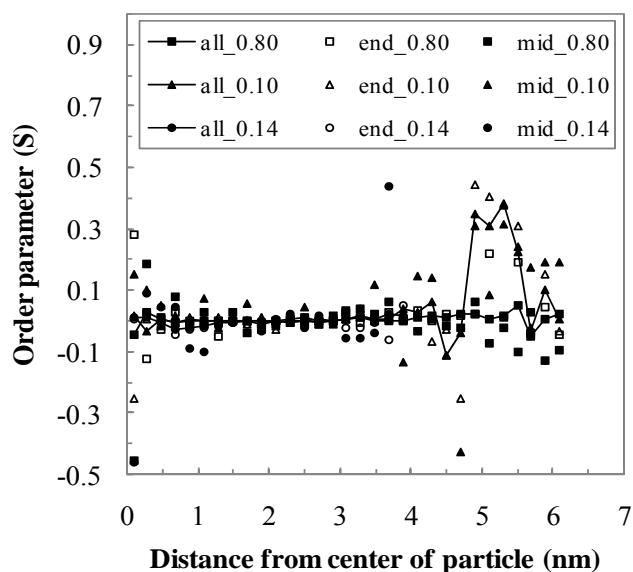


Figure 3.42 The orientation of chords (mid-, end- and all) as a function of the displacement from the center of the nanoparticle.

- Chain orientation

The orientations of the largest and smallest eigenvector of the whole chains (L_1 and L_3 , respectively) display in Figure 3.43. The definition of the order parameter and the reference vector are the same as that present in the chord orientation. Similar with the orientation, the reliable data point is between 0.5 - 4.0 nm. The orientation of the longest (first) principal axis is tended to perpendicular if the center of mass is far away for the nanoparticle under $k = 1.0$ and $k = 1.4$ (poorer solvent condition), while are randomly oriented for the particle under $k = 0.80$. The shortest (third) principal axis is tended to random, perpendicular and parallel orientation with the k value of 0.80, 1.00 and 1.40, respectively.

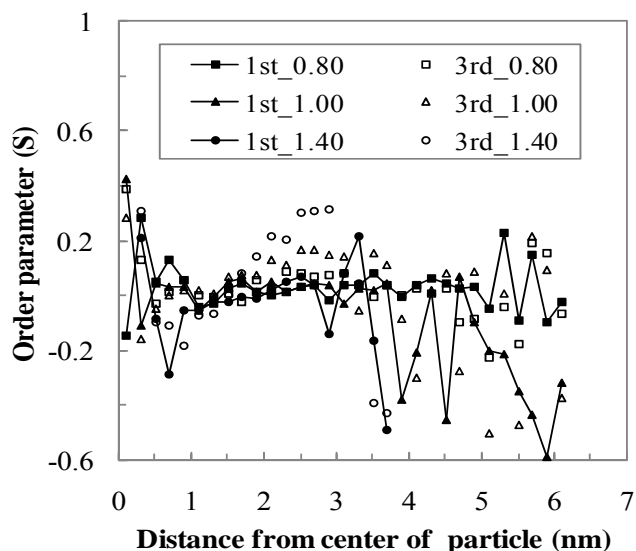


Figure 3.43 The orientation of the largest and smallest principal moment to the reference vector connecting the center of particle to the center of each PEO chain in the nanoparticle.

3.6.3 Summary

MC simulation was modified to model PEO nanoparticle under the variation of solvent quality to study the stability and structure properties at the molecular level as the model for the core part of polymer micelle. The simulation results suggest the PEO chains were denser packed and increased density in bulk region of the nanoparticles. The shape of nanoparticle was nearly ellipsoid when the solvent quality was poorer. The distributions of middle bead in nanoparticle were not significant change by any solvent quality, while the end beads distributions were strongly changed. Most of bond orientation in the nanoparticle was relatively random.

3.7 References

- Abe, A., Jernigan, R. L. and Flory, P. J. (1966). Conformational energies of n-alkanes and the random configuration of higher homologs including polymethylene. **Journal of the American Chemical Society** 88(4): 631-639.
- Amoskov, V. M. and Birshtein, T. M. (2001). Polydisperse anisotropic brushes. **Macromolecules** 34(15): 5331-5341.
- Auroy, P., Mir, Y. and Auvray, L. (1992). Local structure and density profile of polymer brushes. **Physical Review Letters** 69(1): 93-95.
- Baker, S. M., Smith, G. S., Anastassopoulos, D. L., Toprakcioglu, C., Vradis, A. A. and Bucknall, D. G. (2000). Structure of polymer brushes under shear flow in a good solvent. **Macromolecules** 33(4): 1120-1122.
- Balijepalli, S. and Rutledge, G. C. (1998). Molecular simulation of the intercrystalline phase of chain molecules. **The Journal of Chemical Physics** 109(16): 6523-6526.
- Baschnagel, J. and Binder, K. (1995). On the influence of hard walls on structural properties in polymer glass simulation. **Macromolecules** 28(20): 6808-6818.
- Baschnagel, J., Paul, W., Tries, V. and Binder, K. (1998). Statics and dynamics of bidisperse polymer melts: a Monte Carlo study of the Bond-fluctuation model. **Macromolecules** 31(12): 3856-3867.
- Binder, K. and Paul, W. (1997). Monte Carlo simulations of polymer dynamics: Recent advances. **Journal of Polymer Science Part B: Polymer Physics** 35(1): 1-31.

- Birshtein, T. M., Liatskaya, Y. V. and Zhulina, E. B. (1990). Theory of supermolecular structures of polydisperse block copolymers: 1. Planar layers of grafted chains. **Polymer** 31(11): 2185-2196.
- Chakrabarti, A. and Toral, R. (1990). Density profile of terminally anchored polymer chains: a Monte Carlo study. **Macromolecules** 23(7): 2016-2021.
- Cho, J. and Mattice, W. L. (1997a). Estimation of Long-Range Interaction in Coarse-Grained Rotational Isomeric State PE Chains on a High Coordination Lattice. **Macromolecules** 30(3): 637-644.
- Cho, J. and Mattice, W. L. (1997b). Estimation of long-range interaction in coarse-grained rotational isomeric state polyethylene chains on a high coordination lattice. **Macromolecules** 30(3): 637-644.
- Dan, N. and Tirrell, M. (1993). Effect of bimodal molecular weight distribution on the polymer brush. **Macromolecules** 26(24): 6467-6473.
- de Gennes, P. G. (1980). Conformations of polymers attached to an interface. **Macromolecules** 13(5): 1069-1075.
- Deutsch, H. P. and Binder, K. (1991). Interdiffusion and self-diffusion in polymer mixtures: A Monte Carlo study. **The Journal of Chemical Physics** 94(3): 2294-2304.
- Devos, W. and Leermakers, F. (2009). Modeling the structure of a polydisperse polymer brush. **Polymer** 50(1): 305-316.
- Doruker, P. and Mattice, W. L. (1997). Reverse Mapping of Coarse-Grained Polyethylene Chains from the Second Nearest Neighbor Diamond Lattice to an Atomistic Model in Continuous Space. **Macromolecules** 30(18): 5520-5526.

- Doruker, P. and Mattice, W. L. (1998a). Mobility of the surface and interior of thin films composed of amorphous polyethylene. **Macromolecules** 32(1): 194-198.
- Doruker, P. and Mattice, W. L. (1998b). Simulation of polyethylene thin films on a high coordination lattice. **Macromolecules** 31(4): 1418-1426.
- Fried, H. and Binder, K. (1991). The microphase separation transition in symmetric diblock copolymer melts: A Monte Carlo study. **The Journal of Chemical Physics** 94(12): 8349-8366.
- Harris, J. G. (1992). Liquid-vapor interfaces of alkane oligomers: structure and thermodynamics from molecular dynamics simulations of chemically realistic models. **The Journal of Physical Chemistry** 96(12): 5077-5086.
- Hastings, W. K. (1970). Monte Carlo sampling methods using Markov chains and their applications. **Biometrika** 57(1): 97-109.
- Huang, J., Jiang, W. and Han, S. (2001). Dynamic Monte Carlo simulation on the polymer chain with one end grafted on a flat surface. **Macromolecular Theory and Simulations** 10(4): 339-342.
- Kent, M. S., Factor, B. J., Satija, S. and Smith, G. S. (1996). Structure of bimodal polymer brushes in a good solvent by neutron reflectivity. **Macromolecules** 29(8): 2843-2849.
- Kritikos, G. and Terzis, A. F. (1976). Theoretical study of polymer brushes by a new numerical mean field theory. **Polymer** 48(2): 638-651.
- Kritikos, G. and Terzis, A. F. (2005). Structure of bimodal and polydisperse polymer brushes in a good solvent studied by numerical mean field theory. **Polymer** 46(19): 8355-8365.

- Lai, P. Y. and Zhulina, E. B. (1992). Structure of a bidisperse polymer brush: Monte Carlo simulation and self-consistent field results. **Macromolecules** 25(20): 5201-5207.
- Laub, C. F. and Koberstein, J. T. (1994). Effect of brush polydispersity on the interphase between end-grafted brushes and polymeric matrices. **Macromolecules** 27(18): 5016-5023.
- Lindberg, E. and Elvingson, C. (2001). Monte Carlo simulation of polymer brushes attached to a spherical surface. **The Journal of Chemical Physics** 114(14): 6343-6352.
- Metropolis, N., Rosenbluth, A. W., Rosenbluth, M. N., Teller, A. H. and Teller, E. (1953). Equation of state calculations by fast computing machines. **The Journal of Chemical Physics** 21(6): 1087-1092.
- Milner, S. T. (1991a). POLYMER BRUSH. **Science** 251.
- Milner, S. T. (1991b). Polymer brushes. **Science** 251(4996): 905-914.
- Milner, S. T., Witten, T. A. and Cates, M. E. (1988a). Theory of the grafted polymer brush. **Macromolecules** 21: 2610-2619.
- Milner, S. T., Witten, T. A. and Cates, M. E. (1988b). Theory of the grafted polymer brush. **Macromolecules** 21(8): 2610-2619.
- Milner, S. T., Witten, T. A. and Cates, M. E. (1989). Effects of polydispersity in the end-grafted polymer brush. **Macromolecules** 22(2): 853-861.
- Murat, M. and Grest, G. S. (1989). Structure of a grafted polymer brush: a molecular dynamics simulation. **Macromolecules** 22(10): 4054-4059.

- Pant, P. V. K. and Theodorou, D. N. (1995). Variable connectivity method for the atomistic monte carlo simulation of polydisperse polymer melts. **Macromolecules** 28(21): 7224-7234.
- Paul, W., Binder, K., Kremer, K. and Heermann, D. W. (1991). Structure-property correlation of polymers, a Monte Carlo approach. **Macromolecules** 24(23): 6332-6334.
- Rapold, R. F. and Mattice, W. L. (1995a). New high-coordination lattice model for rotational isomeric state polymer chains. **J. Chem. Soc., Faraday Trans.** 91(16): 2435-2441.
- Rapold, R. F. and Mattice, W. L. (1995b). New high-coordination lattice model for rotational isomeric state polymer chains. **Journal of the Chemical Society, Faraday Transactions** 91(16): 2435-2441.
- Rapold, R. F. and Mattice, W. L. (1996). Introduction of short and long range energies to simulate real chains on the 2nd lattice. **Macromolecules** 29(7): 2457-2466.
- Scheutjens, J. M. H. M. and Fleer, G. J. (1979). Statistical theory of the adsorption of interacting chain molecules. 1. Partition function, segment density distribution, and adsorption isotherms. **The Journal of Physical Chemistry** 83(12): 1619-1635.
- Schwartz, D. K., Steinberg, S., Israelachvili, J. and Zasadzinski, J. A. N. (1992). Growth of a self-assembled monolayer by fractal aggregation. **Physical Review Letters** 69(23): 3354-3357.
- Solc, K. (1971). Shape of a random-flight chain. **The Journal of Chemical Physics** 55(1): 335-344.

- Taunton, H. J., Toprakcioglu, C., Fetters, L. J. and Klein, J. (1990). Interactions between surfaces bearing end-adsorbed chains in a good solvent. **Macromolecules** 23(2): 571-580.
- Terzis, A. F. (2002). Bidisperse melt polymer brush studied by self-consistent field model. **Polymer** 43(8): 2435-2444.
- Theodorou, D. N. and Suter, U. W. (1985). Shape of unperturbed linear polymers: polypropylene. **Macromolecules** 18(6): 1206-1214.
- Vao-soongnern, V. (2006). Nanostructure of the interface modified by grafted polymers: a Monte Carlo simulation. **J. Nanosci. Nanotechnol.** 6(12): 3977-3980.
- Vao-soongnern, V., Doruker, P. and Mattice, W. L. (2000). Simulation of an amorphous polyethylene nanofiber on a high coordination lattice. **Macromol. Theory Simul.** 9(1): 1-13.
- Vao-Soongnern, V., Xu, G. and Mattice, W. L. (2004). Structure formation in the crystallization and annealing of tetracontane nanoparticles. **Macromol. Theory Simul.** 13(6): 539-549.
- Verdier, P. H. and Stockmayer, W. H. (1962). Monte Carlo calculations on the dynamics of polymers in dilute solution. **The Journal of Chemical Physics** 36(1): 227-235.
- Xu, G., Rane, S. S., Helfer, C. A., Mattice, W. L. and Pugh, C. (2004). Monte Carlo simulation of solvent effects on the threading of poly(ethylene oxide) **Modelling and Simulation in Materials Science and Engineering** 12.
- Zhao, B. and Brittain, W. J. (2000). Polymer brushes: surface-immobilized macromolecules. **Progress in Polymer Science** 25(5): 677-710.

CHAPTER IV

MESOSCALE SIMULATION OF TRIBLOCK COPOLYMER MICELLE

4.1 Abstract

The aggregation behavior of three ABA (A = PEO, B = PPO) triblock copolymer model (PEO-PPO-PEO) was investigated by mesoscale simulation *i.e.* MesoDyn. Parameterization strategies based upon atomistic models and experimental data were used. The effects of A/B block ratio, polymer concentrations and the third component addition on the morphology of polymer aggregation at fixed total number of beads were studied. The calculated results show that with increasing polymer concentration, polymer micelles with different shapes were observed *i.e.* spherical micelle, dis-like micelle, worm-like micelle and biphasic. An increasing in A/B block ratio causing lower critical micelle concentration (cmc) but the size was larger. Moreover, adding the model drug *i.e.* Haloperidol into the solution caused easier micelle formation and gave bigger micelle size and Haloperidol was located between PEO and PPO interface. In order to investigate the effect of hydrophilicity of triblock copolymer structure, the hydrophobic part of polymer was changed. The PPO was replaced with PLA. The simulation results revealed that the change in hydrophilicity of the ABA triblock copolymer can cause a difference in its phase morphology.

The series of triblock copolymer of PLA_x - PEG_y - PLA_x with different LA/EG block ratio were simulated for molecular design before later synthesis. The simulation was performed using both MesoDyn and DPD to gain more understanding about the phase morphology, cmc and kinetic of micelle formation. The simulation results shown that only the appropriated LA/EG block ratio can induce the formation of spherical micelle. Smaller LA/EG ratio cans have phase morphology at quite high concentration. In addition, the drug model was added to polymer solution to study the effect of content on aggregation behavior of spherical micelle formation. With adding drug, the micelle was formed easier with larger size. Introducing of a large amount of drug can be causing the phase transition to morphology of spherical micelle.

4.2 Introduction

With the growing interests in polymer micelle of triblock copolymers, understanding the relationship between their structure and properties needs more attention. Molecular modeling and simulation methods can be used to gain a better understanding of the systems and processes at the molecular level, as well as the driving forces and mechanisms behind these phenomena. Simulations can also help to interpret and inspire experiments to provide a picture of the underlying microscopic processes at a single molecule resolution frequently not accessible experimentally. Multiscale computer simulation covers a range of sizes and scale time is used in order to give sufficient information of material systems (Fermeglia and Pricl, 2007; Kremer, 2003). Many important phenomena of polymers that involve the large distance or time scales, for examples, microphase separation in copolymers cannot be studied by fully atomistic simulations. Simulation technique so-called 'coarse-grained'

continuous spaces based on the bead-spring model of polymer have been developed to reduce the number of degrees of freedom of the system, enabling to investigate larger systems. Mesoscopic simulation technique, Mesoscopic Dynamics (Mesodyn) and Dissipative Particle Dynamics (DPD), provide a powerful approach to predict the mesoscopic phenomena and kinetic process of complex fluids and soft materials *i.e.* surfactants, emulsions, colloids, block copolymers, and polymer blends. The models form a bridge between fast molecular kinetics and slow thermodynamic relaxation of macroscale properties. They treat the real polymer chains by grouping atoms together up to the persistence length of polymer chain, which can be extended to length and time scales by several orders of magnitude as compared to all-atomistic simulations. To model a specific chemical nature of the system in mesoscopic simulation, there are two sets of parameters have to be defined (Lam and Goldbeck-Wood, 2003). The first parameter is the Gaussian chain architecture that depends on the degree of coarsening of the original system. The second parameter is the interaction between the different chemical components, which also captures the hydrophilicity and hydrophobicity of the components. Mesodyn is based on the free energy of an inhomogeneous liquid which can be solved to obtain all thermodynamic functions. Phase transition can be investigated as a functional of the density distribution (Yang *et al.*, 2008b). MesoDyn has been applied for studying the long length and time behavior of complex fluid systems. It has gained wide respect in the literatures and commercial circles with scientifically astute algorithms aimed at elucidating important mesoscale structure and kinetics *i.e.* polymer, polymer blend and copolymer in pure and multicomponent system (Guo *et al.*, 2002; Jawalkar and Aminabhavi, 2006; Lam and Goldbeck-Wood, 2003).

Another method developed for simulation of the complex fluids is DPD. It was introduced by Hoogerbrugge and Koelman for hydrodynamic simulation method (Hoogerbrugge and Koelman, 1992). For examples, it has been successfully applied to investigate the and revised (Español and Warren, 1995). This technique is based on the simulation of soft spheres. The motion is governed by certain collision rules. This simulation technique has also been used as an effective tool to investigate the complex system. aggregation behavior of self-assembled micelles from amphiphilic polymers, and the simulation results were found to be qualitatively consistent with the experimental results (Xin *et al.*, 2009). It can provide additional information about an insight of the mechanism of mesoscopic structures which is more efficiently guide to experimental preparation of chemical system with desired properties (Guo *et al.*, 2007; Wu *et al.*, 2006; Zhang *et al.*, 2007; Zhao *et al.*, 2009).

4.3 Research methods

4.3.1 Mesoscopic Dynamics (Mesodyn)

The idea of MesoDyn is that the free energy, F , of an inhomogeneous liquid is a function of the local density function, ρ , from which all thermodynamic functions can be derived. The model used in the MesoDyn project consists of beads of various types *i.e.* i and j with interactions described by harmonic oscillator potentials for intra-molecular interactions and a mean field potential for all other interactions (Doi and Edwards, 1988). Each bead is of a certain component type representing covalently bonded groups of atoms such as those given by one or a few structural units of a polymer chains. The dynamic of the system is described by a set of

functional Langevin equations, which are diffusion equations in the component densities by taking into account of the noise in the system

On a coarse-grained time scale, $\rho^0(r)$ is defined as a collective concentration field for the type i beads at an instant of time and serves as a reference level. There would be a certain distribution of bead positions, defined as $\Psi(R_{11}, \dots, R_{\gamma s})$. Given the distribution Ψ , the collective concentration of the bead s from all chains can be defined by the average of a microscopic density operator:

$$\rho_1 \Psi(r) \equiv \sum_{r=1}^n \sum_{s=1}^N \delta_{1s}^k \text{Tr} \Psi \delta(r - R_{\gamma s}) \quad (4.1)$$

Where δ_{1s}^k is the Kronecker function with value 1 when bead is of type i and 0 otherwise and $R_{\gamma s}$ is the position of bead s from chain γ . It is assumed that in the liquid with slow relaxation the interactions do not depend on the momenta. A set of distribution functions Ψ is defined with the constraint $\rho_1^0(r) = \rho_1[\Psi](r)$. All distributions Ψ lead to the same density $\rho^0(r)$ to form an equivalent class Ω of distribution functions:

$$\Omega = \left\{ \Psi(R_{11}, \dots, R_{nN}) \mid \rho_1[\Psi](r) = \rho_1^0(r) \right\} \quad (4.2)$$

On the basis of this set of distribution functions, an intrinsic free energy function $F[\Psi]$ can be defined:

$$F[\Psi] = \text{Tr}(\Psi H^{id} + \beta^{-1} \Psi \ln \Psi) + F^{mid}[\rho^0] \quad (4.3)$$

The first term is the average value of the Hamiltonian for internal Gaussian chain interactions. The second and third terms represent the Gibbs entropy of the distribution $-k_B T \Psi \ln \Psi$ and the mean-field nonideal contribution, respectively. Ψ is independent of the system history and is fully characterized by the constraint

that represents the density distribution and minimizes the free-energy function. This constraint on the density fields is realized by means of an external potential U_i . The constraint minimization of the free energy function leads to an optimal distribution, which in turn, by the one-to-one relation between densities, distributions, and external potential, can be written as:

$$\beta F[\rho] = n \ln \Phi + \beta^{-1} \ln n! - \sum_1 \int U_1(r) \rho_1(r) dr + \beta F^{\text{nid}}[\rho] \quad (4.4)$$

Now the nonideal free energy function F^{nid} is introduced,

$$\begin{aligned} F^{\text{nid}}[\rho] = & \frac{1}{2} \int \int \epsilon_{ii}(|r-r'|) \rho_i(r) \rho_i(r') + \\ & \epsilon_{ij}(|r-r'|) \rho_i(r) \rho_j(r') + \epsilon_{ji}(|r-r'|) \rho_j(r) \rho_i(r') + \\ & \epsilon_{jj}(|r-r'|) \rho_j(r) \rho_j(r') dr dr' \end{aligned} \quad (4.5)$$

where $\epsilon_{ij}(|r-r'|)$ is a mean-field energetic interaction between beads of type i at r and type j at r' . The mean-field intrinsic chemical potentials can easily be derived by functional differentiation of the free energy $\mu_i(r) = \delta F / \delta \rho_i(r)$. At equilibrium, $\mu_i(r) = \text{constant}$, which results in the familiar self-consistent field equations for the mean-field Gaussian chain model. In general, these equations have many solutions, one of which will be a state of lowest free energy, while most other states will be metastable. On the basis of these equations, the generalized time-dependent Ginzburg-Landau theory can be set up.

The following functional Langevin equations for the diffusive dynamics of the density fields are also introduced:

$$\frac{\partial \rho_i}{\partial t} = M \nu_j \nabla \rho_i \rho_j \nabla [\mu_i - \mu_j] + \eta \quad (4.6)$$

$$\frac{\partial \rho_j}{\partial t} = M \nu_j \nabla \rho_i \rho_j \nabla [\mu_j - \mu_i] + \eta \quad (4.7)$$

The distribution of the Gaussian noise satisfies the fluctuation dissipation theorem:

$$\langle \eta(r, t) \rangle = 0 \quad (4.8)$$

$$\langle \eta(r, t) \rangle \langle \eta(r', t') \rangle = -\frac{2M\nu_j}{\beta} \delta(t-t') \nabla_r \times \delta(r-r') \rho_i \rho_j \nabla_{r'} \quad (4.9)$$

where M is a bead mobility parameter. The kinetic coefficient $M\nu\rho_i\rho_j$ models a local exchange mechanism. The Langevin equations are constructed for an incompressible system with dynamic constraint:

$$(\rho_i(r, t) + (\rho_j(r, t))) = \frac{1}{\nu_j} \quad (4.10)$$

where ν_j is the average bead volume. Generally, to map the representative polymer chains onto the coarse-grained chains, the bead number (N_{meso}) and the unit chain length of the coarse-grained chain (a_{meso}) are estimated by (Mu *et al.*, 2011)

$$N_{meso} = \frac{N_{mon}}{C_\infty} \quad (4.11)$$

where N_{mon} is the number of repeating units in the polymer chain. a_{mon} is the reference unit monomer length, and C_∞ is the characteristic ratio of a chain of infinite length. The interaction between beads $\nu^{-1} \varepsilon_{ij}$ connection is as follows:

$$\nu^{-1} \varepsilon_{ij} = \chi_{ij} RT \quad (4.12)$$

where the parameter χ_{ij} is the interaction between A and B at different temperatures. R is the molar gas constant, 8.314 J/molK, and T is the simulation temperature.

4.3.2 Dissipative Particle Dynamic (DPD)

Dissipative particle dynamics (DPD) is a stochastic coarse-grained simulation technique in which each bead represents a group of atoms or a volume of fluid that is large than the atomistic scale but still macroscopically small. The force between each pair of beads is a sum of a conservative force F_{ij}^C , a dissipative force F_{ij}^D and a random force F_{ij}^R (Groot and Warren, 1997)

$$f_i = \sum_{j \neq i} (F_{ij}^C + F_{ij}^D + F_{ij}^R) \quad (4.13)$$

these three contributions are defined as follows

$$F_{ij}^C = \begin{cases} a_{ij}(1-r_{ij})\hat{r}_{ij} & (r_{ij} < 1) \\ 0 & (r_{ij} \geq 1) \end{cases} \quad (4.14)$$

$$F_{ij}^D = \frac{-\sigma^2(\omega(r_{ij}))^2}{2kT} (\hat{r}_{ij} \cdot \mathbf{v}_{ij}) \hat{r}_{ij} \quad (4.15)$$

$$F_{ij}^R = \frac{\sigma\omega(r_{ij})\hat{r}_{ij}\zeta}{\sqrt{\delta_t}} \quad (4.16)$$

where $r_{ij} = r_i - r_j$, $r_{ij} = |r_{ij}|$, $\hat{r}_{ij} = r_{ij} / r_{ij}$ and $\mathbf{v}_{ij} = \mathbf{v}_i - \mathbf{v}_j$. k is the Boltzman constant, T is the system temperature, σ is the noise strength, ζ is a randomly fluctuating variable with zero mean and unit variance, δ_t is simulation time

step, the r -dependent weight function $\omega(r) = (1 - r)$ for $r < 1$ and $\omega(r) = 0$ for $r > 1$, and a_{ij} is the maximum repulsion between beads i and j . The parameter a_{ij} depends on the underlying atomistic interactions and is related to the Flory-Huggins (χ_{ij}) parameters through

$$a_{ij} = a_{ii} + 3.27 \chi_{ij} \quad (4.17)$$

$$\chi_{ij} = \frac{(\delta_i - \delta_j)^2 V_{ij}}{RT} \quad (4.18)$$

where V_{ij} is the arithmetic average of molar volumes of beads i and j .

δ_i and δ_j are the solubility parameters of beads i and j , respectively, which were depend on the chemical nature of species and was obtained by simulation or experiment. In addition, the particles can be interconnected to complex topologies by a spring force acts between beads (Español and Warren, 1995).

4.4 Mesoscale simulation of ABA triblock copolymer model based on Pluronic® (PEO-PPO-PEO)

4.4.1 Simulation detail

MesoDyn was used to investigate the aggregation behavior of designed ABA triblock copolymer based on Pluronic® (PEO-PPO-PEO). Effects of A/B block ratio on cmc and micelle formation were studied, when the hydrophilic EO and hydrophobic PO block represented by A and B bead, respectively. In MesoDyn simulations, two sets of parameters must be defined to specify the chemical nature of the system: one is the chain topology in terms of repeat segments (or beads), and the

other is the interaction energy between different components. For the first set, MesoDyn uses a Gaussian chain “springs and beads” description, where each bead in the Gaussian chain is a statistical unit, representing a number of “real” monomers and different types of beads correspond to diverse components. All ABA sequence Gaussian chain topology were illustrated in Table 4.1. The relationship between the real atomic molecule and Gaussian chain model was approximated which was corresponded to number of monomer unit/bead ratio of 4.3 for the PEO and 3.3 for the PPO (van Vlimmeren *et al.*, 1999). A water molecule and Haloperidol drug were approximated with single bead as W and H, respectively.

The interaction energy ($v^{-1}\epsilon_{ij}$) between various type of beads were presented in Table 4.2 (Lam *et al.*, 2004). The bond length was 1.1543 nm. All bead diffusion coefficients were 1.0×10^{-7} cm²/s. A box size $32 \times 32 \times 32$ with periodic boundary conditions was used. The total simulation time was 20,000 time steps.

Table 4.1 Designated Gaussian chain for ABA triblock copolymers.

Real copolymer chain	Gaussian chain	A/B (LA) block ratio
(1) PEO ₃₄ PPO ₂₆ PEO ₃₄	A ₈ B ₈ A ₈	2.00
(2) PEO ₂₆ PPO ₄₀ PEO ₂₆	A ₆ B ₁₂ A ₆	1.00
(3) PEO ₁₇ PPO ₅₃ PEO ₁₇	A ₄ B ₁₆ A ₄	0.50
(4) -	A ₄ LA ₁₆ A ₄	0.50

Table 4.2 Interaction parameters for polymer, water and Haloperidol drug molecule.

	A	B	W	H
A	-	7.30	3.34	5.13
B	7.30	-	4.07	2.79
W	3.34	4.07	-	12.09
H	5.13	2.79	12.09	-
L	2.52	-	14.18	-

4.4.2 Results and discussion

- The effect of polymer concentration

The Gaussian chain models of the amphiphilic triblock copolymer of PEO and PPO (A and B bead, respectively) with the same total length but different A/B block ratio ($A_4B_{16}A_4$, $A_6B_{12}A_6$ and $A_8B_8A_8$) in aqueous solution were studied. The isosurface of three dimensional density field of B block for each chain topologies on its concentration show in Figure 4.1. The density field suggests the dependence of polymer morphology on its concentration. The phases of $A_4B_{16}A_4$ and $A_6B_{12}A_6$ have a similar trend changed. The morphologies were transformed from disorder phase to spherical micelle, disk-like micelle and bi-phase region with increasing polymer concentration. The change of micelle phase for $A_6B_{12}A_6$ was good agreement with previous study (Yang *et al.*, 2008a). In contrast, the spherical micelle for $A_8B_8A_8$ cannot obtain. Instead, the morphologies were skipped from a disorder phase and transform directly to disk-like micelle. That means only appropriated A/B block ratio (< 1.00) can induce spherical micelle to form. As shown in the Figure 4.1, the

concentration for spherical micelles is ranging between 8 - 15% v. and 23 - 27% v. for $A_4B_{16}A_4$ and $A_6B_{12}A_6$, respectively. For smaller A/B ratio, spherical micelle was formed at lower concentration. To understand more detail about the structure of each spherical micelle, 12% v. of $A_4B_{16}A_4$ was chosen to picture out the structures of spherical micelles through the density field of different beads that represent each different species. First, the best density slices of A, B and W along the reference axis of a cubic grid was created. Then, three slices of each bead in the same spherical micelle are divided as shown in Figure 4.2. The structure of spherical micelle is present by the A part forms the corona of the micelle whereas the B part forms the micelle core. Some water molecules still remaining in the micelle core as suggested by Yang *et al.* (Yang *et al.*, 2008a). This may be due to the fact that this spherical micelle is composed of loosely core of hydrophobic part as finding in typical experimental result of Pluronic[®] (Batrakova and Kabanov, 2008; Kabanov *et al.*, 2002).

- The effect of A/B block ratio

Furthermore, to investigate the effect of the A/B block ratio on the morphology change and micelle formation kinetic, the behavior of $A_6B_{12}A_6$ (A/B = 0.5) and $A_4B_{16}A_4$ (A/B = 0.25) were compared by looking at the aggregated morphology of these copolymers in Figure 4.1. The spherical micelles start to grow at different concentration. The micelle size of $A_4B_{16}A_4$ is larger than that of $A_6B_{12}A_6$. The spherical micelle of $A_6B_{12}A_6$ and $A_4B_{16}A_4$ was compare in Figure 4.3. $A_6B_{12}A_6$ was more difficult to form spherical micelles than the $A_4B_{16}A_4$ as confirm by the order parameter that the system need more time evolution to reach the equilibrium point.

This may be because there is smaller amount of the hydrophobic content to form the phase separation. However, at a rough approximation, it seem like that there is no significant difference in the micelle size, but $A_4B_{16}A_4$ has slightly more number of aggregated particles than those of $A_6B_{12}A_6$. In order to gain insight into phase separation kinetics, the order parameter for each component of $A_6B_{12}A_6$ with the simulation time were carefully analyzed as shown in Figure 4.4. There are about four states for micelle growth as suggested by the change in order parameter. The first state takes about 0.1 microseconds (or 1000 time steps), in which the order parameter is slightly changes from beginning. The phase is still homogeneous. Then, the order parameter was largely increased resulting from the transition of disorder to a partial spherical micelle and is then rearranges themselves to form a spherical micelle in the second and the third state. After that, the system was changed slowly to overcome their initial morphology in the last state with slowly changed in order parameter before reached their equilibrium (Guo *et al.*, 2002; Yang *et al.*, 2008b). The phase transition of the second and the third states is very fast especially at high concentration. It was took shorter time for micelles grow and reach the equilibrium. Therefore, the micelle formation rate at high concentration needs less time step to phase separate. The phase transition of other triblock copolymers also has similar process. The aggregation characteristics have a similar trend as well.

Similar copolymer topology reported in the literature (Yang *et al.*, 2008b), $PEO_{17}PPO_{60}PEO_{17}$ (P103) which can be mapped to Gaussian chain model as $A_4B_{18}A_4$ ($A/B = 0.22$), shows the critical micelle concentration (cmc) at 4% v., while the cmc of the $A_4B_{16}A_4$ ($A/B = 0.25$) in this study gives cmc at 8% v.. In addition, simulation results give similar morphology change with increasing concentration;

from disorder to spherical micelle, disk-like micelle and bi-phase region which is in good agreement with experiment findings (Alexandridis *et al.*, 1995).

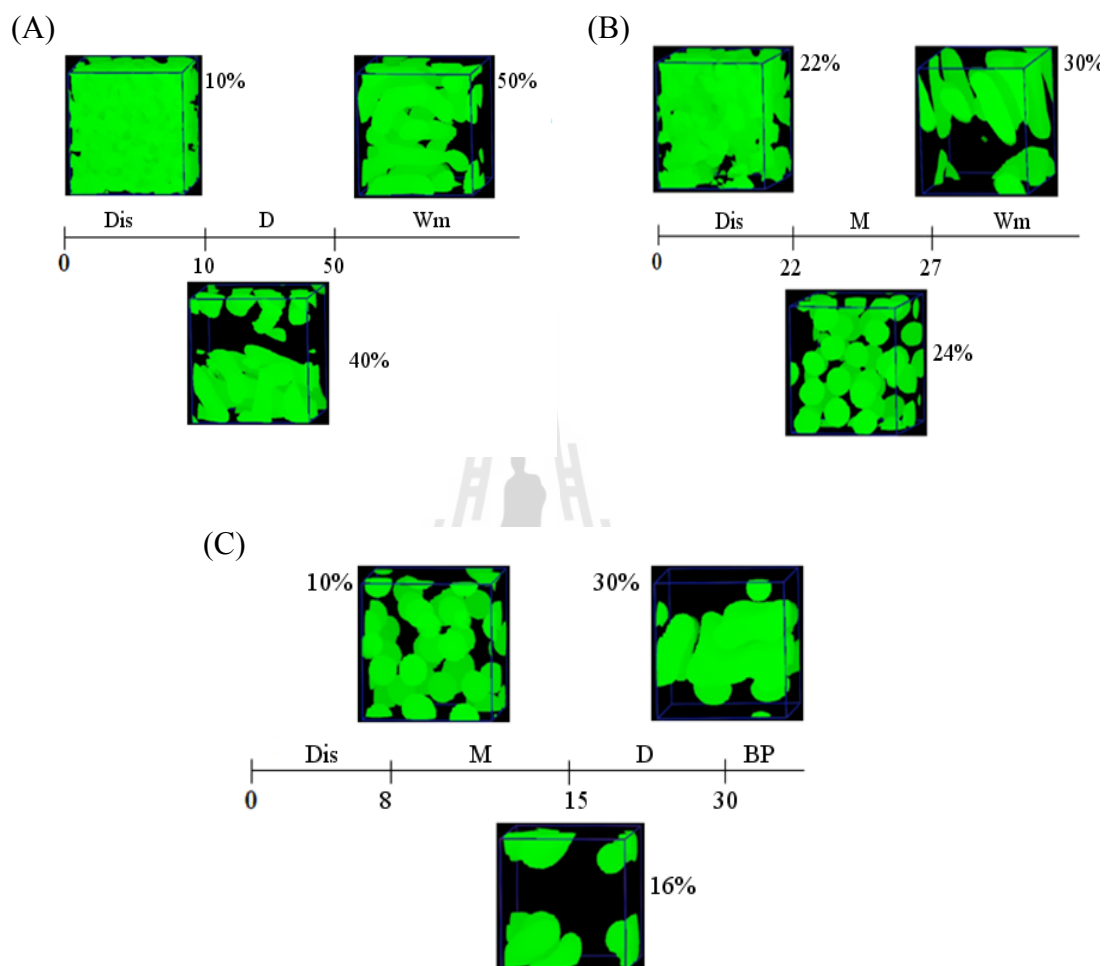


Figure 4.1 Phase morphology in aqueous solution at 298 K for (A) $A_8B_8A_8$, (B) $A_6B_{12}A_6$ and (C) $A_4B_{16}A_4$. Dis (disorder phase), M (micelle), D (disk-like micelle), Wm (worm-like micelle) and BP (bi-phase).

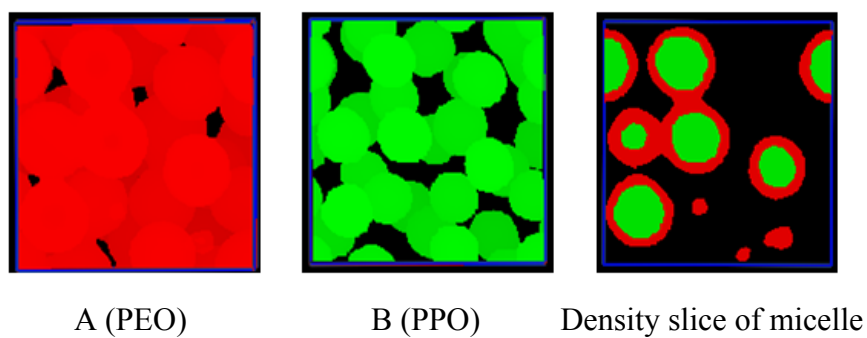


Figure 4.2 The isosurface of A and B species and the density slices for 12% v. of $A_4B_{16}A_4$ in aqueous solution at 298 K.

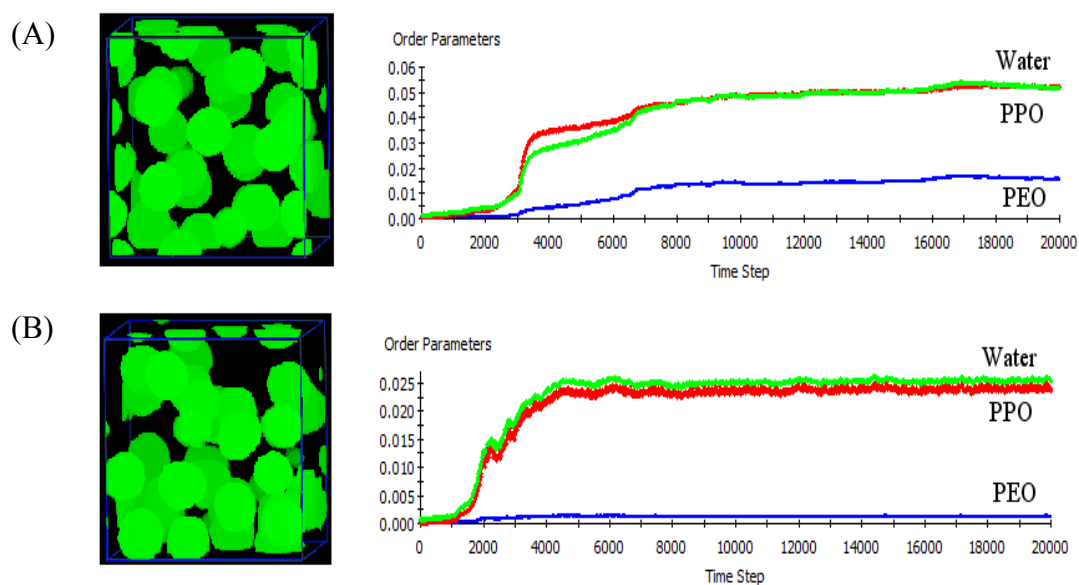


Figure 4.3 The isosurface of B part and the order parameter plot simulation time step in aqueous solution at 298 K for (A) 24% v. of $A_6B_{12}A_6$ and (B) 12% v. of $A_4B_{16}A_4$.

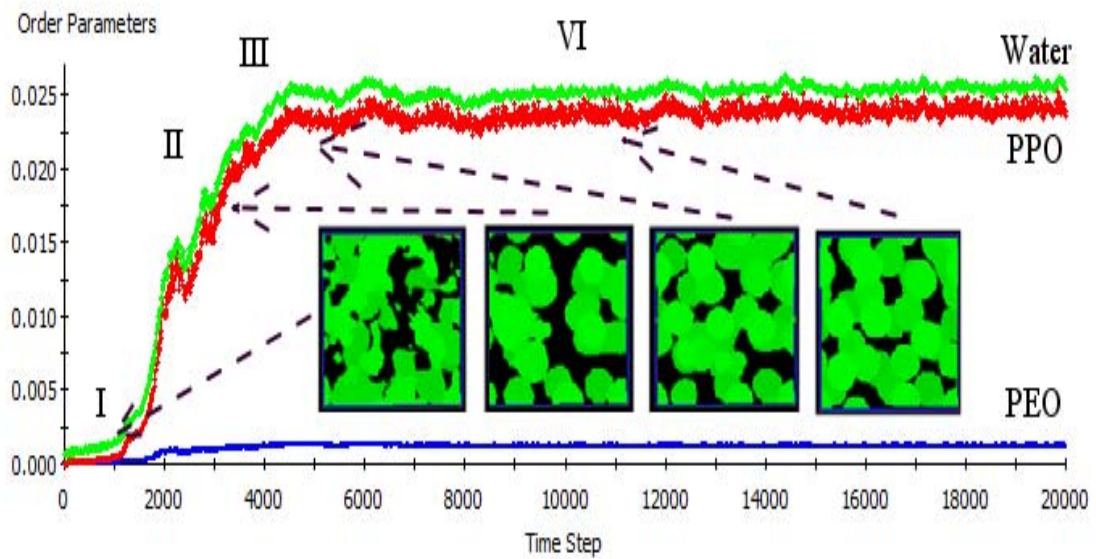


Figure 4.4 The order parameter versus the simulation time for 12% v. of $A_4B_{16}A_4$ in water.

- **The effect of adding third component (drug)**

To observe effect of the third component addition on aggregation behavior and micelle formation, the 12% v. of $A_4B_{16}A_4$ in the absence and presence of drug model *i.e.* Haloperidol were investigated as show in Figure 4.5. The isosurface of each species in the spherical micelle reveal that, the size of micelle for the system with adding drug is larger, but is less number of micelle than the system without drug. Moreover, the drug was located between interface between A and B part of micelle. To gain more insight about the micelle formation rate and the kinetics of phase transition, the order parameter for each component for 12% v. of $A_4B_{16}A_4$ with and without drug addition with the simulation time were analyzed as shown in Figure 4.6.

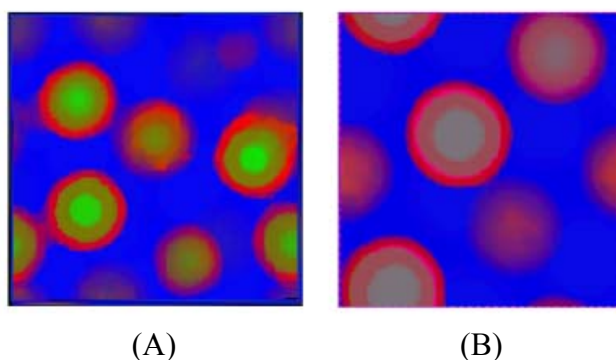


Figure 4.5 Sketch morphology for 12 % v. of $A_4B_{16}A_4$ in aqueous solution at 298 K. (A) without and (B) with adding 2% v. of drug model.

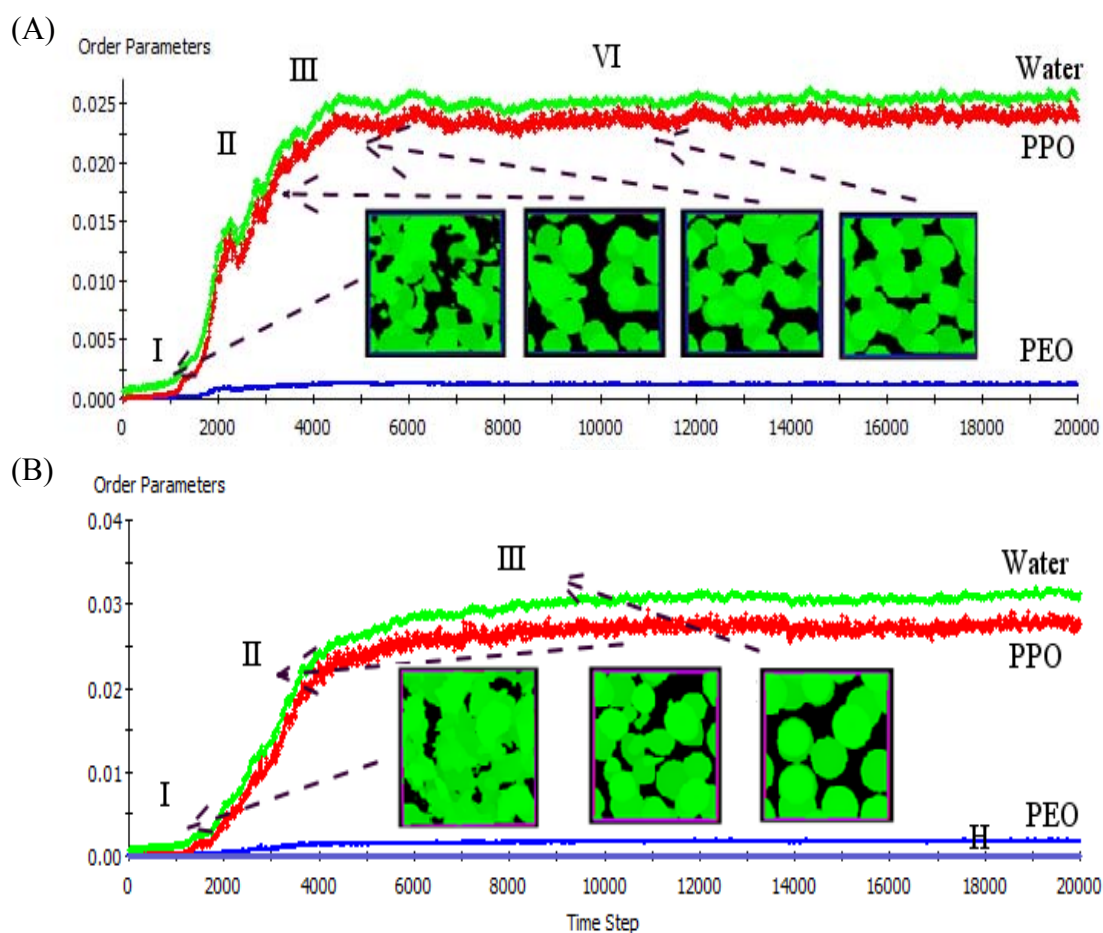


Figure 4.6 Time evolution for 12% v. of $A_4B_{16}A_4$ in aqueous solution at 298 K. (A) without and (B) with 2% v. of drug

There are three major states for micelle growth when the drug molecule was added into polymer solution as suggested by the change in the order parameter. The first state takes about 0.1 microseconds (or 1,000 time steps), the phase solution was still homogeneous in which the order parameter was unchanged from the beginning. Then, the order parameter was largely increased resulting from the phase transition from disorder phase to a spherical micelle in the second state. After that, the system was slowly changed to overcome their morphology in the initial state. The order parameter in this last state is still slowly changed and reaches their equilibrium compared with the micelle in the solution without drug addition. A difference in the number of micelle formation state between these two systems suggests that, it was harder for micelle to form and reach the equilibration state with incorporated drug molecule into the solution. Moreover, the solution needs slightly longer time consuming to transform the phase from a disorder to a spherical micelle and reach their equilibrium.

- **The effect of hydrophobicity of ABA block copolymer**

To investigate effect of increasing the strength of the hydrophobic block on aggregation behavior of the ABA triblock copolymer micelle in aqueous solution was investigated. Here, the PPO was replaced by PLA block. The simulation result was compared between 12 % v. of $A_4B_{16}A_4$ and the $A_4C_{16}A_4$ ($C = \text{PLA}$) as shown in Figure 4.7, where C block has larger hydrophobicity than B. The results indicated that increasing hydrophobic properties of hydrophobic part was affected both on phase morphology and the aggregation mechanism. The morphology was largely changed from spherical to cylindrical-like structure. The formation rate of was

very fast. The phase was strong separated as soon as dissolved in water. That mean, both two input parameter in coarse grain model, chain topology and interaction parameter, are importance for the simulation to give reasonable simulation results.

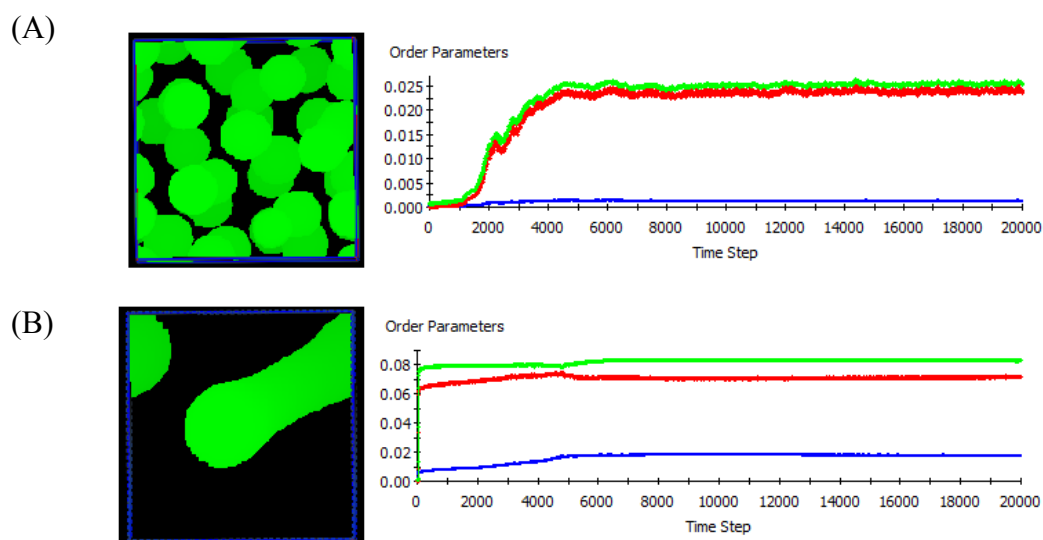


Figure 4.7 The isosurface of the hydrophobic part for 12% v. of (A) $A_4B_{16}A_4$ and (B) $A_4C_{16}A_4$.

4.4.3 Summary

In this section, the influences of A/B block ratio on the morphology of designed triblock copolymer at fixed total number of beads were studied using MesoDyn. The simulation results suggested that the A/B block ratio has a significant effect on phase aggregation, cmc and the formation rate of micelle. The cmc was increased with increasing the block ratio and only appropriate ratio can induce a spherical micelle formation. In addition, the triblock copolymer with longer B block length was easier for micelle formation and its size become bigger. The present of drug model, *i.e.* Haloperidol inducing easier micelle formation and gave bigger

micelle size. The order parameters suggest the drug model was located at the interface between A and B part. Moreover, the strength of hydrophobic part of the triblock copolymer plays an important role on the micelle formation and its morphology.

4.5 Mesoscale simulation of $\text{PLA}_x\text{-PEG}_y\text{-PLA}_x$ triblock copolymer

4.5.1 Simulation detail

The MesoDyn and DPD were used to study the associative structures in aqueous solution of triblock copolymer consisted of polylactide (PLA) and polyethylene glycol (PEG). The effect of the LA/EG block ratio and the third component addition (hydrophobic drug model) on polymer morphology in aqueous solutions were investigated. A $20 \times 20 \times 20$ cubic simulation box with periodic boundary condition was applied in all three directions. The total simulation time of 20,000 with 0.05 integration time step were used.

Gaussian Chain Topology

The Gaussian chain topology is depended on the degree of coarseness of the system. There were two main factors which were crucial to developing the Gaussian chain model *i.e.* the chain length and the bead size. Simple coarse-grained beads of the components used in this study are shown in Table 4.3. The molecular structure of triblock copolymer divided into two types of particle, LA and EG beads which were connected together by harmonic springs. Water and drug model were represented as a particle W and D, respectively.

Table 4.3 Designated Gaussian chain for PLA_x-PEG_y-PLA_x triblock copolymers.

Real system	LA/EG block ratio	Coarse grain bead
PLA ₁₅ PEG ₂₃ PLA ₁₅	0.65	LA4EG5LA4
PLA ₂₈ PEG ₂₃ PLA ₂₈	1.22	LA8EG5LA8
PLA ₄₁ PEG ₂₃ PLA ₄₁	1.78	LA12EG5LA12
Haloperidol	-	D1
Water	-	W 1

Table 4.4 The interaction parameters for DPD (Guo *et al.*, 2009).

α_{ij}	W	D	LA	EG
W	25.00			
D	107.03	25.00		
LA	71.37	30.29	25.00	
EG	36.92	38.49	33.24	25.00

Table 4.5 The interaction parameters for MesoDyn.

$v^{-1}\epsilon_{ij}$	W	D	LA	EG
W	-			
D	25.09	-		
LA	14.18	1.62	-	
EG	3.65	4.13	2.52	-

Interaction parameters between LA, EG, Water and drug model

The interaction energy among chemical entities is the parameters which quantify the characteristics such as hydrophobicity. The parameter represents the pair wise interactions of beads. In order to calculate this parameter for DPD (α_{ij}), the interaction parameter which is related to the Flory-Huggins parameter was calculated using Equation (4.12). Similarly, the repulsive parameters ($v^{-1}\epsilon_{ij}$) for MesoDyn were utilized as the relationship shown in Equation (4.17) and (4.18), respectively. All interaction parameters used summarize in Table 4.4 and 4.5.

4.5.2 Results and discussion

- The effect of polymer concentration

The coarse-grained models of the designated amphiphilic triblock copolymer consisting of PLA and PEG with different LA/EG block ratio ($LA_4EG_5LA_4$, $LA_8EG_5LA_8$ and $LA_{12}EG_5LA_{12}$) in aqueous solution were simulated. The isosurface of three dimensional density field of LA block for each chain topologies on its concentration demonstrate in Figure 4.8. The density field suggests the dependence of the polymer morphology on their concentration. All $LA_4EG_5LA_4$, $LA_8EG_5LA_8$ and $LA_{12}EG_5LA_{12}$ can form micelles in different way by transformed from a disorder to any form of micelle *i.e.* cylindrical shape and lamellar with increasing concentration. As shown in Figure 4.8, the first concentrations to aggregate are 20, 1 and 0.5% v. of $LA_4EG_5LA_4$, $LA_8EG_5LA_8$ and $LA_{12}EG_5LA_{12}$, respectively. For smallest LA/EG block ratio, the micelle was formed at quite high concentration with very large micelle size.

To understand more details in the structure of each spherical micelle, the 8% v. of LA₈EG₅LA₈ choose to point out the structures of spherical micelles through the density field of different beads that represent different species in triblock copolymer. The best density slices of each species along the reference axis of the cubic grid were created. Then, three slices for total spherical micelle, LA and EG bead in the same spherical micelle were divided as shown in Figure 4.9. From this sketch, the structure of spherical micelle is drawing by the dispersion of the EG part in water whereas the LA part forms the micelle core (He *et al.*, 2007; Xiao *et al.*, 2010). There are no water molecules remaining in the micelle core as also suggested by Yang *et al.* for triblock copolymer of PEO and PPO. (Yang *et al.*, 2008a). It may be due to the fact that this spherical micelle is composed of denser core of hydrophobic part which is higher hydrophobicity than that of PPO. To present more details about the spherical micelle in the triblock copolymer solution, DPD simulation snapshot for the 8% v. of the LA₈EG₅LA₈ also illustrate in Figure 4.10. A section view of one spherical micelle at the final simulation time step at 20,000 (2 microseconds) show the distribution of LA blocks as the micelle core and surrounded with the looped EG part as the corona. The morphology of an aggregation looks like a flower-like micelle.

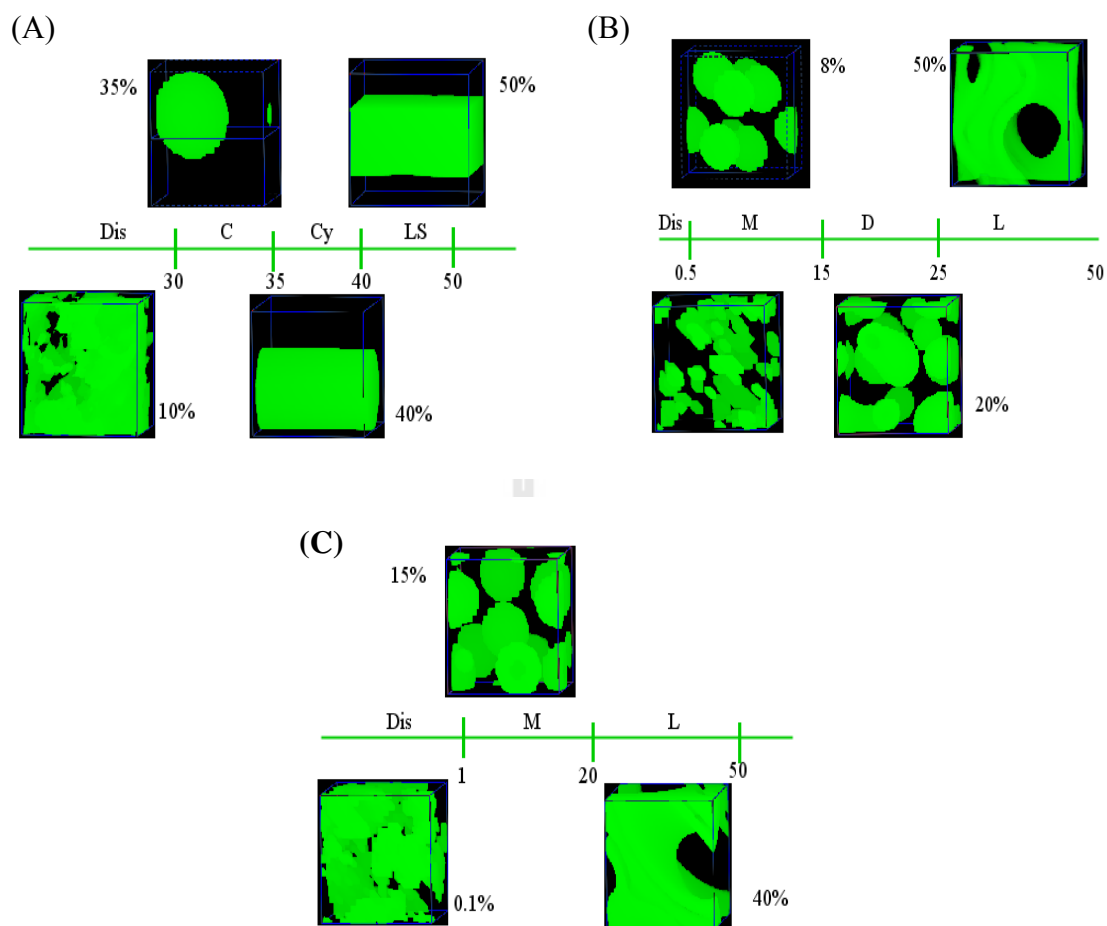


Figure 4.8 Phase morphology in aqueous solution at 298 K for (A) $\text{LA}_4\text{EG}_5\text{LA}_4$, (B) $\text{LA}_8\text{EG}_5\text{LA}_8$ and (C) $\text{LA}_{12}\text{EG}_5\text{LA}_{12}$. Dis (disorder phase), M (micelle), C (big cluster), Cy (cylindrical), D (disk-like micelle) and L (lamellar).

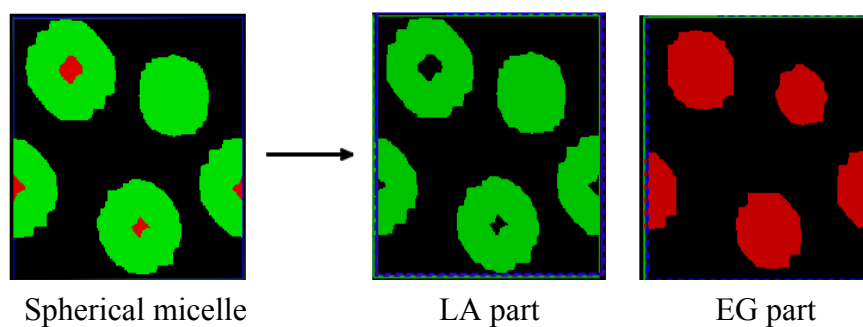


Figure 4.9 The isosurface of LA and EG species in the spherical micelle for 8% v. of $\text{LA}_8\text{B}_5\text{A}_8$ in aqueous solution. Water bead is not present.

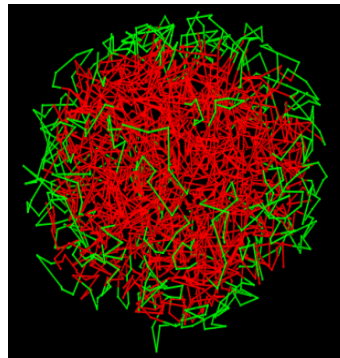


Figure 4.10 Section view of one spherical micelle for 8% v. of $LA_8B_5A_8$. Red color = LA block and Green color = EG block.

- The effect of LA/EG block ratio

The aggregation of triblock copolymer quickly takes place as soon as the polymers reach their cmc in water. MesoDyn method cannot capture the time evolution during the phase transition. The data reported here were mainly about the morphology change by mean of DPD results. In order to investigate the effect of the LA/EG block ratio on the morphology of spherical micelle, $LA_8EG_5LA_8$ and $LA_{12}EG_5LA_{12}$ were carefully analyzed. Figure 4.11, the snapshot of spherical micelle of $LA_8EG_5LA_8$ and $LA_{12}EG_5LA_{12}$ at the same concentration was illustrated. The result shown that, the spherical micelle of $LA_{12}EG_5LA_{12}$ was larger in size than those of $LA_8EG_5LA_8$. This is well corresponding to experimental results that the size of PLA-PEG-PLA triblock copolymer micelle with higher LA/EG block ratio is bigger than the lower LA/EG block ratio (Venkatraman *et al.*, 2005). The important data obtained from DPD is the micelle size in term of the average radial center of mass of end-to-end distance for spherical micelle (DPD unit) as summarize in Table 4.6. In can be concluded that the size of micelle increase with their polymer concentration. However, the dependence of micelle size with concentration was stronger for

LA₁₂EG₅LA₁₂ than those of LA₈EG₅LA₈ as can be clearly illustrate in plot between the micelle sizes as a function of polymer concentration in Figure 4.12. The relation each of them was fitted with linear relation. The slopes of each system were 0.98 and 0.17 for LA₁₂EG₅LA₁₂ and LA₈EG₅LA₈, respectively. These difference dependent may be the major effect of LA/EG block ratio.

Table 4.6 The effect of polymer concentration on micelle size of LA_x-EG_y-LA_x triblock copolymer in term of end to end distance (DPD unit) from DPD simulation.

Polymer concentration	LA ₁₂ EG ₅ LA ₁₂		LA ₈ EG ₅ LA ₈	
	Size	S.D.	Size	S.D.
0.5	1.76	0.58	1.73	0.62
1	2.41	0.91	1.92	0.70
2	2.45	0.92	2.83	1.01
4	3.19	1.21	2.81	1.05
6	3.56	1.39	2.90	1.01
8	3.69	1.39	3.22	1.14
12	3.87	1.56	3.30	1.25

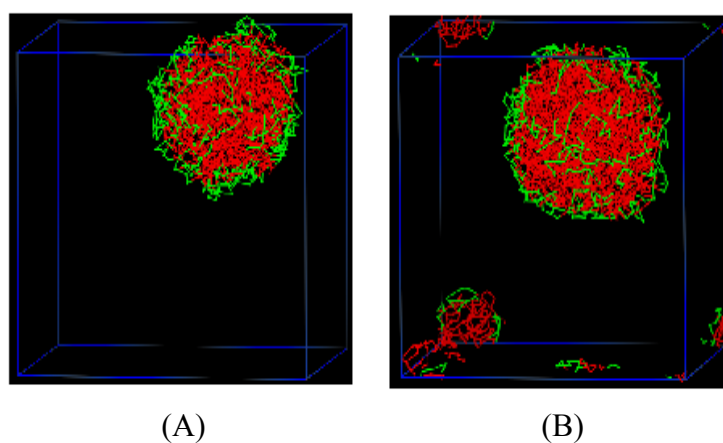


Figure 4.11 Snapshot of spherical micelle for 8% v. of (A) $LA_8EG_5LA_8$ and (B) $LA_{12}EG_5LA_{12}$ in aqueous solution.

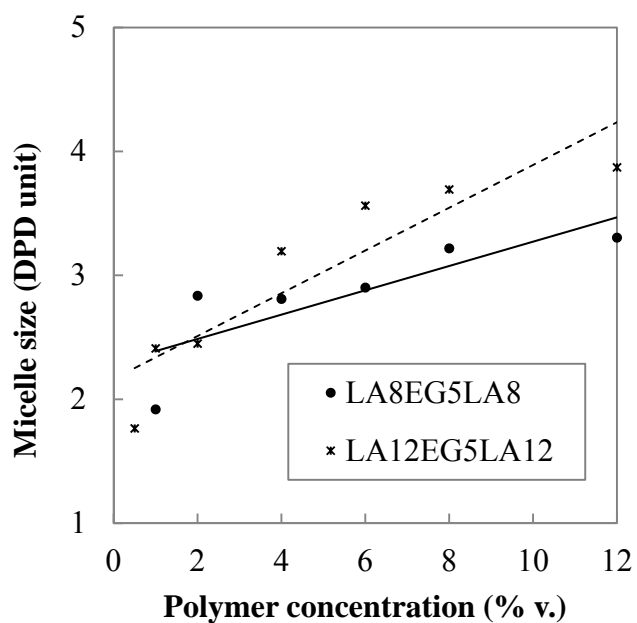


Figure 4.12 The size of micelle as a function of polymer concentration in water.

- **The effect of adding third component (hydrophobic drug model)**

The aggregated morphologies for 8% v. of $LA_8EG_5LA_8$ at different level of drug contents were investigated by DPD simulation. Results of simulation

show in Figure 4.13. A stable microsphere was observed at all drug molecules distributed inside the polymer micelle when the drug content is low (1 – 4% v.) and it was caused the micelle size become bigger. With increasing drug content up to 4 % v., drug molecules can be distributed in the outer region of the spherical micelle. At that point the spherical micelle cannot encapsulated all drug molecules and small amount of drug molecules can formed aggregates outside the micelle as show in Figure 4.13. These phenomena can also be found in the experimental result.

Table 4.7 The effect of drug content on micelle size of $LA_x-EG_y-LA_x$ triblock copolymer in term of end to end distance (DPD unit) from DPD simulation.

drug content	$LA_{12}EG_5LA_{12}$		$LA_8EG_5LA_8$	
	Size	S.D.	Size	S.D.
0.0	3.69	1.39	3.22	1.14
1.0	3.68	1.30	3.27	1.26
2.0	3.86	1.58	3.12	1.17
4.0	3.92	1.52	3.47	1.38
8.0	4.07	1.67	3.47	1.42
12.0	4.50	1.92	3.78	1.60

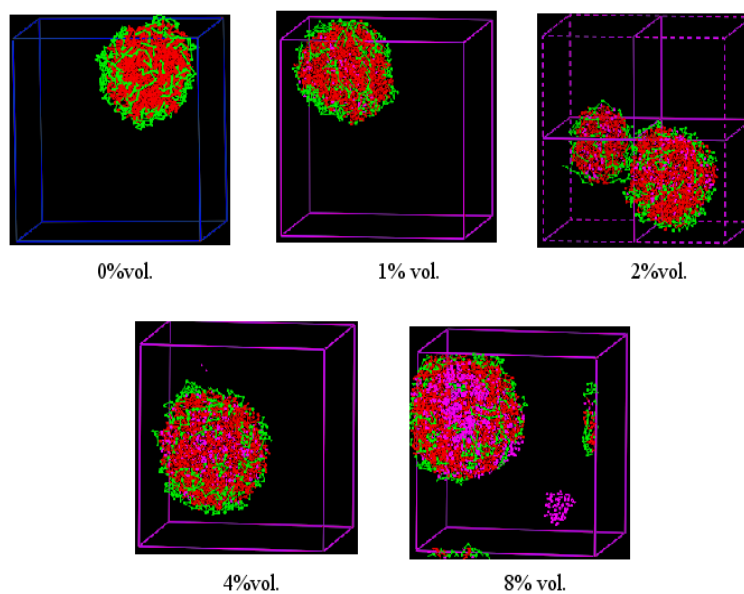


Figure 4.13 Aggregation morphologies for 8% v. of LA₈EG₅LA₈ at various drug contents.

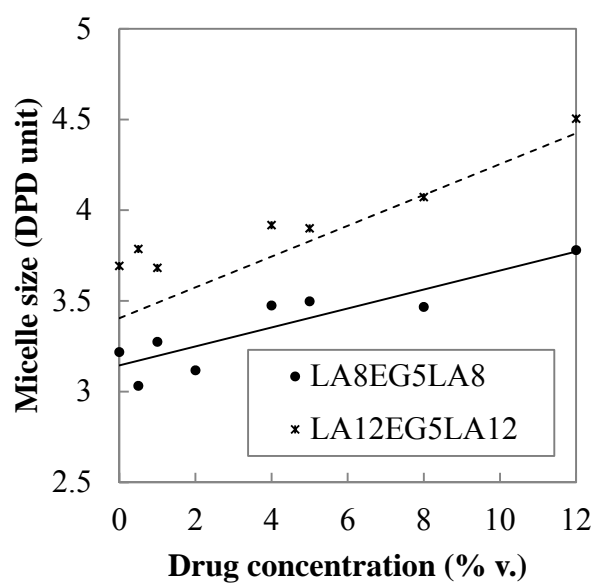


Figure 4.14 The size of micelle as a function of drug concentration in aqueous solution.

In order to study the effect of drug content in difference LA/EG block ratio, the introducing of various concentration of drug to LA₁₂EG₅LA₁₂ solution was

also investigated. The distribution of drug within the micelle was presented similar trend with LA₈EG₅LA₈ system (not shown here). The size of micelle increased with an increase of drug content. However, the critical concentration of drug encapsulation of LA₁₂EG₅LA₁₂ micelle was higher. The size of spherical micelle as a function of the drug content for LA₈EG₅LA₈ and LA₁₂EG₅LA₁₂ were summarized in Table 4.7. In addition, the plots of the relation between the sizes of micelle with drug concentration image in Figure 4.14. The slope of linear relation between the micelle size and the drug content are 0.08 and 0.05 for LA₈EG₅LA₈ and LA₁₂EG₅LA₁₂, respectively. This can be indicated that LA₁₂EG₅LA₁₂ was more effective in encapsulated hydrophobic drug than those of LA₈EG₅LA₈.

4.5.3 Summary

In this section, the influences of LA/EG block ratio, polymer concentration and the third component addition (drug model) on phase aggregation of designed LA_x-EG_y-LA_x were studied using both MesoDyn and DPD simulation. The simulation results suggested that the LA/EG block ratio play an importance role in micelle formation. Only the appropriated ratio can induce spherical micelle formation. With increasing the block ratio was increased in cmc and micelle size. Unfortunately, the aggregation was very strong and it hardly to get more details about the micelle formation step using the order parameter from MesoDyn. The present of drug model into the solution can induce larger micelle size and drug was distributed everywhere inside the core at low drug concentration. The polymer with higher LA/EG block ratio was more efficiency to encapsulate hydrophobic drug model.

4.6 References

- Alexandridis, P., Olsson, U. and Lindman, B. (1995). Self-assembly of amphiphilic block copolymers: the (EO)₁₃(PO)₃₀(EO)₁₃-water-p-xylene system. **Macromolecules** 28(23): 7700-7710.
- Batrakova, E. V. and Kabanov, A. V. (2008). Pluronic block copolymers: evolution of drug delivery concept from inert nanocarriers to biological response modifiers. **Journal of Controlled Release** 130(2): 98-106.
- Doi, M. and Edwards, S. F. (1988). The theory of polymer dynamics. United Kingdom, Oxford Univ Pr on Demand.
- Español, P. and Warren, P. (1995). Statistical mechanics of dissipative particle dynamics. **EPL (Europhysics Letters)** 30(4): 191.
- Fermeglia, M. and Pricl, S. (2007). Multiscale modeling for polymer systems of industrial interest. **Progress in Organic Coatings** 58(2): 187-199.
- Groot, R. D. and Warren, P. B. (1997). Dissipative particle dynamics: bridging the gap between atomistic and mesoscopic simulation. **The Journal of Chemical Physics** 107(11): 4423-4435.
- Guo, S. L., Hou, T. J. and Xu, X. J. (2002). Simulation of the phase behavior of the (EO)₁₃(PO)₃₀(EO)₁₃(pluronic L64)/water/p-xylene system using MesoDyn. **The Journal of Physical Chemistry B** 106(43): 11397-11403.
- Guo, X. D., Tan, J. P. K., Zhang, L. J., Khan, M., Liu, S. Q., Yang, Y. Y. and Qian, Y. (2009). Phase behavior study of paclitaxel loaded amphiphilic copolymer in two solvents by dissipative particle dynamics simulations. **Chemical Physics Letters** 473(4): 336-342.

- Guo, X. D., Zhang, L., Qian, Y. and Zhou, J. (2007). Effect of composition on the formation of poly(dl-lactide) microspheres for drug delivery systems: mesoscale simulations. **Chemical Engineering Journal** 131(1): 195-201.
- He, G., Ma, L. L., Pan, J. and Venkatraman, S. (2007). ABA and BAB type triblock copolymers of PEG and PLA: a comparative study of drug release properties and “stealth” particle characteristics. **International Journal of Pharmaceutics** 334(1): 48-55.
- Hoogerbrugge, P. J. and Koelman, J. M. V. A. (1992). Simulating microscopic hydrodynamic phenomena with dissipative particle dynamics. **EPL (Europhysics Letters)** 19(3): 155-161.
- Jawalkar, S. S. and Aminabhavi, T. M. (2006). Molecular modeling simulations and thermodynamic approaches to investigate compatibility/incompatibility of poly(l-lactide) and poly(vinyl alcohol) blends. **Polymer** 47(23): 8061-8071.
- Kabanov, A. V., Batrakova, E. V. and Alakhov, V. Y. (2002). Pluronic® block copolymers as novel polymer therapeutics for drug and gene delivery. **Journal of Controlled Release** 82(2): 189-212.
- Kremer, K. (2003). Computer simulations for macromolecular science. **Macromolecular Chemistry and Physics** 204(2): 257-264.
- Lam, Y.-M. and Goldbeck-Wood, G. (2003). Mesoscale simulation of block copolymers in aqueous solution: parameterisation, micelle growth kinetics and the effect of temperature and concentration morphology. **Polymer** 44(12): 3593-3605.

- Lam, Y.-M., Goldbeck-Wood, G. and Boothroyd, C. (2004). Mesoscale simulation and cryo-TEM of nanoscale drug delivery systems. **Molecular Simulation** 30(4): 239-247.
- Mu, D., Li, J.-Q. and Zhou, Y.-H. (2011). Modeling and analysis of the compatibility of polystyrene/poly(methyl methacrylate) blends with four inducing effects. **Journal of Molecular Modeling** 17(3): 607-619.
- van Vlimmeren, B. A. C., Maurits, N. M., Zvelindovsky, A. V., Sevink, G. J. A. and Fraaije, J. G. E. M. (1999). Simulation of 3D mesoscale structure formation in concentrated aqueous solution of the triblock polymer surfactants (ethylene oxide)₁₃(propylene oxide)₃₀(ethylene oxide)₁₃ and (propylene oxide)₁₉(ethylene oxide)₃₃(propylene oxide)₁₉: application of dynamic mean-field density functional theory. **Macromolecules** 32(3): 646-656.
- Venkatraman, S. S., Jie, P., Min, F., Freddy, B. Y. C. and Leong-Huat, G. (2005). Micelle-like nanoparticles of PLA-PEG-PLA triblock copolymer as chemotherapeutic carrier. **International Journal of Pharmaceutics** 298(1): 219-232.
- Wu, H., Xu, J., He, X., Zhao, Y. and Wen, H. (2006). Mesoscopic simulation of self-assembly in surfactant oligomers by dissipative particle dynamics. **Colloids and Surfaces A: Physicochemical and Engineering Aspects** 290(1-3): 239-246.
- Xiao, R. Z., Zeng, Z. W., Zhou, G. L., Wang, J. J., Li, F. Z. and Wang, A. M. (2010). Recent advances in PEG-PLA block copolymer nanoparticles. **International Journal of Nanomedicine** 5(1): 1057-1065.

- Xin, D. G., Jeremy, P. K. T., Sung, H. K., Li, J. Z., Ying, Z., James, L. H., Yi, Y. Y. and Yu, Q. (2009). Computational studies on self-assembled paclitaxel structures: Templates for hierarchical block copolymer assemblies and sustained drug release. **Biomaterials** 30(33): 6556-6563.
- Yang, S., Yuan, S., Zhang, X. and Yan, Y. (2008a). Phase behavior of tri-block copolymers in solution: Mesoscopic simulation study. **Colloids and Surfaces A: Physicochemical and Engineering Aspects** 322(1-3): 87-96.
- Yang, S., Zhang, X. and Yuan, S. (2008b). Mesoscopic simulation studies on micellar phases of Pluronic P103 solution. **Journal of Molecular Modeling** 14(7): 607-620.
- Zhang, X., Yuan, S., Xu, G. and Liu, C. (2007). Mesoscopic simulation of the phase separation on triblock copolymer in aqueous solution. **Acta Physico-Chimica Sinica** 23(2): 139-144.
- Zhao, Y., You, L.-Y., Lu, Z.-Y. and Sun, C.-C. (2009). Dissipative particle dynamics study on the multicompart ment micelles self-assembled from the mixture of diblock copolymer poly(ethyl ethylene)-block-poly(ethylene oxide) and homopolymer poly(propylene oxide) in aqueous solution. **Polymer** 50(22): 5333-5340.

CHAPTER V

POLYLACTIDE-POLYETHYLENE GLYCOL - POLYLACTIDE (PLA_x-PEG_y-PLA_x) TRIBLOCK COPOLYMER MICELLE

5.1 Abstract

Three PLA_x-PEG_y-PLA_x triblock copolymers were synthesized by bulk ring opening polymerization using stannous octoate as the catalyst. The PEG block lengths was fixed ($\overline{M}_n = 1,000$ g/mol, 23 ethylene oxide units) with three different PLA block lengths. The triblock copolymer composition and molecular weight were determined by ¹H NMR and GPC. The critical micelle concentration (cmc) of these amphiphilic triblock copolymers in aqueous solutions was determined by using the fluorescent probe technique. The results revealed that only the appropriated balancing of hydrophobic and hydrophilic LA/EG block ratio in the copolymer can induce the micelle formation. In addition, light scattering technique was applied to study hydrodynamic radius of these copolymer micelle. For illustration of the concept of drug delivery system, pyrene was used to mimic the behavior of the hydrophobic drug model to investigate an ability of this copolymer micelle to encapsulate drug molecule in term of the partition coefficient between water phase and micelle core.

5.2 Introduction

The earliest pharmaceutical method usually exhibits a specific problem causing a reduction of an efficiency of drug therapy. To gain the most effective therapy, understanding of the human body and the discovery of new and potential treatments are necessary. Drug delivery systems (DDSs) have been used to solve the pharmaceutical therapy problem based on an idea that drug should be released at the right site, in the right dose and for the required time without any side effect (Mishra *et al.*, 2010; Whittlesey and Shea, 2004). Biocompatible or biodegradable properties are required especially for implantable drug delivery system (IDDS). It should be a nontoxic fragment which can be eliminated harmlessly from the body (Kumari *et al.*, 2010; Nair and Laurencin, 2007; Winzenburg *et al.*, 2004). The successful of pharmaceutical therapy by DDS is largely dependent on the delivery carrier and controlled release system. The drug carriers evade recognition and uptake by mononuclear phagocyte system (MPS) (Ganta *et al.*, 2008; Sung *et al.*, 2007). Among nanoscopic carriers, polymer micelles with advances in the chemistry of amphiphilic, biocompatible and biodegradable polymer have been highly interested for an effective drug deliver application due to their performance to self-organize at nanoscales in an appropriate condition (Cho *et al.*, 2010; Gaucher *et al.*, 2005; Torchilin, 2007). Especially, their self-assembled in solution states have already been shown to be useful for many applications in gene therapy, nanotechnology and drug delivery.

Initially, studies of most block copolymer micelle-based delivery systems are focused on Pluronic® (BASF), the triblock copolymer of polyethylene oxide (PEO) and polypropylene oxide (PPO). PEO is the polymer with ethylene oxide, but with a

relatively low molecular weight (Almgren *et al.*, 1995; Kwon and Okano, 1999; Linse, 1994). It is generally considered to be inert and possess a low order of toxicity in animals and humans. In addition, it has been widely investigated and often shows extended circulation through modification with other polymers (Loh, 2002). The micellization and aggregation behavior of pure and multicomponent in aqueous solution and their application as drug delivery carriers have been much considered (Alexandridis *et al.*, 1994; Mata *et al.*, 2004; Rapoport, 2004).

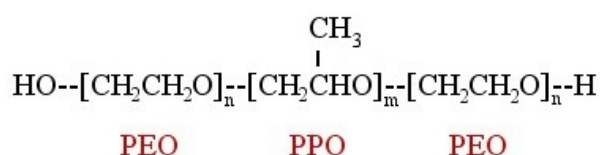


Figure 5.1 Molecular structure of polyethylene oxide - polypropylene oxide - polyethylene oxide (PEO-PPO-PEO) triblock copolymer.

Nowadays, biodegradable polymer is widely interesting as they are friendly with an environment. Block copolymers made of PLA and PEG has evoked considerable interest as biodegradable drug carriers (Nair and Laurencin, 2007). The triblock copolymer of PLA and PEG can be synthesized as designed properties by varying chemical composition, molecular weight and block ratio, which allows control micelle properties in many applications (Agrawal *et al.*, 2006; Lee *et al.*, 2002; Li *et al.*, 1996). With an amphiphilic property their micelle forms self-assemble in selective solvent. The PLA part is form the hydrophobic core of the micelles, while the PEG shell forms a dynamic molecular shield *i.e.* corona over the surface that provides interactions with the solvent and makes these nanoparticles stable in the

medium. Hydrophobic drugs can be physically entrapped in the micelle core which can evade the immune system and circulate for longer period of time after administration without any takeover causing these structures is great interest for hydrophobic drug delivery applications (Oh, 2011). To control over the chain length, the ratio of hydrophilic and hydrophobic components and copolymer structure are possible and offer the possibility of modifying the size and surface characteristics of the association complexes formed in water. The complexes can be considered to be a micelle type and this form may be utilized directly for drug delivery application. An efficient application of polymer micelles as drug carriers is considered by their loading capacity, size, circulation time, stability, release kinetics, and biodistribution (Lee *et al.*, 2002). Their encapsulation efficiency was involved by the relevancy of the drug molecule with the micelle cores, the volume of hydrophobic cores, and the hydrophilicity of drugs (Venkatraman *et al.*, 2005).

In order to synthesize PLA-PEG-PLA triblock copolymer, ring opening polymerization is the most popular method to polymerize lactide monomer into a preformed dihydroxy ended polyethylene oxide. A number of catalysts have been used for this purpose *i.e.* stannous octoate, SnO, SnO₂, Sb₂O₃, PbO, GeO₂, SnCl₂, zinc powder, and NaH (Cohn and Younes, 1988; Kricheldorf and Meier-Haack, 1993; Xiao *et al.*, 2010; Zhu *et al.*, 1990). Among of them, stannous octoate is the most frequently used because it leads to high yield and high molecular weights (Kricheldorf and Meier-Haack, 1993).

In this research, the PLA_x-PEG_y-PLA_x triblock copolymers were synthesized via ring opening polymerization by using stannous octoate and dihydroxy PEG as the catalyst and the initiator. The characteristic of triblock copolymer was determined by

^1H NMR and GPC. Effect of the LA/EG block ratio on critical micelle concentration (cmc) and ability of polymer micelle to encapsulate pyrene drug model were investigated. In addition, the hydrodynamic radius (R_H) of polymer micelle was observed.

5.3 Materials and methods

5.3.1 Materials

- L-lactide (Sigma-Aldrich, 98%)
- Polyethylene glycol ($\overline{M_n} \sim 1,000$ g/mol, HO-[CH₂CH₂O]₂₃-H)
- Ethyl acetate (Sigma-Aldrich, 99.5%)
- Stannous octoate (Aldrich, ~95%)
- Toluene (Sigma-Aldrich, >99.5%)
- Dichloromethane (Sigma-Aldrich, 99.8%)
- Petroleum ether (Sigma-Aldrich, ACS reagent)
- Calcium hydride (Sigma-Aldrich, anhydrous grade)
- Molecular sieves 3 Å (Sigma-Aldrich, beads 4-8 mesh)
- Pyrene (Sigma-Aldrich, 98%)

5.3.2 Analysis instrument

- Proton Nuclear Magnetic Resonance (^1H NMR) (JEOL JNM LA500 spectrometry, Osaka university)
- Gel permeation chromatography (GPC) (JASCO GPC-900/ Shodex Asahipak GF-7M HQ column, Osaka University)

- Fluorescence (Hitachi F-4500 fluorescence spectrophotometer, Osaka University)
- Dynamic and static light scattering (LS) (ALV/DLS/SLS-5000 light scattering photometer, Osaka University)

5.3.3 Research methods

- Lactide recrystallization

Ethyl acetate was first poured into a 500 mL three necks round bottom flask and heated by rising the temperature of the oil bath to 328 K. Place a beaker of L-lactide with a magnetic stirrer on hot plate (around 328 K), slowly added hot ethyl acetate to the monomer until monomer was completely dissolved. After that, removed the beaker from the heat and allowed the flask to cool at room temperature. The monomer solution was then placed in to the refrigerator for one hour. The ethyl acetate was rinsed out and do the recrystallizations step again for 2 times. Finally, the solution was filtered through sinter glass to collect monomer crystal. Then lactide monomer crystals were dried overnight in the vacuum oven before further use.

- Ethyl acetate distillation

Ethyl acetate was used as the solvent to recrystallize lactide monomer. Dried toluene was obtained by a simple distillation at 353 K (boiling point 349-351 K). Dried CaH_2 was used to absorb the moisture from solvent before distillation. The dried ethyl acetate was soaked in 3Å molecular sieve before used.

- **Toluene distillation**

Toluene was used as the solvent to prepared catalyst solution. Toluene was distilled over sodium/benzophenone at 383 K. The dried toluene was soaked in molecular sieve 3Å before further used.

- **Triblock copolymer synthesis**

Premeasured amount of dried L-lactide and PEG were first added to a three neck flask connected to T-joint adapter. Through the upper neck was capped with a rubber septum. To another neck was attached a vacuum pump. The atmosphere within the flask was slowly pumped out and filled with argon gas. The catalyst solution was injected and flow argon through the flask again before it was placed in an oil bath at 383 K for 20-24 h. After a given amount of time, the reaction was removed from heating and it was placed under the room temperature before dissolution/precipitation in dichloromethane and petroleum ether. The polymer was filtered and dried under vacuum oven for one day. Information details of the triblock copolymer, which denoted as TB were shows in Table 5.1.

Table 5.1 Polymerization conditions used in the triblock copolymer synthesis.

System	LA/EG block ratio	Weight of LA in feed (g)	Weight of PEG in feed (g)
TB1	0.61	1.0000	0.4953
TB2	1.22	1.0000	0.2480
TB3	2.00	1.0000	0.1510

- **Triblock copolymer characterization**

Proton Nuclear Magnetic Resonance (^1H NMR)

Varian 300 MHz ^1H NMR at Chemistry Department (Osaka University) was used to confirm the structure of prepared triblock copolymer. Solvent used in this experiment was deuterium chloroform. The using temperature was 298 K.

Gel Permeation Chromatography (GPC)

Molecular weight and its distribution were performed using JASCO GPC-900 equipped with a Shodex Asahipak GF-7M HQ column in combination with JASCO UV-975 and RI-930 detectors. In general 5 mg samples were used to dissolve in 1 mL of THF for a complete dissolution. The temperature was set at 313 K using THF as the elution at flow rate 1 mL/min. Polyethylene glycol and polyethylene oxide standard ($\overline{M}_n \sim 6,000, 21,000, 44,900$ and $255,000$ g/mol) purchased from Scientific Polymer Products were used for molecular weights calibration.

- **Triblock copolymer micelle characterization**

Fluorescence

Fluorescence measurements were carried out at Laboratory of Polymer Assemblies, Osaka University to determine the critical micelle concentration of $\text{PLA}_x\text{-PEG}_y\text{-PLA}_x$ triblock copolymer micelles using pyrene as a molecular probe. The measurement was recorded on a Hitachi F - 4500 fluorescence spectrophotometer at 298 K. The changing in excitation spectra of pyrene in different polymer solution was monitored with the emission spectra at 390 nm. The slit widths for both the

excitation and emission sides were 2.5 nm. Stock solution of triblock copolymer and pyrene were first separately prepared.

- Triblock copolymer solutions: The triblock copolymer was first dissolved in a little amount of THF. Pure water was following added with gentle agitation.
- Pyrene solution: pyrene was dissolved in acetone to prepare 0.01 g/L of pyrene solution.

After that, predetermined amount of pyrene stock solution was added into a series of small test tube. After acetone was evaporated, the triblock copolymer solution was added and was adjusted its volume using pure water. The series of various triblock copolymer concentrations in range of 0.00005 - 4.0 g/L contain the final pyrene concentration at 6×10^{-7} mol/L were obtained.

Light scattering (LS)

Light scattering measurements were carried out on an ALV/DLS/SLS-5000 light scattering photometer (Photal Otsuka Electronics, Japan) equipped with a multi- τ digital time correlator (ALV-5000E). Vertically polarized light with the wavelength of 532 nm emitted from a Nd:YAG laser (model 532, Coherent) was used as the incident light, and the scattered light was measured with no analyzer. The light scattering system was calibrated using toluene as the reference material to determine the excess Rayleigh ratio R_θ of the solution over that of the solvent at the scattering angle θ . The intensity of the scattered light was detected at a scattering angular range from 30 to 150°. The apparent hydrodynamic radius R_H at each concentration was determined. Moreover, intensity autocorrelation functions

$g^{(2)}(t)$ were obtained to analyze the relaxation time spectrum $A(\tau)$. Sample for light scattering measurement was prepared by directly dissolving triblock copolymer in pure water. The solution was stirred overnight before measurement.

5.4 Results and discussion

5.4.1 Triblock copolymer characterization

To confirm the results in Chapter IV that balancing between the LA/EG block ratio was affected the micelle formation, three $\text{PLA}_x\text{-PEG}_y\text{-PLA}_x$ triblock copolymers with different PLA block lengths at fixed PEG block were synthesized by ring opening polymerization using stannous octoate as catalyst. In order to obtain desired polymer structure, the monomer and initiator were used as shown in Table 5.1. The

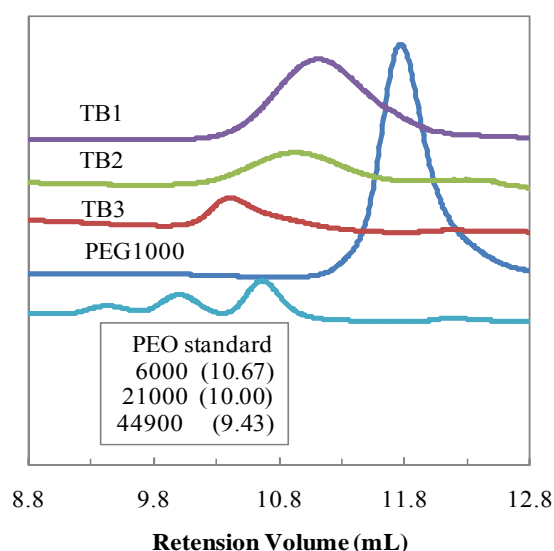
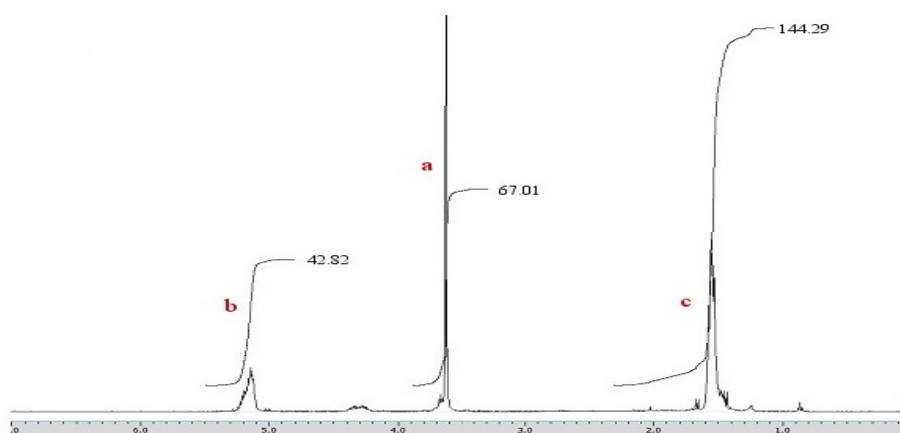
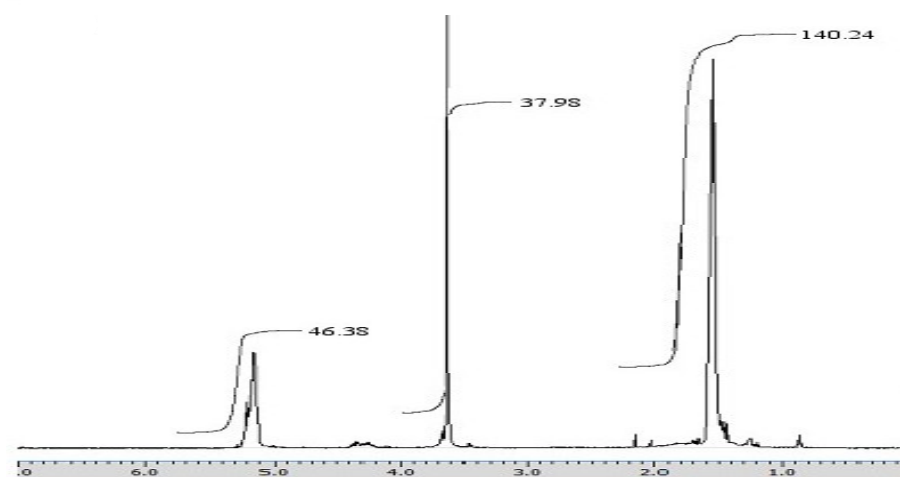


Figure 5.2 Gel permeation chromatogram of $\text{PLA}_x\text{-PEG}_y\text{-PLA}_x$ triblock copolymer.

(A)



(B)



(C)

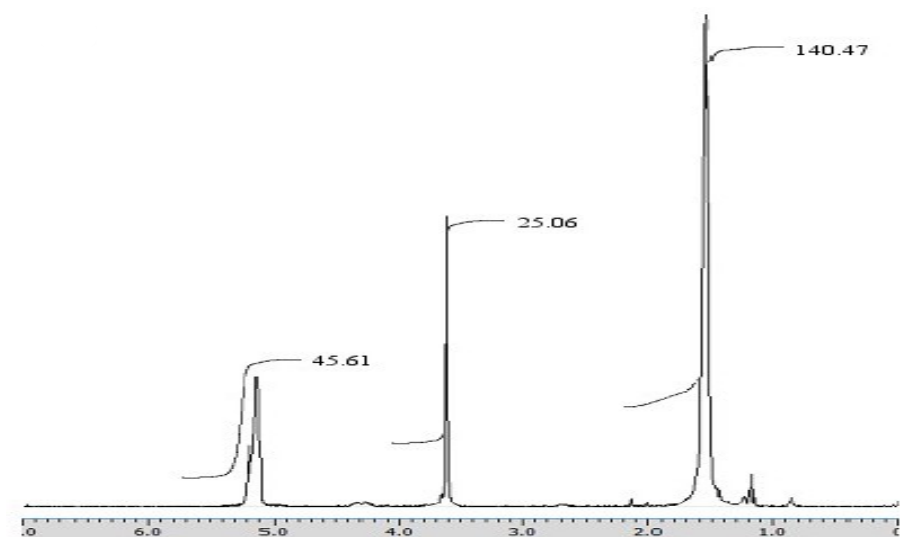


Figure 5.4 The ^1H NMR spectra of (A) TB1, (B) TB2 and (C) TB3 in CDCl_3 at 298 K. The labels are according to character label in Figure 5.3.

As this triblock copolymers consist only of PLA and PEG in their chemical structure. So, the molecular weight or degree of polymerization (\overline{DP}) for each of them can be determined by following relationship (Venkatraman *et al.*, 2005)

$$\overline{DP}_{PLA} \approx \overline{DP}_{PEG} \times (LA/EG) / 2 \quad (5.1)$$

$$\overline{Mn}_{PLA} \approx \overline{DP}_{PLA} \times 144 \quad (5.2)$$

$$\overline{Mn}_{Total} \approx \overline{Mn}_{PLA} + \overline{Mn}_{PEG} \quad (5.3)$$

where \overline{Mn} and \overline{DP} are the number average molecular weight and degree of polymerization, respectively. The LA/EG is the fractional which is according to number of proton for each species and can be determined by 1H NMR.

Example: LA/EG in product and \overline{DP}_{PLA} of TB1 were determined from the integration ratio of resonance due to PEG blocks at 3.6 ppm ($-O-CH_2CH_2-$) and to the PLA blocks at 5.2 ppm ($Me-CH^*<$) in the 1H NMR. The integration are 42.82 and 67.01 for ($Me-CH^*<$) and ($-O-CH_2CH_2-$), respectively.

$$\begin{aligned} \overline{DP}_{PLA} &\approx \overline{DP}_{PEG} \times (LA/EG) / 2 \\ &\approx \left(\frac{1,000}{44} \right) \times \left(\frac{(42.82)}{(67.01/4)} \right) / 2 \\ &\approx 29 \end{aligned}$$

$$\begin{aligned} \overline{Mn}_{PLA} &\approx \overline{DP}_{PLA} \times 144 \\ &\approx 29 \times 144 \\ &\approx 4,183 \end{aligned}$$

Therefore, the structure of this triblock copolymer is PLA₂₉-PEG₂₃-PLA₂₉. Other triblock copolymers were calculated as the above explanation and summarized in Table 5.2. The obtained triblock copolymer did not successful synthesize as aspect. The LA/EG ratio in the products was quite higher than in feed. However, the remaining system can be used to study the effect of LA/EG ratio on micelle properties and ability of them to encapsulate pyrene drug model.

Table 5.2 Characteristic of PLA_x-PEG_y-PLA_x triblock copolymers.

System	Polymer	LA/EG	LA/EG	\overline{DP}_{PLA}^b	\overline{Mn}_{total}^c
		block in feed	block in product ^a		
TB1	PLA ₂₉ PEG ₂₃ PLA ₂₉	0.61	2.56	29	5,188
TB2	PLA ₅₆ PEG ₂₃ PLA ₅₆	1.22	4.88	56	9,076
TB3	PLA ₈₃ PEG ₂₃ PLA ₈₃	2.00	7.28	83	12,964

^a Integration ratio of resonance due to PEG blocks at 3.6 ppm (–O–CH₂CH₂–) and to the PLA blocks at 5.2 ppm (Me–CH*–) in the ¹H NMR

$$^b \overline{DP}_{PLA} \approx \overline{DP}_{PEG} \times (LA/EG) / 2$$

$$^c \overline{Mn}_{total} \approx (\overline{DP}_{PLA} \times 144) + (\overline{DP}_{PEG} \times 44)$$

5.4.2 Triblock copolymer micelle characterization

- Critical micelle concentration (cmc)

The critical micelle concentration (cmc) of the triblock copolymer was determined using fluorescent probing. The fluorescent of pyrene molecule is

largely depending on its environment, which is providing the localized information. The pyrene excimer can be formed when aromatic rings closely approach to each other within 4 - 5 Å, which is quite sensitive to the small aggregates containing two or more pyrene groups. Obviously the fluorescence intensity increases tremendously and the maximal peak position shifts with increasing polymer concentration depend mainly on the relative hydrophobic nature of the micelle cores *i.e.* more hydrophobicity of micelle core should induce larger maximal peak shift (Dai *et al.*, 2004). Fluorescence excitation spectra of pyrene in the presence of various concentrations ranging between 0.00005 - 4.0 g/L of three PLA_x-PEG₂₃-PLA_x systems are shown in Figure 5.5. As clearly see from Figure 5.5, the spectra of TB2 and TB3 were revealed the peak shift between 334 to 336 nm which is attributed to pyrene probe molecules entering the micelle core. The spectrum of the TB1 was not changed this because micelle formation cannot occurred. On the basis of the peak shift, the cmc for each system were determined (Dai *et al.*, 2004; Wilhelm *et al.*, 1991). The plot of the selected fluorescence intensity ratio (I_{336}/I_{334}) as a function of the concentration of TB2 and TB3 were demonstrated in Figure 5.6. A little distort S-shaped curve is obtained, which reflects the whole process of micellization. The intersection of the lower horizontal tangent and the slope tangent corresponds to the cmc for each system. As expected, the cmc were increased with increasing LA/EG block ratio (He *et al.*, 2007) as summarized in Table 5.4. The cmc of TB2 and TB3 are 0.46 and 0.63 mg/L, respectively. The results are good agreement with other studies that the trends of cmc is increasing with LA/EG block ratio (Venkatraman *et al.*, 2005).

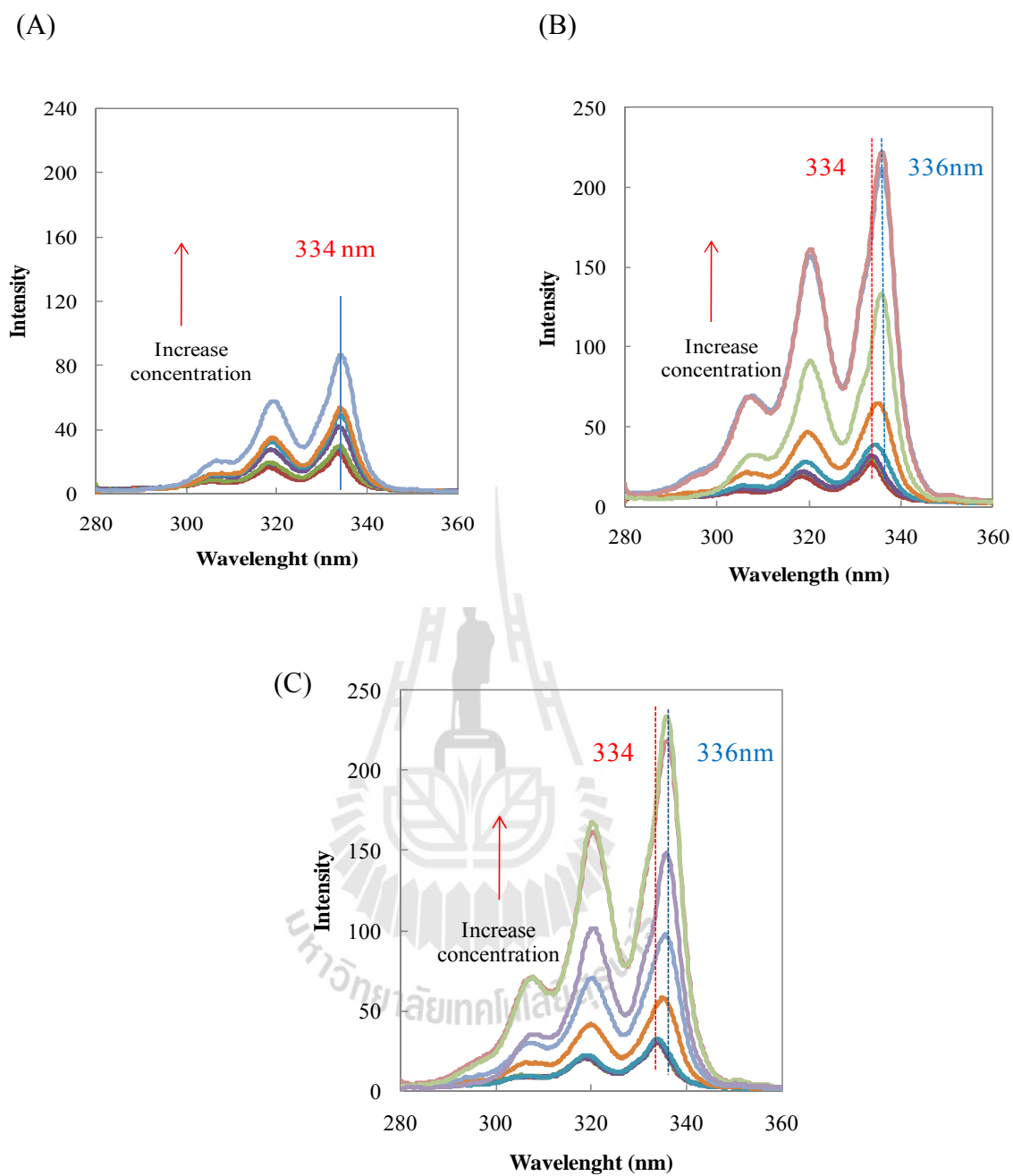


Figure 5.5 Pyrene excitation spectra (at emission wavelength 390 nm) as a function of polymer concentration of (A) TB1, (B) TB2 and (C) TB3.

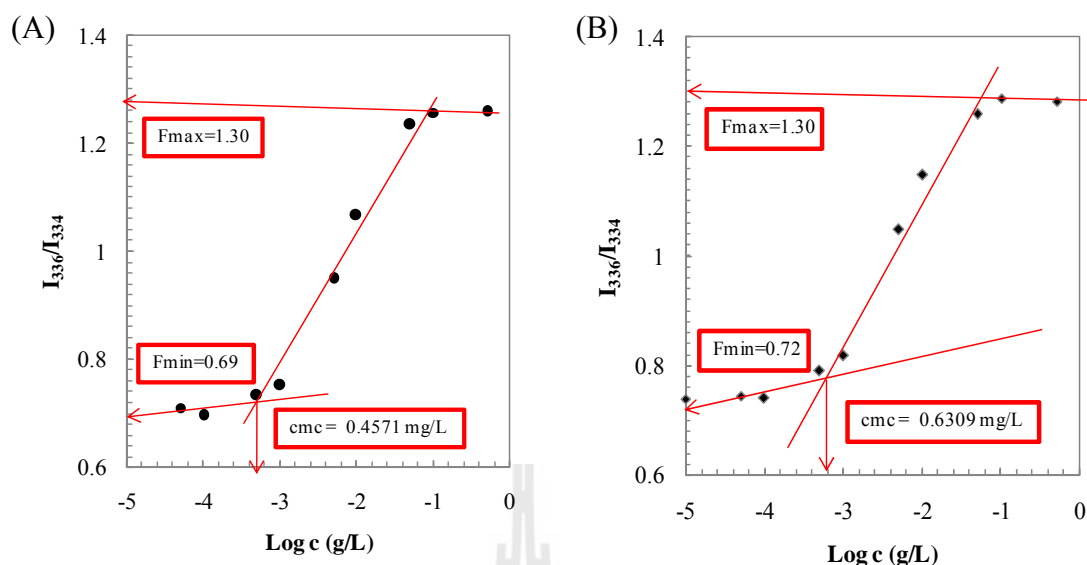


Figure 5.6 Plots of the intensity ratio I_{336}/I_{334} versus $\log c$ for (A) TB2 and (B) TB3.

- The micelle size

The suitable balancing of hydrophilic/hydrophobic ratio of the amphiphilic $PLA_x-PEG_y-PLA_x$ triblock copolymers, which is consisting of hydrophilic PEG and hydrophobic PLA blocks, provides an opportunity to form micelles in water. Light scattering results of triblock copolymer in solution were investigated. The intensity autocorrelation function $g^{(2)}(t)$ obtained by dynamic light scattering was analyzed to estimate the spectrum $A(s, k)$ of the relaxation time s (in the logarithmic scale) at each k . The aggregated particle from $PLA_x-PEG_y-PLA_x$ triblock copolymer in solution, for example in Figure 5.7, show the unimodal spectra $A(s, k)$ and gives a single hydrodynamic radius (R_H) after an extrapolation to zero c and k . The R_H each concentration was determined using the semilogarithmic plot of $g^{(2)}(t) - 1$ versus t . Figure 5.8 presents the R_H as a function of concentration for TB2 and TB3. The results revealed that the particle size of TB3 was increased with their concentration, whereas the particle size of TB2 was independent from its

concentration. The mean diameters of the micelles which are relative to their structure and concentration for each system were summarized in Table 5.3.

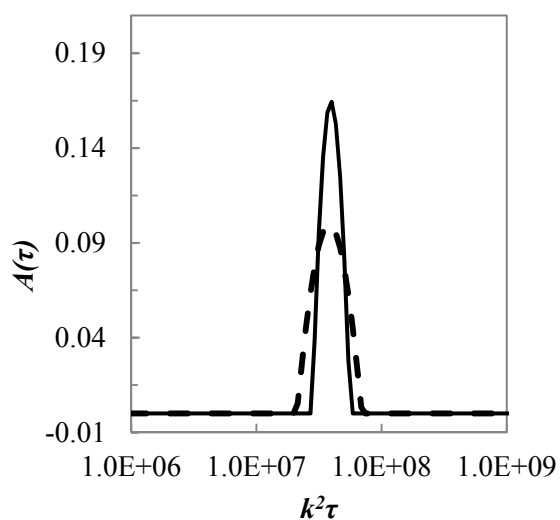


Figure 5.7 Relaxation spectra $A(\tau, k)$ at $\theta=90^\circ$ for 0.01 g/L of TB2 (---) and TB3 (—).

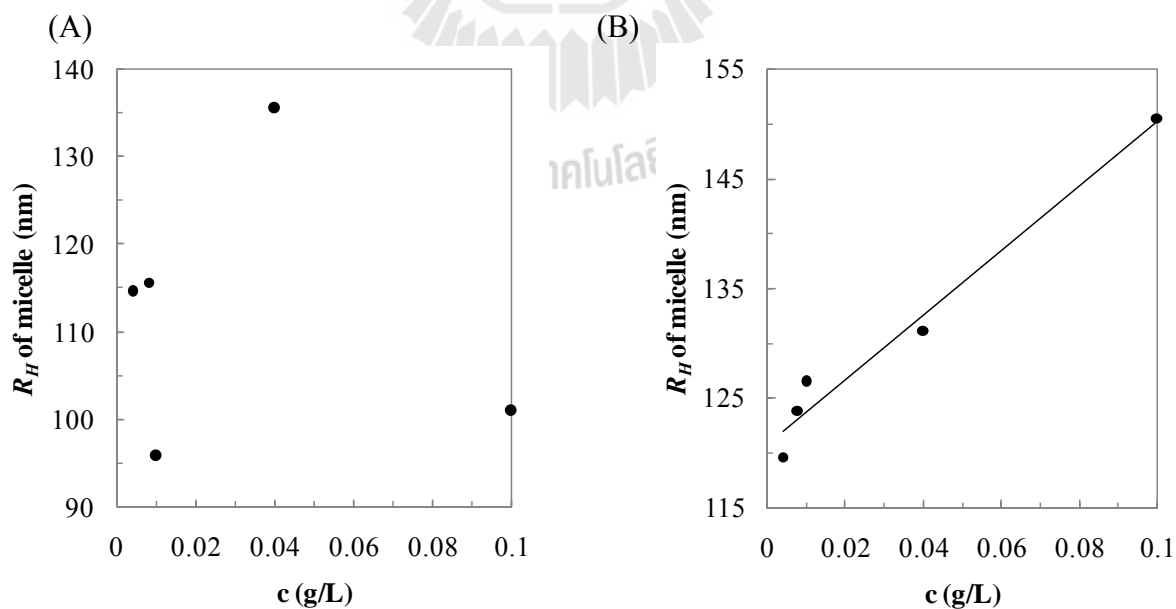
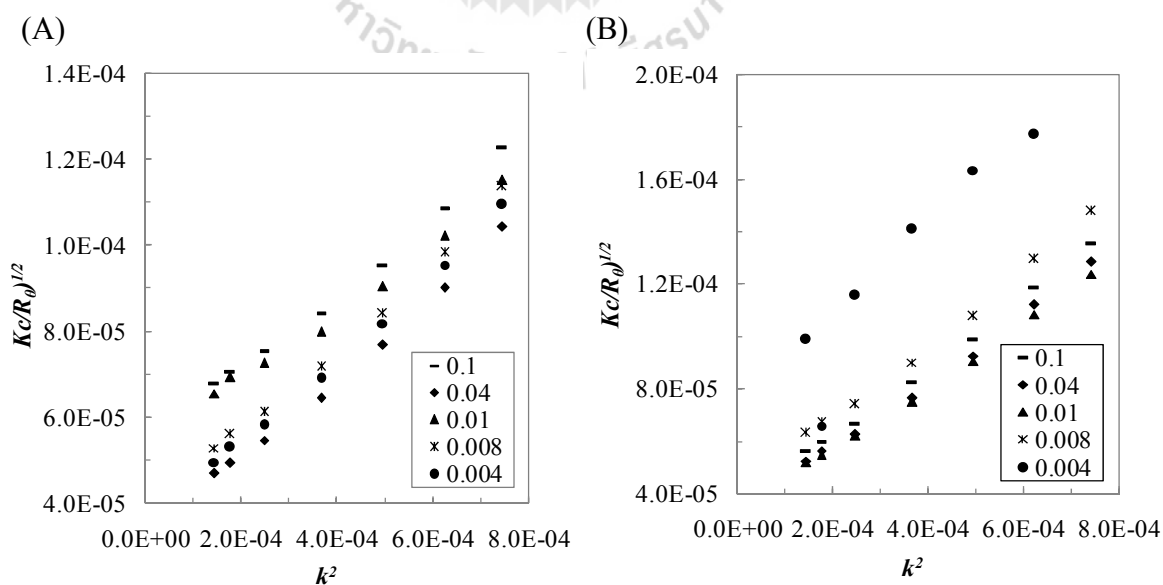


Figure 5.8 Hydrodynamic radius (R_H) plotted against the triblock copolymer concentration of (A) TB2 and (B) TB3.

Table 5.3 Light scattering results for PLA_x-PEG_y-PLA_x in water at 298 K.

Polymer	c (g/L)	τ/k^2 (10^{-8})	$R_{H, app}$ (nm)
PLA ₁₅ PEG ₂₃ PLA ₁₅	-	-	-
PLA ₂₈ PEG ₂₃ PLA ₂₈	0.1	2.85	100.96
	0.04	2.89	135.55
	0.01	2.93	95.84
	0.008	2.97	115.73
	0.004	2.83	114.64
PLA ₄₁ PEG ₂₃ PLA ₄₁	0.1	2.73	150.52
	0.04	2.99	131.19
	0.01	2.96	126.46
	0.008	2.93	123.91
	0.004	3.83	119.68

**Figure 5.9** Static light scattering results for (A) TB2 and (B) TB3 in aqueous solutions.

The structure factor $S(k)$ which is presented in term of Kc/R_θ was plotted as a function of k in Figure 5.9. Data point of $S(k)$ for TB2 was randomly scattered with k . In contrast, the $S(k)$ for TB3 was qualitatively dependent with the concentration.

- Partition coefficients of pyrene (Drug model)

As a hydrophobic molecule, pyrene prefers to incorporate into the hydrophobic part of micelle. Pyrene as a model for a hydrophobic drug had been studied by several previous researches (Dai *et al.*, 2004; Jiao *et al.*, 2010; Kwon *et al.*, 1994; Xiaozhi *et al.*, 2009). The cmc measurements with pyrene as the fluorescent probe are actually based on the partition of pyrene between water and micelle phases. Therefore a measurement of the partition coefficient of pyrene as a model hydrophobic drug can provide information on its affinity to the micelle phase or micelle cores. Moreover, it provides information on the chemical composition and the structure of micelle core.

To determine the partition of pyrene between water and the core of micelle, a similar method with Dai is applying (Dai *et al.*, 2004);

$$\frac{[Py]_m}{[Py]_w} = \frac{K_v \chi_{PLA} (c - cmc)}{1000 \rho_{PLA}} \quad (5.4)$$

$$\frac{[Py]_m}{[Py]_w} = \frac{F - F_{\min}}{F_{\max} - F} \quad (5.5)$$

where $[Py]_m$, $[Py]_w$ are the pyrene concentration in micelle core and water phase, respectively. K_v is the equilibrium partition coefficient of pyrene between the micelle core and water phase, c is the total copolymer concentration in

grams per liter, χ_{PLA} is the weight fraction of PLA in copolymer, and ρ_{PLA} is the density of the PLA core (1.2 g/ml). In experiment, the partition of pyrene can be obtained from fluorescence spectra as plotted in Figure 5.10 and was analyzed the data by using equation (5.5). The F , F_{min} and F_{max} are intensity ratio I_{336}/I_{334} , minimum ratio and maximum ratio, respectively. Figure 5.10 illustrates the plot between $[Py]_m/[Py]_w$ as a function of triblock copolymer concentration for TB2 and TB3. The K_v was calculated and summarized in Table 5.4. The K_v values are 1.62×10^5 and 3.42×10^5 for TB2 and TB3, respectively. The appearing results indicated that the micelle core can encapsulated more pyrene molecule with increased PLA block length. This result is fair agree with other work that encapsulation efficiency is higher with increasing PLA block length (Ruan and Feng, 2003). The observed K_v values were higher than those of diblock copolymer of PLA and MeOPEG (K_v ranging from 0.2×10^5 to 1.9×10^5) (Dai *et al.*, 2004), this is because the micelle from triblock copolymer prefer to form flower-like micelle and it is better structure to encapsulate the hydrophobic molecule than diblock copolymer. However, this triblock copolymer micelle still gave lower K_v than those of PS – PEO (K_v ranges from 2×10^5 to 4×10^5). This implies the PLA core is less hydrophobic than those of the PS core.

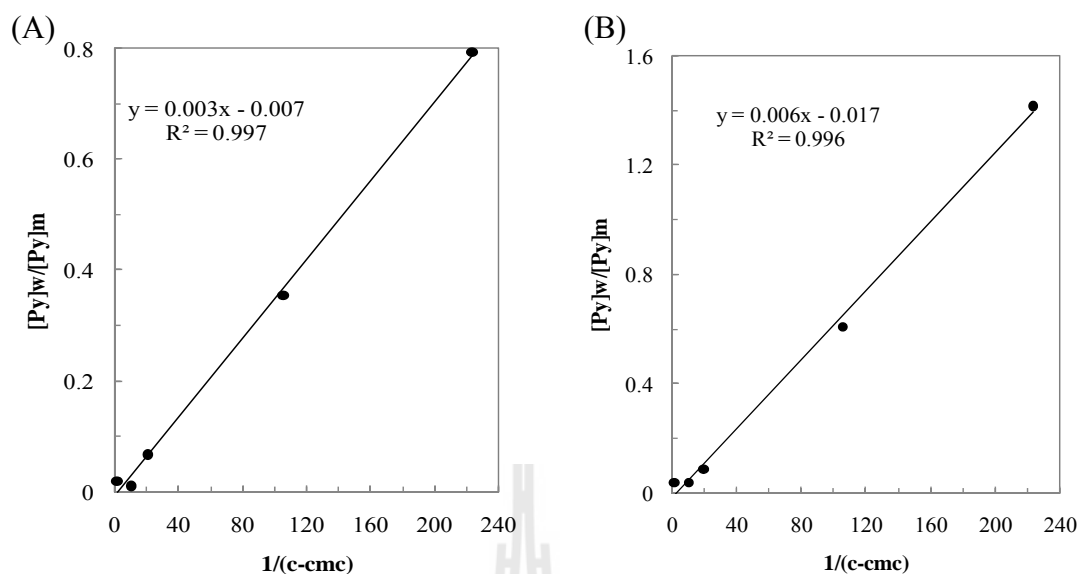


Figure 5.10 Plot of $[Py]_m/[Py]_w$ versus concentration of (A) TB2 and (B) TB3.

Table 5.4 Summarization of the $PLA_x-PEG_y-PLA_x$ triblock copolymer properties.

System	Triblock copolymer	LA/EG ratio	PLA fraction	cmc (mg/L)	K_v ($\times 10^5$)
TB1	$PLA_{29}PEG_{23}PLA_{29}$	2.56	0.80	- *	- *
TB2	$PLA_{56}PEG_{23}PLA_{56}$	4.88	0.89	0.46	1.60
TB3	$PLA_{83}PEG_{23}PLA_{83}$	7.28	0.92	0.63	3.42

* No micelle formation was detected by pyrene probing fluorescence

5.5 Conclusions

Three $PLA_x-PEG_y-PLA_x$ triblock copolymers at fixed PEG block lengths (1,000 g/mol, HO-[CH₂CH₂O]₂₃-H) with varying LA/EG block ratio were synthesized using stannous octoate as catalyst. Experimental results indicated only the appropriated LA/EG block ratio can inducing micelle formation. The cmc and hydrodynamic radius were increased with increasing LA/EG block ratio at fixed PEG

block length. Moreover, the ability of the triblock copolymer micelle system composed of larger LA/EG block ratio to encapsulate pyrene as the hydrophobic drug model was higher than those of the lower.

5.6 References

- Agrawal, S. K., Sanabria-DeLong, N., Coburn, J. M., Tew, G. N. and Bhatia, S. R. (2006). Novel drug release profiles from micellar solutions of PLA-PEO-PLA triblock copolymers. **Journal of Controlled Release** 112(1): 64-71.
- Alexandridis, P., Holzwarth, J. F. and Hatton, T. A. (1994). Micellization of poly(ethylene oxide)-poly(propylene oxide)-poly(ethylene oxide) triblock copolymers in aqueous solutions: thermodynamics of copolymer association. **Macromolecules** 27(9): 2414-2425.
- Almgren, M., Brown, W. and Hvidt, S. (1995). Self-aggregation and phase behavior of poly(ethylene oxide)-poly(propylene oxide)-poly(ethylene oxide) block copolymers in aqueous solution. **Colloid and Polymer Science** 273(1): 2-15.
- Cho, H., Cheong, I., Lee, J. and Kim, J. (2010). Polymeric nanoparticles, micelles and polymersomes from amphiphilic block copolymer. **Korean Journal of Chemical Engineering** 27(3): 731-740.
- Cohn, D. and Younes, H. (1988). Biodegradable PEO/PLA block copolymers. **Journal of Biomedical Materials Research** 22(11): 993-1009.
- Dai, Z., Piao, L., Zhang, X., Deng, M., Chen, X. and Jing, X. (2004). Probing the micellization of diblock and triblock copolymers of poly(L-lactide) and

- poly(ethylene glycol) in aqueous and NaCl salt solutions. **Colloid and Polymer Science** 282(4): 343-350.
- Ganta, S., Devalapally, H., Shahiwala, A. and Amiji, M. (2008). A review of stimuli-responsive nanocarriers for drug and gene delivery. **Journal of Controlled Release** 126(3): 187-204.
- Gaucher, G., Dufresne, M.-H., Sant, V. P., Kang, N., Maysinger, D. and Leroux, J.-C. (2005). Block copolymer micelles: preparation, characterization and application in drug delivery. **Journal of Controlled Release** 109(1-3): 169-188.
- Hagan, S. A., Coombes, A. G. A., Garnett, M. C., Dunn, S. E., Davies, M. C., Illum, L., Davis, S. S., Harding, S. E., Purkiss, S. and Gellert, P. R. (1996). Polylactide-poly(ethylene glycol) copolymers as drug delivery systems. 1. characterization of water dispersible micelle-forming systems. **Langmuir** 12(9): 2153-2161.
- He, G., Ma, L. L., Pan, J. and Venkatraman, S. (2007). ABA and BAB type triblock copolymers of PEG and PLA: a comparative study of drug release properties and “stealth” particle characteristics. **International Journal of Pharmaceutics** 334(1): 48-55.
- Jiao, Y.-H., Li, Y., Wang, S., Zhang, K., Jia, Y.-G. and Fu, Y. (2010). Layer-by-layer assembly of poly(lactic acid) nanoparticles: a facile way to fabricate films for model drug delivery. **Langmuir** 26(11): 8270-8273.
- Kricheldorf, H. R. and Meier-Haack, J. (1993). Polylactones, 22 ABA triblock copolymers of L-lactide and poly(ethylene glycol). **Die Makromolekulare Chemie** 194(2): 715-725.

- Kumari, A., Yadav, S. K. and Yadav, S. C. (2010). Biodegradable polymeric nanoparticles based drug delivery systems. **Colloids and Surfaces B: Biointerfaces** 75(1): 1-18.
- Kwon, G. S., Naito, M., Kataoka, K., Yokoyama, M., Sakurai, Y. and Okano, T. (1994). Block copolymer micelles as vehicles for hydrophobic drugs. **Colloids and Surfaces B: Biointerfaces** 2(4): 429-434.
- Kwon, G. S. and Okano, T. (1999). Soluble self-assembled block copolymers for drug delivery. **Pharmaceutical Research** 16(5): 597-600.
- Lee, S.-H., Kim, S. H., Han, Y.-K. and Kim, Y. H. (2002). Synthesis and characterization of poly(ethylene oxide)/polylactide/poly(ethylene oxide) triblock copolymer. **Journal of Polymer Science Part A: Polymer Chemistry** 40(15): 2545-2555.
- Li, S. M., Rashkov, I., Espartero, J. L., Manolova, N. and Vert, M. (1996). Synthesis, characterization, and hydrolytic degradation of PLA/PEO/PLA triblock copolymers with long poly(L-lactic acid) blocks. **Macromolecules** 29(1): 57-62.
- Linse, P. (1994). Adsorption and phase behaviour of pluronic block copolymers in aqueous solution. **Colloids and Surfaces A: Physicochemical and Engineering Aspects** 86: 137-142.
- Loh, W. (2002). Block copolymer micelles. **Encyclopedia of Surface and Colloid Science**: 802-813.
- Mata, J., Joshi, T., Varade, D., Ghosh, G. and Bahadur, P. (2004). Aggregation behavior of a PEO-PPO-PEO block copolymer + ionic surfactants mixed

- systems in water and aqueous salt solutions. **Colloids and Surfaces A: Physicochemical and Engineering Aspects** 247(1): 1-7.
- Mishra, B., Patel, B. B. and Tiwari, S. (2010). Colloidal nanocarriers: a review on formulation technology, types and applications toward targeted drug delivery. **Nanomedicine: Nanotechnology, Biology and Medicine** 6(1): 9-24.
- Nair, L. S. and Laurencin, C. T. (2007). Biodegradable polymers as biomaterials. **Progress in Polymer Science** 32(8): 762-798.
- Oh, J. K. (2011). Polylactide (PLA)-based amphiphilic block copolymers: synthesis, self-assembly, and biomedical applications. **Soft Matter** 7(11): 5096-5108.
- Rapoport, N. (2004). Combined cancer therapy by micellar-encapsulated drug and ultrasound. **International Journal of Pharmaceutics** 277(1): 155-162.
- Ruan, G. and Feng, S.-S. (2003). Preparation and characterization of poly(lactic acid) – poly(ethylene glycol) – poly(lactic acid) (PLA–PEG–PLA) microspheres for controlled release of paclitaxel. **Biomaterials** 24(27): 5037-5044.
- Sung, J. C., Pulliam, B. L. and Edwards, D. A. (2007). Nanoparticles for drug delivery to the lungs. **Trends in Biotechnology** 25(12): 563-570.
- Torchilin, V. P. (2007). Micellar nanocarriers: pharmaceutical perspectives. **Pharmaceutical Research** 24(1): 1-16.
- Venkatraman, S. S., Jie, P., Min, F., Freddy, B. Y. C. and Leong-Huat, G. (2005). Micelle-like nanoparticles of PLA–PEG–PLA triblock copolymer as chemotherapeutic carrier. **International Journal of Pharmaceutics** 298(1): 219-232.

- Whittlesey, K. J. and Shea, L. D. (2004). Delivery systems for small molecule drugs, proteins, and DNA: the neuroscience/biomaterial interface. **Experimental Neurology** 190(1): 1-16.
- Wilhelm, M., Zhao, C. L., Wang, Y., Xu, R., Winnik, M. A., Mura, J. L., Riess, G. and Croucher, M. D. (1991). Poly(styrene-ethylene oxide) block copolymer micelle formation in water: a fluorescence probe study. **Macromolecules** 24(5): 1033-1040.
- Winzenburg, G., Schmidt, C., Fuchs, S. and Kissel, T. (2004). Biodegradable polymers and their potential use in parenteral veterinary drug delivery systems. **Advanced Drug Delivery Reviews** 56(10): 1453-1466.
- Xiao, R. Z., Zeng, Z. W., Zhou, G. L., Wang, J. J., Li, F. Z. and Wang, A. M. (2010). Recent advances in PEG-PLA block copolymer nanoparticles. **International Journal of Nanomedicine** 5(1): 1057-1065.
- Xiaozhi, Z., Dongsheng, M., Jiangling, W., Huibi, X. and Xiangliang, Y. (2009). A novel method for the separation and determination of non-encapsulated pyrene in plasma and its application in pharmacokinetic studies of pyrene-loaded MPEG-PLA based nanoparticles. **Nanotechnology** 20(12): 125701.
- Zhang, Y., Jin, T. and Zhuo, R.-X. (2005). Methotrexate-loaded biodegradable polymeric micelles: Preparation, physicochemical properties and in vitro drug release. **Colloids and Surfaces B: Biointerfaces** 44(2-3): 104-109.
- Zhu, K. J., Xiangzhou, L. and Shilin, Y. (1990). Preparation, characterization, and properties of polylactide (PLA)-poly(ethylene glycol) (PEG) copolymers: A potential drug carrier. **Journal of Applied Polymer Science** 39(1): 1-9.

CHAPTER VI

CONCLUSIONS

In this research, both computational and experimental were used as the effective tools to investigate the detailed knowledge of amphiphilic triblock copolymer micelle in various aspects. In the first part of thesis, a novel lattice Monte Carlo simulation of coarse-grained polymer model mapped on the high coordination (second nearest neighbor diamond, 2nnd) lattice was applied to study polymer brushes and nanoparticle as the conceptual model of the corona and the core part of polymer micelle. Base on the model of PE and PEO, both $-\text{CH}_2\text{CH}_2-$ and $-\text{CH}_2\text{CH}_2\text{O}-$ unit are represented by a bead. The interaction between each bead is described by short- and long-range interactions based on the modified rotational isomeric state (RIS) model and Lennard-Jones (LJ) potential energy, respectively. The MC simulation was applied to study the effect of polydispersity on bidisperse polymer brush which is composed of a mixture of short and long chains. The simulation results reveal that, as N_S increases at constant N_L , both short and long chains are affected. On other hand, as N_L is increased, the short chains are more compressed in the inner layer whereas the long chains are more stretched to the outer layer. Strong difference in bead distribution cans cause two main features of the bimodal brushes *i.e.* vertical segregation and the difference of local degree of stretching between long and short chains. In addition, end bead distribution show an interpenetration of the short chain

ends into the outer layer. The effect of solvent quality on mono- and bidisperse PEO brush were also investigated as a model of corona part of micelle model. The results show that both polydispersity and solvent quality could affect to the brush properties. Due to different interaction between polymer-polymer and polymer-solvent interaction, the brush under poor solvent was more compressed as confirmed by the density profile, the orientation of bond and the polymer bead distribution. Moreover, this MC simulation was additionally modified to model PEO nanoparticle under the variation of solvent quality to study the stability and structure at the molecular level for the core part of micelle. The observed properties suggest the denser packing of chains in nanoparticles and increased density in bulk region. The shape of nanoparticle was nearly ellipsoid when the solvent quality was poorer. The distribution of middle beads in nanoparticle had no significant change by any solvent quality, while the end beads distribution was strongly changed. Most of bond orientation in the nanoparticle was relatively random.

The second part of thesis is about an application of the mesoscale simulation to study the aggregation behavior of amphiphilic ABA triblock copolymer micelle in water for molecular design. The influence of A/B block ratio to the morphology of designed ABA triblock copolymer based on Pluronic® (A = PEO and B = PPO) at fixed total number of beads were studied using MesoDyn method. The simulation results suggest that the A/B block ratio has a significant effect on phase aggregation, critical micelle concentration (cmc) and the formation rate of micelle. The cmc was increased with increasing A/B block ratio. In addition, the triblock copolymer with longer B block length was easier inducing micelle formation and its size become bigger. The present of drug model *i.e.* Haloperidol to the solution inducing easier

micelle formation and larger micelle size. The order parameters suggest the Haloperidol drug was placed at the interface between A and B part. The strength of hydrophobic part, by replacing PPO with PLA, of the triblock copolymer plays an important role on both the micelle formation and its morphology. Moreover, the influence of LA/EG block ratio, polymer concentration and third component addition (drug model) on morphology of designed $\text{PLA}_x\text{-PEG}_y\text{-PLA}_x$ were studied using both MesoDyn and DPD method before synthesis. The results suggest that only appropriated LA/EG ratio can be induced the spherical micelle formation. With increasing the LA/EG block ratio, there was an increased cmc and larger micelle size. Unfortunately, the aggregation was very strong making it was hardly to get more details about the micelle formation. The present of adding drug model in the solution can induce larger micelle size. Moreover, the drug was distributed everywhere inside the micelle core at low drug concentration. The triblock copolymer with higher LA/EG block ratio had more efficiency to encapsulate the hydrophobic drug model.

For the last part of this work, three $\text{PLA}_x\text{-PEG}_y\text{-PLA}_x$ triblock copolymers at fixed PEG block lengths ($\text{HO-[-CH}_2\text{CH}_2\text{O-]}_{23}\text{-H}$) with varying LA/EG block ratio based on the molecular simulation designed were synthesized using stannous octoate as the catalyst. Experimental results which were in qualitatively good agreement with the prediction from mesoscale simulation showed that the cmc and hydrodynamic radius were increased with increasing PLA block length at fixed PEG block. Moreover, moreover, the ability of the triblock copolymer micelle system compose of larger LA/EG block ratio to encapsulate pyrene as the hydrophobic drug model was higher than those of the lower.

CURRICULUM VITAE

Name : Mantana Chansuna

Date of birth : April 18th, 1984

Address : 27 Moo 11 Namakhue, Sahasakhan, Kalasin, Thailand

E-mail : pakat9@yahoo.com **Tel.** : +668-4028-6520

Education :

2002-2005 : Bachelor degree of Science in Chemistry, Mahasarakham University,
Mahasarakham

2006 : Graduate Diploma in Teaching (Chemistry), Mahasarakham
University, Mahasarakham

2007- 2013 : Ph.D. candidate in Chemistry, Suranaree University of Technology,
Nakhon Ratchasima

Experience :

- Teaching Practice (Chemistry): Sarakhampittayakom School, October 2006 – March 2007.
- Workshop in Simulations: Ubon Ratchathani University, August 20th – 22nd, 2008.
- The Japan Society for the Promotion of Science (JSPS) student exchange: Yamagata University (Yonezawa campus), Japan. September - October 2011
- Special research student in the Department of Macromolecular Science, Graduate School of Sciences, Osaka University, Japan. September 2012 - February 2013.